Diffusion Magnetic Resonance Imaging Tractography of the Fornix in Pediatric and Adult Multiple Sclerosis

by

Carly Weber

A thesis submitted in partial fulfillment of the requirements for the degree of

Master of Science

in

Biomedical Sciences

Department of Biomedical Engineering

University of Alberta

Abstract

The fornix is the main white matter output tract of the hippocampus and part of the limbic system, which is involved in aspects of memory and cognition. High-resolution, fluid-suppressed diffusion tensor imaging tractography has identified marked volume and diffusion abnormalities of the fornix in adults with multiple sclerosis (MS), with greater fornix changes in those with cognitive impairment. Fornix microstructural changes have also been identified across the healthy lifespan and across limited age ranges of disease cohorts, including MS, using lower resolution diffusion tensor imaging tractography without fluid-suppression, which is not ideal for measuring the fornix. Therefore, the objectives of this thesis were to use high-resolution, fluid-suppressed diffusion tractography to (i) determine if the fornix is affected in child/adolescent pediatric-onset MS using the same imaging protocols used to study the fornix in adults with MS, which would suggest its early involvement in the disease course, and (ii) analyze fornix microstructure changes across the MS lifespan, compared to healthy controls.

High-resolution, fluid-suppressed diffusion tractography was used to identify the fornix in 42 MS patients (13-63 years old), including 11 pediatric-onset MS (≤19 years of age), and 103 healthy controls (12-65 years). First, fornix volume and diffusion metrics were compared between the 11 pediatric-onset MS patients and 26 age/sex matched controls, as well as total/regional brain volumes, and correlated with cognitive/clinical scores (Chapter 3). Fornix volume/diffusion metrics and total/regional brain volumes of all 42 MS patients were then compared to all 103 healthy controls across age (Chapter 4).

Chapter 3 results showed that relative to controls, pediatric-onset MS patients had significantly smaller fornix (-26%), which was greater than other proportional losses in total/regional brain volumes. Notably, hippocampus volume was not significantly lower in

pediatric-onset MS. Fornix diffusion tensor imaging metrics yielded significantly lower fractional anisotropy (-7%), as well as higher mean (12%), axial (7%), and radial (16%) diffusivities in pediatric-onset MS. There were no significant correlations between fornix volume/diffusion metrics and cognitive/clinical scores. Fornix volume/diffusion metrics in pediatric-onset MS were similarly affected relative to controls as in our lab's previous adult MS study, and showed marked injury to the fornix that precedes injury to connected gray matter such as the hippocampus, implicating the fornix as an early brain region affected in MS, possibly by demyelination as indicating by the largest diffusion metric change in radial diffusivity.

Chapter 4 results showed that control fornix volume increased until 33 years and then declined, fractional anisotropy showed no age relationship, and mean, axial and radial diffusivities decreased until 33, 30, and 32 years, respectively, and then increased with age. MS fornix volume and fractional anisotropy followed similar trends as controls across age, but remained below controls at all ages, and mean, axial and radial diffusivities did not show age relationships but remained above controls at all ages, especially fornix volume and radial diffusivity. Presumably, pathological effects on fornix diffusion metrics overwhelmed expected age relationships in MS, and showed deviations from controls indicative of MS injury across all ages, suggesting the fornix is an early and consistent target of injury in MS, and that fornix injury is not progressive in MS.

These findings implicate the fornix as an early brain region affected in MS and may be largely related to its location within cerebrospinal fluid, which may contain MS inflammatory factors early on in the disease course.

Preface

This thesis is an original work by Carly Weber. The research projects, of which this thesis is a part, received research ethics approval from the University of Alberta Human Research Ethics Board, including project name "Advanced Magnetic Resonance Imaging of Pediatric-Onset Multiple Sclerosis", No. Pro00112979, and "Development of Magnetic Resonance Imaging and Its Application to Human Disease (Patients without Contract)", No. Pro00002112. All participants were scanned at the University of Alberta Peter S. Allen MR Research Centre.

A version of Chapter 3 of this thesis was presented at the 2024 International Society for Magnetic Resonance in Medicine (ISMRM) Annual Meeting in Singapore as Weber C, Wilbur C, Beaulieu C "High-resolution Fluid-Suppressed Diffusion Tractography Shows Altered Fornix Volume and Diffusion Metrics in Pediatric Multiple Sclerosis" (Abstract #0117). Chapter 3 of this thesis has been submitted for publication as Weber C, Wilbur C, Blevins G, Beaulieu C "Disproportional Smaller Fornix with Altered Microstructure in Pediatric Multiple Sclerosis Shown by High-Resolution Fluid-Suppressed Diffusion Tractography."

Chapter 4 is an original contribution to this thesis and has not yet been published elsewhere.

Acknowledgments

This work was funded by the Canadian Institutes of Health Research (CIHR). I would like to thank my supervisory committee, Dr. Christian Beaulieu and Dr. Colin Wilbur, as well as MS nurses, Leah White and Pam Dumont, and neurologists, Dr. Gregg Blevins and Dr. Penelope Smyth, all of whom were part of this research. Christian, thank you for being an incredible mentor and providing feedback that has improved my capabilities as a researcher immensely. Leah and Pam, thank you for teaching me how to administer clinical and cognitive testing, and taking the time to help me recruit patients. Colin, Gregg, and Penny, thank you for helping me recruit patients, and showing me what it means to be an excellent physician that is deeply appreciated by each and every one of their patients.

I would also like to thank all of the staff at the Peter S. Allen MR Research Centre, especially Carol Hartle, for always keeping me organized, and Peter Seres for his assistance during scans. Also, many thanks to the faculty and students of the Department of Biomedical Engineering. Alan and Rob, thank you for your guidance and support in teaching MRI physics and engineering principles to a former biological sciences major. Sarah Treit, thank you for your advice and encouragement prior to my first participant scan. To my fellow labmates, I am so grateful to have met, learned from, and bonded with all of you - I could not have done this without you.

Finally, thank you to my family and friends for their unwavering support, especially Colton. Above all, thank you to all of the children and adults with multiple sclerosis, and their families who participated in this research and gave it purpose.

Table of Contents

List of Tables

List of Figures

Symbols and Abbreviations

δ	Gradient Duration
γ	Gyromagnetic Ratio
Δ	Time Between Diffusion Gradients
ω_0	Larmor Frequency
χ	Magnetic Susceptibility
$\lambda_{1,2,3}$	Eigenvalues
$\varepsilon_{1,2,3}$	Eigenvectors
^{1}H	Hydrogen Proton
9HPT	Nine-Hole Peg Test
AD	Axial Diffusivity
ADC	Apparent Diffusion Coefficient
ADHD	Attention Deficit Hyperactivity Disorder
AIC	Akaike Information Criterion
b	Diffusion Sensitivity
B_0	Uniform Magnetic Field
B_1	Radiofrequency Magnetic Field
BDI-II	Beck's Depression Inventory-II
BVMT-R	Brief Visuospatial Memory Test-Revised
CNS	Central Nervous System
CSF	Cerebrospinal Fluid
CVLT-II	California Verbal Learning Test-II
D	Diffusion Coefficient
D	Diffusion Tensor
DIR	Dual Inversion Recovery
DMTs	Disease-Modifying Therapies
DTI	Diffusion Tensor Imaging
DWI	Diffusion Weighted Imaging
EDSS	Expanded Disability Status Score

FA	Fractional Anisotropy
FACT	Fiber Assignment by Continuous Tracking
FDR	False Discovery Rate
FID	Free Induction Decay
FLAIR	Fluid-Attenuated Inversion Recovery
FSS	Fatigue Severity Scale
G	Gradient Magnitude
GM	Gray Matter
GRAPPA	GeneRalized Autocalibrating Partially Parallel Acquisitions
ICC	Intracranial Cavity
M_0	Net Equilibrium Magnetization
MD	Mean Diffusivity
MFIS	Modified Fatigue Impact Scale
MNI	Montreal Neurological Institute
MPRAGE	Magnetization Prepared Rapid Acquisition Gradient Echo
MRI	Magnetic Resonance Imaging
MS	Multiple Sclerosis
M_{xy}	Net Transverse Magnetization
M_z	Net Longitudinal Magnetization
NA2BS	Non-Local Automatic Brain Hemispheric Segmentation
NAGM	Normal-Appearing Gray Matter
NAWM	Normal-Appearing White Matter
NICE	Non-Local Intracranial Extraction
NLM	Non-Local Means
NMR	Nuclear Magnetic Resonance
OGSE	Oscillating-gradient spin-echo
PASAT-3	Paced Auditory Serial Addition
PEC	Patch-based Ensemble Corrector
PGSE	Pulsed Gradient Spin Echo
POMS	Pediatric-onset Multiple Sclerosis
PPMS	Primary Progressive Multiple Sclerosis

RD	Radial Diffusivity
RF	Radiofrequency
ROI	Region-of-Interest
RRMS	Relapsing-remitting Multiple Sclerosis
S_0	b0 signal intensity
SDMT	Symbol Digit Modalities Test
SNR	Signal-to-noise Ratio
SPACE	Sampling Perfection Application Contrast Evolution
SPMS	Secondary Progressive Multiple Sclerosis
SS-EPI	Single-Shot Echo-Planar Imaging
t	Diffusion Time
T	Tesla
T1	Longitudinal Relaxation
T2	Transverse Relaxation
T25FW	Timed 25-Foot Walk
TBSS	Tract-Based Spatial-Statistics
TBV	Total Brain Volume
TE	Echo Tim
TI	Inversion Time
TLV	Total Lesion Volume
TR	Repetition Time
TSE	Turbo Spin Echo
WM	White Matter

1. Introduction

1.1 Multiple Sclerosis

Multiple sclerosis (MS) is an autoimmune disorder characterized by demyelination, inflammation and neurodegeneration of the central nervous system (CNS), and often results in long-term physical and cognitive impairments (Ghasemi 2017). Approximately 2.8 million people worldwide have MS, and 90,000 of which live in Canada, making Canada one of the leading hotspots of MS in the world, particularly Alberta (MFIS 2020). Most individuals are diagnosed with MS in adulthood, and twice as many females are diagnosed with MS than males on average, however children and adolescents account for at least 30,000 of the MS cases around the world. Pediatric-onset MS (POMS), where MS onset occurs during childhood/adolescence, accounts for 2-5% of MS cases and is characterized by high rates of disease activity and disability during critical stages of development (Bigi 2012, Wilbur 2019). Although the underlying causes of MS are unknown and symptoms vary widely from patient to patient, MS diagnosis requires evidence of at least one MS attack and visualization of lesions using conventional magnetic resonance imaging (MRI) that disseminate in time and/or space, with or without the presence of cerebrospinal fluid (CSF) oligoclonal bands, according to the 2017 McDonald criteria for MS diagnosis (**Table 1.1**) (Thompson 2018). An MS attack is defined as a distinct period of new or worsening symptoms, accompanied by a demyelinating inflammatory event in the CNS. Most individuals are diagnosed with relapsing-remitting MS (RRMS) (above 80%), which is characterized by unpredictable relapses, or attacks, followed by periods of full or partial remission, although some individuals are diagnosed with progressive subtypes of MS, including primary and secondary progressive MS (i.e. PPMS and SPMS, respectively), whereby patients experience a consistent and gradual worsening of symptoms and often

neurodegeneration (Ghasemi 2017). The Expanded Disability Status Scale (EDSS) is a clinical score that quantifies the severity of MS for each patient. EDSS ranges from 0 (no disability) to 10 (death from MS) with 0.5 increments, and is based on neurological examination by a physician (Meyer-Moock 2014). There is no cure for MS, however symptoms can be mediated using disease-modifying therapies (DMTs), which work to reduce the number of relapses, and slow disease progression and disability (Edinger 2024).

Table 1.1. 2017 McDonald criteria for MS diagnosis (Thompson 2018)

Number of attacks/lesions	Diagnosis Criteria
≥ 2 attacks ≥ 2 lesions	Diagnosis
≥ 2 attacks 1 lesion	Lesion disseminates in space → Diagnosis
1 attack ≥ 2 lesions	Lesion disseminates in time → Diagnosis
1 attack 1 lesion	Lesion disseminates in space/time and CSF oligoclonal bands → Diagnosis

1.2 Conventional Clinical MRI of MS

As mentioned in Section 1.1, the clinical diagnosis of MS requires the use of conventional MRI scans in order to visualize lesions (Hemond 2018, Thompson 2018). Conventional scans typically include anatomical T1-weighted scans, with and without contrast (i.e. Gadolinium), and T2-weighted and/or T2 fluid-attenuated inversion recovery (FLAIR) scans (**Figure 1.1**) (Hemond 2018). T1 scans can be used to identify pathological processes, such as demyelination and axonal loss (or brain atrophy), which appear hypointense (i.e. dark) on T1 images. Gadolinium may also be administered intravenously in order to better visualize

arteries/veins in the brain and identify breakdown of the blood-brain barrier from MS inflammation. Gadolinium can enhance lesions to be hyperintense on T1-weighted scans. T2 scans are primarily used to detect hyperintense (i.e. bright) lesions, which may be from demyelination, axonal loss or other pathological processes. T2 FLAIR scans are especially useful for detecting bright periventricular lesions because FLAIR nulls the bright signal from CSF. Diffusion MRI is primarily being used in MS research, not clinical settings.

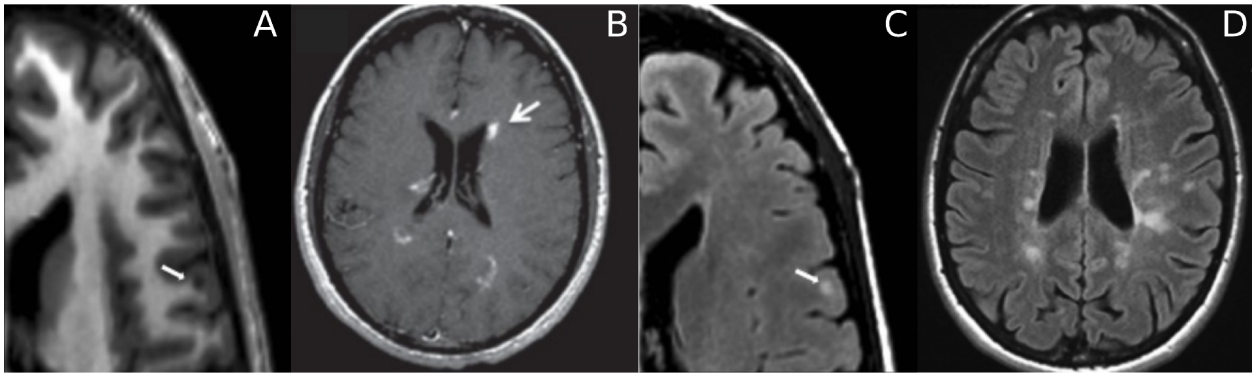

Figure 1.1. Typical Clinical MRI Scans for Diagnosis of Multiple Sclerosis at 3T. (A) T1 scan showing hypointense cortical lesion, (B) T1 scan post Gadolinium showing hyperintense periventricular lesion, (C) T2 FLAIR showing hyperintense cortical lesion, and (D) T2 FLAIR showing hyperintense periventricular lesion. Adapted from Hemond (2018).

1.3 MRI Studies in Adult-Onset MS

1.3.1 Volumetric MRI and Correlates in Adult-Onset MS

Previous studies have used 3D T1-weighted scans to show that adults with MS have reduced deep gray matter (GM) volumes compared to controls, including the accumbens, amygdala, brainstem, caudate, hippocampus, pallidum, putamen, and thalamus (Eshaghi 2018). Notably, the thalamus was shown to be affected early on in the disease course. Hippocampus atrophy has also been consistently reported in adults with all subtypes of MS (Anderson 2010, Kern 2015), in both whole and regional areas of the hippocampus (Sicotte 2008). Adults with MS have also shown reduced volume in cortical and cerebellar gray matter regions compared to

controls, including the precuneus, posterior cingulate cortex, and various regions in the temporal lobe and precentral cortex (Eshaghi 2018). Total cortical and subcortical GM volumes were shown to be lower in adults with MS compared to controls even during early stages of disease (Nygaard 2015).

GM atrophy in adults with MS has also been linked to increased physical and cognitive impairments, especially GM atrophy of the thalamus, hippocampus, and cerebellum. Many volumetric MRI studies have correlated thalamic atrophy with a wide range of disabilities in adults with MS, including cognitive performance (Houtchens 2007, Kern 2015) and fatigue (Bernitsas 2017). There has been particular interest in examining correlates of thalamic atrophy because of its close proximity to the lateral ventricles and third ventricle, which become enlarged in MS and correlate strongly with cognitive impairment, and because of its extensive connectivity, which make it susceptible to Wallerian degeneration from demyelination and axonal loss of connecting white matter (WM) (Houtchens 2007, Sinnecker 2020). Adults with MS showed significantly smaller thalamus (-17%) compared to controls, and thalamic atrophy strongly correlated with decreased measures of processing speed using the Symbol Digit Modalities Test (SDMT) and visuospatial memory using the Brief Visuospatial Memory Test-Revised (BVMT-R) (Houtchens 2007). There have also been strong positive correlations shown between thalamic atrophy and fatigue scores using the Fatigue Severity Scale (FSS) (Bernitsas 2017). Whole and regional hippocampus atrophy was also shown to correlate with worse SDMT and BVMT-R scores, as well as reduced episodic memory, as assessed by the California Verbal Learning Test-II (CVLT-II), and EDSS, which measures degree of MS severity (Koenig 2014). A more recent volumetric MRI study also showed relationships between cerebellar atrophy and physical impairment in adults with MS, including significant positive

correlations between cerebellar cortex volume and walk ratio, which is a measure of coordination and gait control (Kalron 2020). Higher cerebellar lobule volume has been shown to correlate with improved motor and cognitive function in adults with MS, as measured by a variety of walking tests and the SDMT (Fritz 2022). Additionally, most total/regional GM volumes have been shown to decline with age in MS, which is further discussed in Chapter 4.

1.3.2 DTI Studies and Correlates in Adult-Onset MS

Diffusion tensor imaging (DTI) has been used to detect and quantify microscopic injury in MS in otherwise normal-appearing brain tissue, particularly WM. Studies have consistently shown abnormal diffusion metrics, namely increased mean diffusivity (MD) and reduced fractional anisotropy (FA) in MS lesions and normal-appearing WM (NAWM) in adults with MS compared to controls (Filippi 2001, Caranova 2023). A voxel-based DTI analysis found that these abnormal diffusion metrics were even more pronounced in progressive MS subtypes, possibly reflecting a greater degree of axonal injury (Preziosa 2011). Increased axial (AD) and radial (RD) diffusivities have also been reported in NAWM in adults with MS compared to controls, which may specifically reflect axonal loss and demyelination, respectively (Klistorner 2016). Tract-based spatial-statistics (TBSS) have identified abnormal diffusion metrics in most NAWM tracts in adults with MS, notably the corpus callosum, corticospinal tracts, cingulum, optic radiation, inferior longitudinal fasciculus, and fornix, which were found to correlate with greater disease duration and clinical disability (Huang 2018, Roosendaal 2009), as well as physical disability and reduced cognition (Welton 2015), including reduced performance on the SDMT (Yu 2011). DTI tractography has identified similar abnormal diffusion metrics in most NAWM, including the fornix, cingulum, uncinate and longitudinal fasciculus (Fink 2010, Syc 2013, Kern 2015, Keser 2017). DTI tractography abnormalities were shown to correlate with

lower cognitive function as measured by the Paced Auditory Serial Addition (PASAT-3), but not physical disability as measured by the Timed 25-Foot Walk (T25FW) (Syc 2013), as well as cognitive impairment (Keser 2017), processing speed as measured by the SDMT (Kern 2015), and other memory processes as measured by the CVLT (Fink 2010).

Recently, our lab's DTI tractography study identified marked volume and diffusion abnormalities of the fornix in adult MS, including reduced volume and FA, and higher MD and RD compared to controls, which were more extensive than changes to the other WM tracts analyzed (i.e. cingulum and uncinate fasciculus), and were similarly affected across all MS subtypes (i.e. RRMS, PPMS, SPMS) (Valdés Cabrera 2020). Fornix volume and left fornix FA were also shown to correlate negatively with total lesion volume (TLV), suggesting a relationship between MS lesions and fornix integrity. However, the main limitation was the lack of CSF-suppression, which may have altered fornix tractography and DTI metrics by partial volume effects from rapid, isotropic CSF in the ventricles where the fornix is located, which also contributes to the diffusion metrics per voxel. The lack of CSF-suppression may have made fornix tractography and DTI metrics prone to errors, and therefore more difficult to interpret. Further, MS periventricular lesions are common and implicate the role of harmful inflammatory factors that may be contained in CSF, where the fornix is located (Ghasemi 2017). DTI fornix tractography improved with the use of high-resolution fluid-attenuated inversion recovery (FLAIR) DTI, which suppresses confounding CSF and reduces deleterious partial volume effects that arise because of the small tract size of the fornix and its location within CSF (Concha 2005) (**Figure 1.3**). FLAIR-DTI has shown significant volume and diffusion abnormalities of the fornix in adults with MS compared to controls, including lower tract volume and FA, and higher MD, AD and RD, which were most affected in those with cognitive impairment and greater than

other losses in WM and GM (Valdés Cabrera 2022). SDMT was also shown to correlate positively with fornix FA, and negatively with fornix MD and RD. Additionally, fornix volume showed a negative linear relationship, FA showed no relationship, and MD, AD and RD showed positive linear relationships with age (32-71 years). Fornix volume/diffusion metric relationships with age in MS are further discussed in Chapter 4. Others have also found that fornix FA and RD correlated with cognitive impairment in adult MS, measured using the SDMT and other working memory tests (Keser 2017). Further, fornix volume/diffusion metrics in adults with MS have been shown to correlate with multimodal cognitive impairment (Keser 2018), poorer verbal memory performance (Kern 2012), episodic memory performance measured using BVMT-R and processing speed measured using SDMT (Koenig 2014), and lower CVLT scores (Dineen 2012). See **Figure 1.2** for a summary of some published fornix DTI studies in adult MS. Interestingly, hippocampus volume was not shown to be significantly different between adult MS and control groups, and abnormal diffusion metrics were only shown for hippocampus in the cognitively impaired MS group, suggesting that microstructural hippocampus injury precedes atrophy and results from direct injury to connected fornix WM (Valdés Cabrera 2022).

Fewer DTI studies have examined normal-appearing GM (NAGM). High-resolution (1 mm isotropic) DTI showed that compared to controls, adults with MS had higher MD, and lower volume and FA across the whole hippocampus, which correlated with greater physical fatigue (Valdés Cabrera 2023). Relative to controls, adults with MS also showed elevated MD and reduced FA in normal-appearing cortical, but not deep GM, suggestive of microstructural MS injury from inflammation, demyelination and/or Wallerian degeneration (Zhou 2010). Normal-appearing cortical GM diffusion abnormalities were also associated with poorer clinical

disability (Vrenken 2006), and normal-appearing thalamic GM diffusion abnormalities in adults with MS (Tovar-Moll 2009).

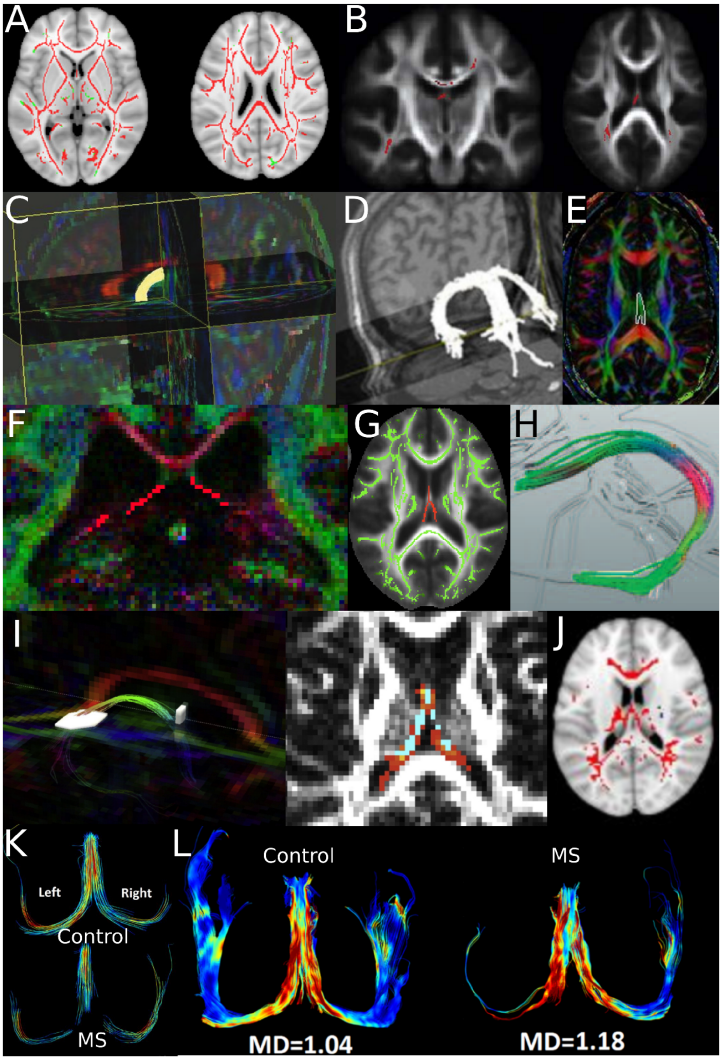

Figure 1.2. Fornix DTI Analyses in Adult MS. (A) TBSS map showing regions with elevated MD in red, adapted from Huang (2018), (B) TBSS map showing regions with reduced FA in red, adapted from Roosendaal 2009, (C) Tractography of the fornix, adapted from Syc 2013, (D Fornix tractography, adapted from Keser 2017, (E) Region-of-interest shown in fornix body, adapted from Keser 2018, (F) Colour FA map with fornix regions-of-interest in red, adapted from Koenig 2013, (G) TBSS map with fornix regions-of-interest manually identified (red) on WM skeleton (green), adapted from Kern 2012, (H) Fornix tractography, adapted from Fink 2012, (I) Fornix tractography (left) and TBSS map (right) with fornix regions-of-interest in red, adapted from Kern 2015, (J) TBSS map showing regions with reduced FA in red, adapted from Welton 2015, (K) Fornix tractography without CSF-suppression at 4.7T, adapted from Valdés Cabrera 2020, (L) Fornix tractography with CSF-suppression at 3T, adapted from Valdés Cabrera 2022.

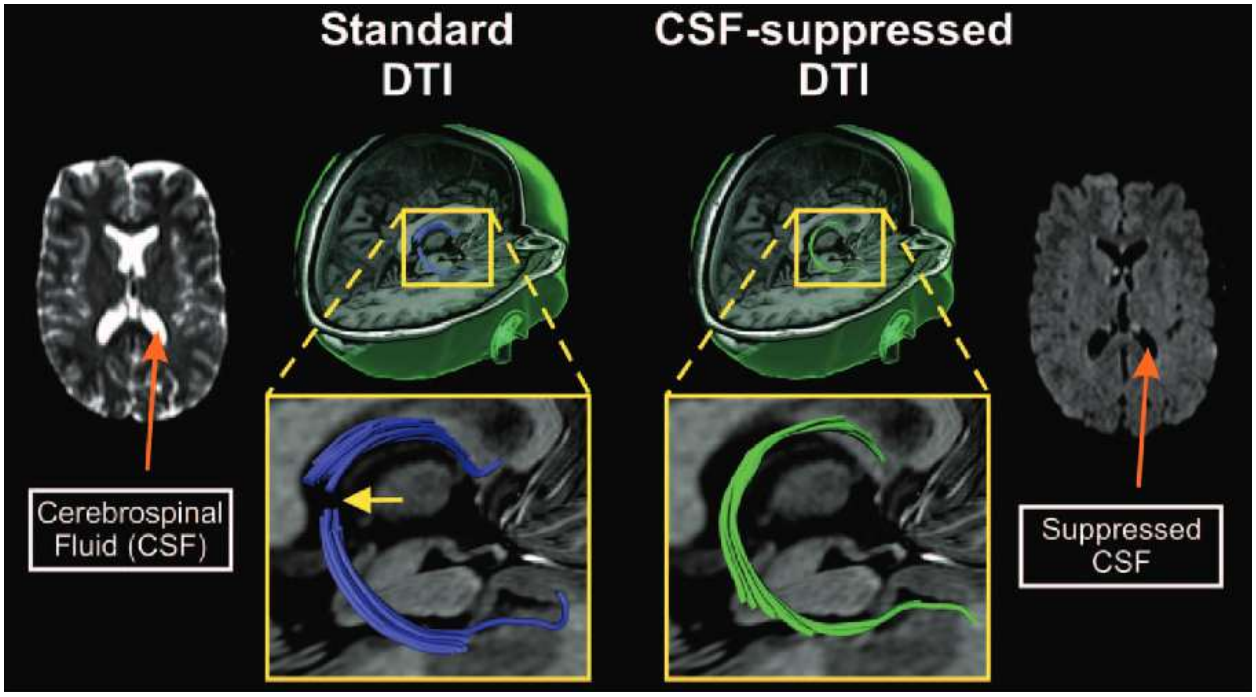

Figure 1.3. Fornix DTI Tractography without CSF-suppression (left) and with CSF-suppression (right), adapted from Concha 2005. Fornix tractography improved with high-resolution, FLAIR DTI, which reduces CSF partial voluming.

1.4 MRI Studies in Pediatric-Onset MS

1.4.1 Volumetric MRI and Correlates in Pediatric-Onset MS

Similar to adult MS, children/adolescents with MS have shown gray matter atrophy across many cortical and subcortical regions compared to controls that progress over time, including the thalamus, hippocampus, insula, caudate, putamen, amygdala, cerebellum, cingulate cortex, and various areas of the frontal, parietal, temporal, occipital lobes (De Meo 2019) and globus pallidus (Aubert-Broche 2011). GM atrophy was shown to correlate positively with EDSS, notably the thalamus, caudate, precuneus, and frontal lobe regions (De Meo 2019). Further, premorbid intelligence correlated positively with cingulate cortex, thalamus, cerebellum, and regional frontal, parietal and temporal lobe volumes (De Meo 2019). Interestingly, pediatric MS has shown inconsistent results regarding hippocampus and thalamus atrophy, compared to

controls. Pediatric MS patients have shown reduced amygdala and thalamus, but not hippocampus volume (Fuentes 2012), although they had similar memory performance as controls. Conversely, reduced global and regional hippocampus volumes have been shown in pediatric MS patients compared to controls, but only regional hippocampal atrophy correlated with clinical measures, namely reduced attention and language abilities (Rocca 2016a). Additionally, cognitively impaired MS showed regional hippocampal reductions compared to MS that were not cognitively impaired.

Similar to adult MS, one pediatric MS study was interested in studying thalamic atrophy because of its interfaces with perivascular WM MS lesions and the ventricles, containing CSF with MS inflammatory factors (Fadda 2019). The study found that relative to controls, pediatric MS patients displayed a surface-in gradient of thalamic atrophy on the ventricular side, which was evident early on in the disease course and progressed over time. However, it was also shown that GM atrophy was restricted to the thalamus in pediatric MS and had no correlations with disease duration or disability, although this may have reflected the fact that the thalamus is one of the first structures affected in MS (Mesaros 2008). This is supported by findings from an older cohort of patients and found that compared to controls, pediatric MS patients had smaller hippocampus, amygdala and thalamus volumes, and that hippocampus and thalamus volumes correlated positively with episodic memory performance (Fabri 2021). No difference in total GM volume between pediatric MS and controls was also shown, but pediatric MS showed reduced total WM (Bartels 2019). Regional cerebellar volume, specifically the posterior lobe, has also been correlated negatively with cognition, notably worse performance on the SDMT in pediatric MS (Weier 2016). See Appendix A for a summary of children/adolescent POMS volumetric studies.

1.4.2 DTI Studies and Correlates in Pediatric-Onset MS

DTI has also detected diffusion abnormalities in a wide range of WM tracts in pediatric MS that are indicative of microstructural injury. Region-of-interest (ROI) and tract-based DTI analyses have shown that relative to controls, pediatric MS patients had higher MD and lower FA in all WM tracts examined, even in NAWM, including the corpus callosum, posterior limb of internal capsule, cerebral peduncle, long association fibers (i.e. superior longitudinal, inferior fronto-occipital, and uncinate fasciculus) (Vishwas 2010, Vishwas 2013). ROI DTI showed that greater lesion volume correlated with reduced FA in pediatric MS corpus callosum and hemispheric NAWM, as well as greater FA with better visual matching and SDMT performance, and no correlations with EDSS (Bethune 2011). Similarly, correlations have been found between corpus callosum FA and math performance in pediatric MS (Till 2011b). ROI DTI also showed elevated RD and reduced AD in early-onset pediatric MS NAWM relative to controls (Tillema 2012). Probabilistic DTI tractography also consistently showed that compared to controls, very early-onset pediatric MS patients (<12 years of age) had higher MD and lower FA in NAWM, including the bilateral superior longitudinal fasciculus and corpus callosum, suggesting early NAWM injury in MS (Rocca 2016b). These abnormal DTI metrics in POMS appear to worsen over time compared to controls (Longoni 2017).

Unlike adult MS, only one study has analyzed the fornix in children/adolescents POMS (Blaschek 2013), presumably because its small structure within the ventricles make it difficult to measure due to partial voluming from rapid, isotropic diffusing CSF, which contributes to the diffusion metrics per voxel, and make measurements prone to error. The study mentions the fornix with elevated MD (**Figure 1.4**), but it used low spatial resolution, no CSF-suppression, and a voxel-based analysis, not ideal for measuring the fornix because it did not minimize the

effects of CSF partial volume (Bach 2014), and the actual MD value was not reported, nor was volume or other diffusion metrics.

Similar to adult MS, there are few POMS NAGM DTI studies, although one recent study by De Meo (2021) found that compared to controls, POMS had higher FA of the whole thalamus, lower FA and elevated MD of thalamic WM, and reduced thalamic volume. These abnormal diffusion metrics were predominantly located in regions of the thalamus nearby CSF and WM, suggestive of CSF and WM-mediated microstructural injury that precedes later macroscopic tissue atrophy. DTI also showed no differences between early-onset pediatric MS and controls in total NAGM, which provided evidence that GM injury may be restricted to the thalamus in pediatric MS (Tortorella 2006). See Appendix B for a summary of children/adolescent POMS DTI studies.

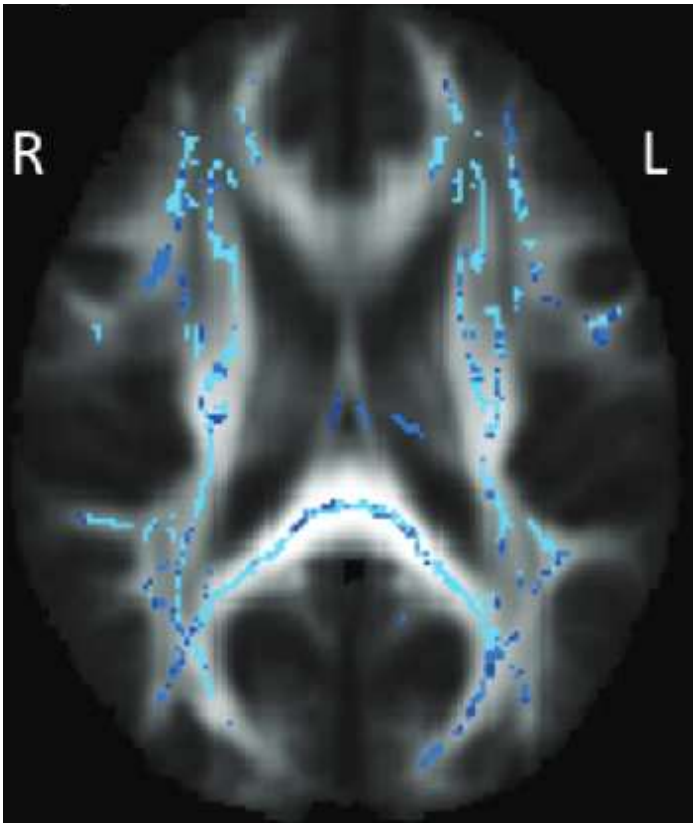

Figure 1.4. Fornix DTI in Pediatric MS. TBSS showing regions with elevated MD in blue, including fornix region (center), adapted from Blaschek 2013.

1.5 Pediatric-Onset vs Adult-Onset MS

Pediatric-onset (diagnosed before 18 years of age) versus adult-onset MS (diagnosed after 18 years of age) studies have shown conflicting results. TBSS showed that adults with relapsing-remitting POMS had lower FA values across widespread WM regions compared to both age-matched and disease duration-matched AOMS (Aliotta 2014). Fewer WM regions with reduced FA were shown for POMS compared to disease duration-matched than age-matched AOMS, although POMS and disease duration-matched AOMS had higher EDSS and lower GM volume than age-matched AOMS. However, adult POMS have also shown lower EDSS and better cognitive scores, with no differences in lesion volume, total GM volume, total WM volume or WM FA, compared to disease duration-matched AOMS (Bonacchi 2021). Although, the rate of WM and then GM atrophy became greater in POMS with age compared to disease duration-matched AOMS.

TBSS and volumetric analyses have shown similar GM volume reductions between early adult POMS (mean age 25 years old, mean disease duration 10 years) and age-matched AOMS (mean age 27 years, mean disease duration 4 years) compared to controls, namely for the thalamus (-8% POMS vs -12% AOMS) and globus pallidus (-10% POMS vs -12%) (Giorgio 2017). POMS and age-matched AOMS also showed similar DTI abnormalities. POMS showed approximately 20% lower FA in regions of the cerebellum, inferior longitudinal fasciculus, inferior fronto-occipital fasciculus, forceps major, fornix, posterior corona radiata and middle frontal gyrus, 28% higher AD in the fornix and posterior corona radiata, and 35% higher RD in the inferior longitudinal fasciculus, and inferior fronto-occipital fasciculus. Age-matched AOMS showed approximately 17% lower FA in the cerebellum WM, inferior longitudinal fasciculus, and inferior fronto-occipital fasciculus, 33% higher AD in the thalamus WM, and 34% higher

RD in the inferior longitudinal fasciculus, inferior fronto-occipital fasciculus, and fornix. POMS only showed greater lesion volume and more affected diffusion metrics relative to controls than age-matched AOMS in the posterior corona radiata. Conversely, older adult POMS (mean age 39 years) showed reduced TBV, total GM, and deep GM volume (i.e. thalamus) compared to age-matched AOMS (Fenu 2018). Similarly adult POMS showed higher lesion volume, and lower TBV, and total GM volume than age-matched AOMS, but higher TBV and total GM volume than disease duration-matched AOMS (Donohue 2014). Adult POMS also showed worse SDMT performance compared to AOMS (McKay 2019).

Compared to children/adolescent POMS (mean age 13 years old), AOMS (mean age 37 years old) showed more cortical lesions, and lower total GM volume baseline, but not after follow-up (3 years) (Calabrese 2012). However, children/adolescents with POMS have also shown more lesions at baseline and follow-up scanned compared to AOMS (Waubant 2009), as well as higher relapse rate compared to disease-duration matched AOMS (Gorman 2009). Children/adolescent POMS also showed similar lesion volume, but higher GM volume compared to disease duration-matched AOMS, whereas adult POMS showed no differences in lesion or WM volume and less progressive MS with lower EDSS, as well as lower GM volumes compared to disease-duration matched AOMS (Yeh 2009).

1.6 The Limbic System: Fornix

The limbic system includes both cortical (i.e. cingulate gyri, parahippocampal gyri, entorhinal cortex) and subcortical (i.e. amygdala, septal nuclei, nucleus accumbens, mammillary bodies, hypothalamus, anterior nucleus of the thalamus, hippocampus, and fornix) structures, involved in emotion and memory processes (Douet 2014a). The fornix is the main output WM tract of the hippocampus, which is the primary memory component of the limbic system, so the fornix has often been studied in relation to memory deficits, particularly episodic memory. The fornix is a small C-shaped tract (sagittal view) that extends from the posterior of the hippocampus to the septal area of the brain and the hypothalamus. The fornix is divided into two fimbria, each of which extend posteriorly from a small section of WM along the ventricular surface of the hippocampus called the alveus and each become a crus (Choi 2021). The crura then merge together and curve both superiorly and anteriorly to form the fornix commissure and then fornix body, which forms beneath the septum pellucidum, and finally converges into two columns that curve inferiorly towards the anterior commissure and ends at the mammillary bodies (**Figure 1.5**).

The fornix is part of what was originally referred to as the Papez circuit, first described by James Papez in 1937, and includes the hippocampus, mammillary bodies of the hypothalamus, thalamus, cingulate gyrus, and parahippocampal gyrus (Papez 1995). The Papez circuit is a major limbic system pathway involved in memory and emotion, and travels through the hippocampal formation (subiculum), fornix, mammillary bodies of the hypothalamus, mammillothalamic tract, anterior thalamic nucleus, cingulum, entorhinal cortex, and then back to the hippocampus (Kamali 2023). Later iterations of the circuit have also proposed connections with other brain regions and structures, including the prefrontal cortex, septum, and amygdala.

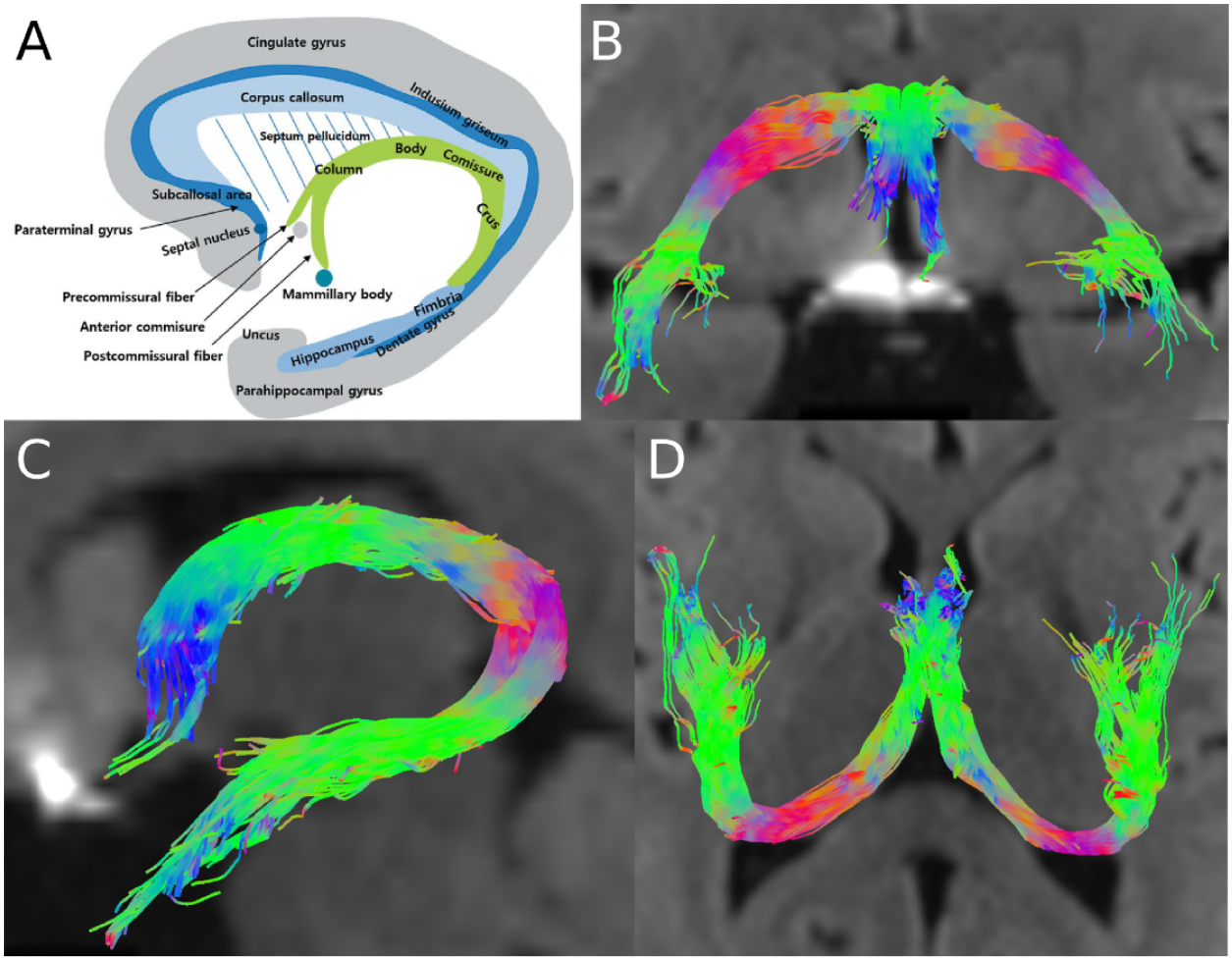

Figure 1.5. Fornix Anatomy. (A) Schematic of the limbic system adapted from Choi 2021 (fornix in green). (B) Coronal (anterior), (C) sagittal (lateral), and (D) axial (superior) view of fornix as depicted by diffusion MRI tractography, colour-coded by fastest direction of diffusion (i.e. anterior-poster tracts in green, left-right tracts in red, superior-inferior tracts in blue).

Fornix microstructure changes, identified using DTI, have primarily been correlated with memory and other cognitive functions, specifically declarative and episodic memory, in healthy aging (Rudebeck 2009), cognitively impaired individuals (Metzler-Baddeley 2012), and many neurodegenerative and neuroinflammatory diseases, including MS (Dineen 2012, Koenig 2013). However, microstructural fornix changes have also been implicated in overall cognition in MS (Keser 2017) and controls (Fletcher 2013). Given its important role, the fornix has also been studied across the healthy lifespan for age-related changes. Fornix volume and FA have shown

inverted U-shaped curves that increases and then decreases with age, whereas fornix MD, AD and RD, have shown opposite U-shaped curves that decrease and then increase with age, as shown in a fornix tractography study of 5-83 year old healthy controls (Lebel 2012) (**Figure 1.6**). Interestingly, there were no significant sex differences shown for fornix FA or MD curves. There are, however, some discrepancies in the age-related changes shown for fornix microstructure (i.e. volume and diffusion metrics) in controls, but these are further discussed in Chapter 4.

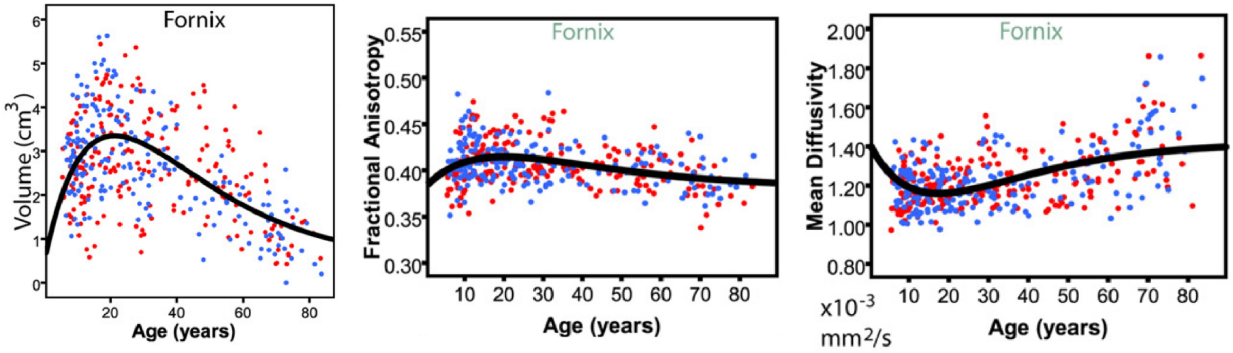

Figure 1.6. Fornix volume (left), FA (middle) and MD (right) relationships with age across 5-83 years in 403 healthy individuals, adapted from Lebel 2012.

1.7 Diffusion Tensor Imaging

Diffusion tensor imaging (DTI) is an MRI technique that has allowed researchers to study the fornix (and other tracts) non-invasively, in-vivo. Although conventional MRI is typically used to clinically diagnose and monitor MS by visualizing inflammatory events over time and in response to treatment, it is unable to detect microstructural WM injury in otherwise NAWM (i.e. normal appearing on conventional MRI but not necessarily normal if measured by other methods), which has been shown to correlate to cognitive dysfunction (Dineen 2009, Valdés Cabrera 2022). One proposed mechanism for cognitive dysfunction in MS asserts that WM injury from demyelination and axonal loss results in disconnections between cortical and subcortical structures involved in cognition. DTI can detect and quantify microscopic pathology

indicative of demyelination and axonal loss in NAWM, as well as virtually identify WM tracts with diffusion tractography to output volume, so it has become a powerful tool for studying demyelinating, inflammatory and neurodegenerative diseases like MS.

1.7.1 MRI Basics

MRI takes advantage of nuclear magnetic resonance (NMR) principles, by imaging water molecules in the body, specifically the hydrogen protons (^1H). This is possible using three distinct steps. First, protons are polarized by applying a strong, uniform magnetic field (B_0), which causes a small surplus of them to align in the direction of the lowest energy state (i.e. parallel to B_0), producing a net equilibrium magnetization vector (M_0) along the longitudinal plane (in equilibrium state $M_z=M_0$). Next, a time-varying excitation radiofrequency (RF) pulse (B_1) is applied at the same frequency as the Larmor frequency (ω_0) of hydrogen (i.e. $\omega_0 = \gamma B_0$ whereby γ is the unique gyromagnetic ratio (MHz/Tesla) of hydrogen and B_0 is the field strength of the scanner in Tesla or T), which disrupts proton alignment and causes M_0 to tip away from B_0 and the longitudinal plane, and into the transverse plane. The rotating net transverse magnetization (M_{xy}) now precesses in the transverse plane at Larmor frequency, which produces a detectable and measurable signal, referred to as the free induction decay (FID), by creating an oscillating magnetic field that induces current in a receiving RF coil. Signal decay occurs when the RF pulse is turned off and excited protons return back to their equilibrium state through T1 and T2 relaxation. T1 relaxation, also called "longitudinal" or "spin-lattice" relaxation, refers to when excited protons return to M_z due to the loss of energy to their surrounding environment, whereas T2 relaxation, also called "transverse" or "spin-spin" relaxation, is the decay of M_{xy} because of gradual dephasing of excited protons perpendicular to B_0. Different MRI sequences

(i.e. flip angles, RF pulses, gradients, time between excitation RF pulses or repetition time (TR), and time between the excitation RF pulse and measurement of the signal or echo time (TE)) yield different image contrast depending on the instrinsic T1 and T2 relaxation times of various tissues. Gradient coils are then used to create linear variations in the magnetic field (i.e. in the X, Y, and Z directions), which are used to encode proton spatial information that a computer console uses to produce the MR image (i.e. through reverse Fourier transform of the signal frequency domain (k-space) to the image domain).

1.7.2 Diffusion MRI

Diffusion MRI is another way to get MR image contrast (i.e. Diffusion Weighted Imaging or DWI) using the diffusion of water molecules within each voxel. Free diffusion is the random motion of molecules (i.e. Brownian) due to thermal energy, and can be described with the following Einstein equation [1], which shows the relationship between the mean squared displacement of water molecules, diffusion coefficient (D) and diffusion time (t).

$$[1] \qquad Displacement^2 = 2Dt$$

That being said, the diffusion of water molecules is hindered by cellular structures in tissues of the body (i.e. by cell membranes), which means that diffusion can sample, or make inferences about cellular micro-structure. This measurement is referred to as the apparent diffusion coefficient (ADC), which will be discussed in greater detail later on. For example, the diffusion of water molecules can have a similar displacement in all directions (i.e. isotropic), which is characteristic of CSF, or it can be directional (i.e. anisotropic), which is characteristic of

WM because of barriers created by myelin and cell membranes that causes water molecules to diffuse further along the length of axons (Beaulieu 2002).

DWI utilizes a pulsed gradient spin echo (PGSE) MRI sequence with "dephasing" and "rephasing" gradients, which was first described by Stejskal-Tanner in 1965 (Stejskal 1965). Below is a basic schematic representation of a PGSE experiment (**Figure 1.7**). At first, protons are aligned with the static magnetic field B_0, producing the net longitudinal magnetization, M_z. Next, a 90° excitation RF pulse is applied, which tips M_z into the transverse plane so that there is a detectable signal (net transverse magnetization, M_{xy}). M_{xy} is then dephased by a diffusion encoding "dephasing" gradient because of the linear variations in the magnetic field created by the gradient, which causes some protons to precess faster/slower than others. A 180° RF pulse is then applied to refocus dephased spins (i.e. from magnetic field inhomogeneities) by flipping M_{xy} 180 degrees around the RF axis. Now, an equal, but opposite diffusion encoding "rephasing" gradient is applied to M_{xy} in order to reverse the dephasing caused by the first gradient. If there is no diffusion, dephasing and rephasing gradients cancel each other out, protons do not accumulate phase, and no signal is lost. However, if there is diffusion, phase accumulates, and there is signal loss.

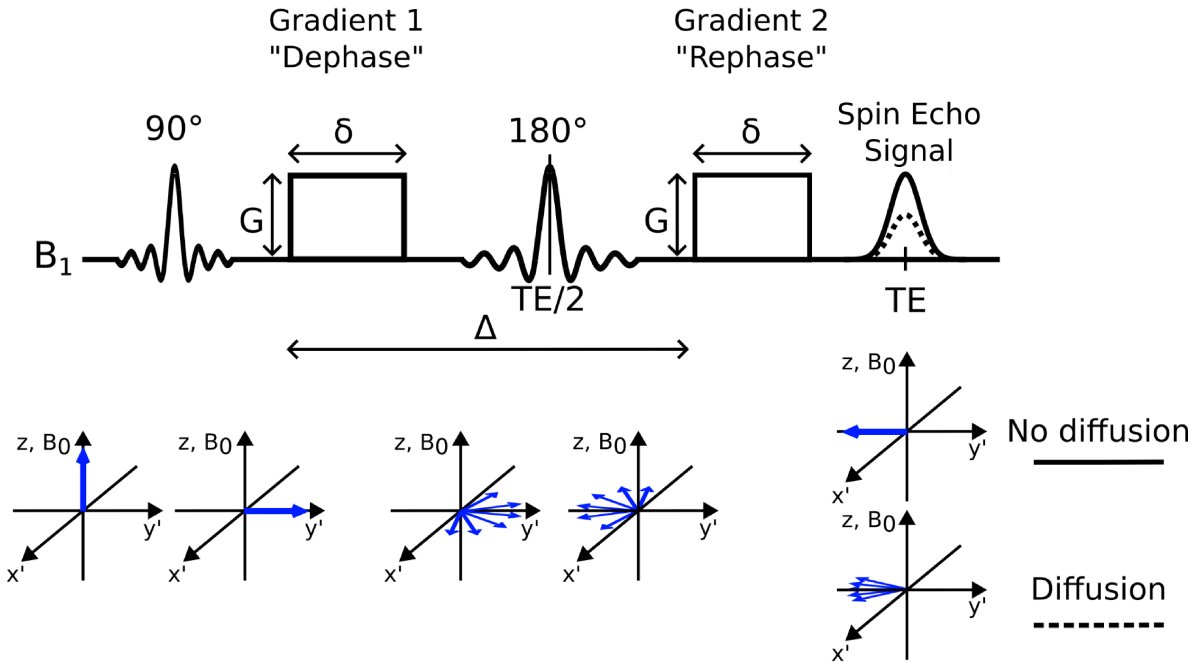

Figure 1.7. PGSE Schematic. M_z tips and becomes M_{xy} using a 90° excitation RF pulse. Proton spins (blue arrows) are dephased by the first gradient, refocussed with a 180° RF pulse, and then rephased with an equal, but opposite second gradient, resulting in a spin echo signal. Spins are shown in the rotating frame of references (‘). G denotes gradient magnitude, δ gradient duration, and Δ the time interval between gradients. T2 relaxation is ignored for simplicity.

The PGSE sequence may be further simplified using the equation [2] introduced by Stejskal and Tanner in 1965 (Stejskal 1965), where the b-value (s/mm^2), defined by Le Bihan in 1986 (Le Bihan 1986), represents diffusion sensitivity of the sequence and is defined in terms of the gyromagnetic ratio of the hydrogen proton (γ), diffusion gradient magnitude (G) and duration (δ), and the time interval between gradients (Δ).

$$[2] \qquad b = \gamma^2 G^2 \delta^2 \left(\Delta - \frac{\delta}{3}\right)$$

Further, signal intensity can be plotted against b-value (minimum two b-values including b=0) to yield the ADC (i.e. the slope) using the equation [3] below.

$$[3] \qquad Signal\ Intensity\ =\ exp(-\ b\ *\ ADC)$$

Essentially, [1] and [3] show that as diffusion gradient magnitude or duration increases, or the time interval between gradients increases, the sequence becomes more sensitive to diffusion (i.e. the b-value increases), and more signal is lost (i.e. less signal intensity or darker) in the DWI. In regards to the brain, areas with a high ADC (i.e. high diffusion), such as CSF, will appear bright on an ADC or mean diffusivity map, but dark on a DWI. The direction of the diffusion gradients is also important as the use of different diffusion gradient directions enables the measurement of diffusion coefficients along various axes. The direction of the diffusion gradient is essentially a snapshot of the diffusion happening in that direction. For example, if the diffusion gradient is aligned along a WM tract, it is most sensitive to the fastest direction of diffusion, so there will be less signal (i.e. appear darker) in the DWI. Diffusion gradient directions are discussed more in Section 1.7.3.

Additionally, a 180^{o} inversion pulse can be applied at the beginning of the PGSE diffusion sequence to obtain fluid-attenuated inversion recovery (FLAIR) (**Figure 1.8**). By implementing a specific inversion time (TI), the signal of CSF will be nulled, as there will be no net transverse magnetization (M_{xy}) for CSF since the 90 degree RF pulse is applied when the longitudinal magnetization (M_z) is zero for CSF. For example, the estimated T1 relaxation value of CSF at 3T (4500 ms) (Bojorquez 2017) and TR (i.e. 9000 ms) can be substituted into equation [4] (Bernstein 2004) to solve for TI of CSF (i.e. approximately 2550 ms, which is consistent with

the actual TI of 2300 ms). Note that a 180º inversion RF pulse is applied inverting the signal ($-M_z$), after which point the magnetization grows in the period TI until it reaches zero.

$$[4] \qquad TI = T1 \times ln\left(\frac{2}{1+e^{-TR/T1}}\right)$$

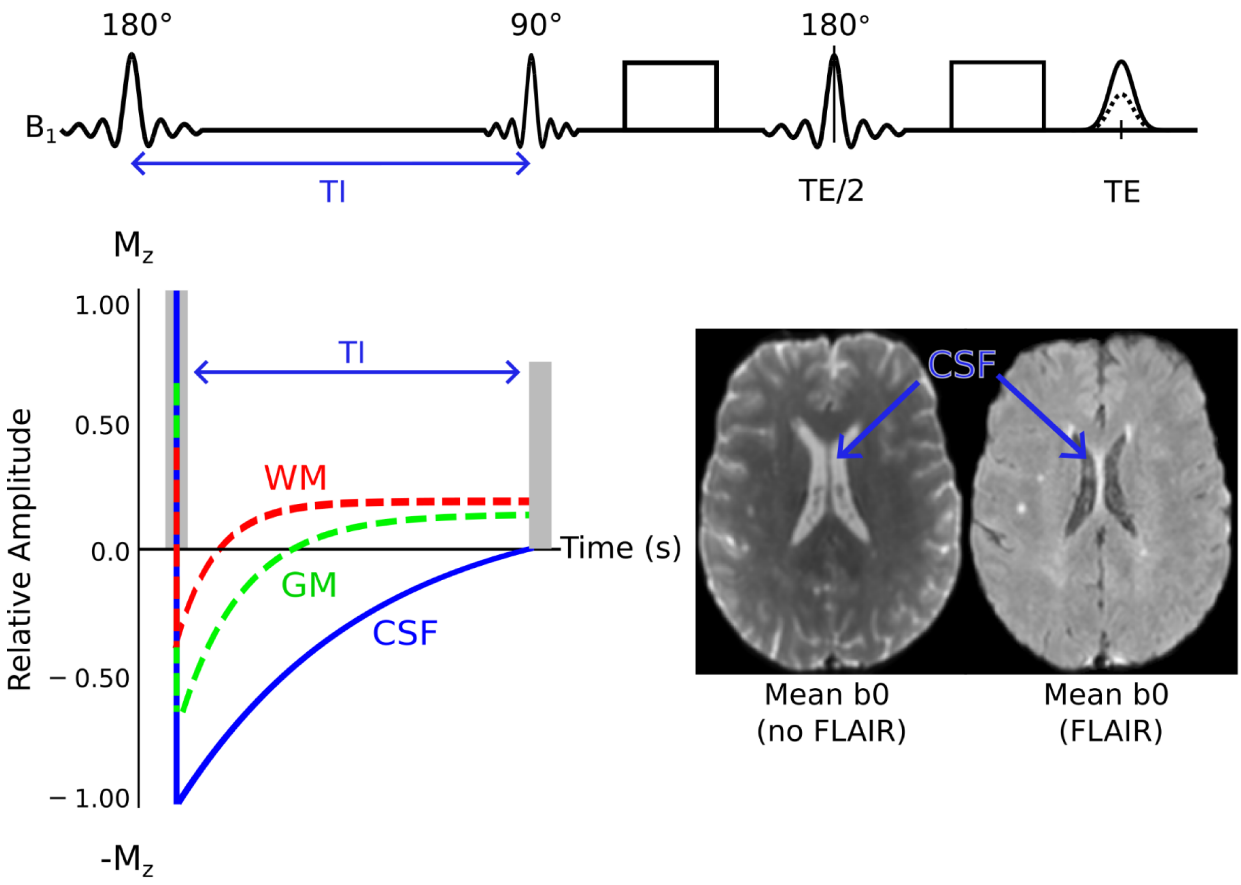

Figure 1.8. PGSE Schematic with FLAIR. PGSE diffusion sequence has an additional 180º inversion pulse at the beginning with an inversion time (TI) that nulls CSF signal (in blue) (i.e. CSF has no net longitudinal magnetization to flip 90º into the transverse plane). T2 relaxation is ignored for simplicity.

It is important to note that shortening TR by reordering slice acquisition and using a non-zero minimum diffusion weighting b-value has also been shown to reduce CSF signal and partial volume effects, and improve fornix tractography and diffusion metrics in healthy controls (Baron 2015), but this method was not achievable in the studies within this thesis.

The downsides of using an inversion recovery pulse before DTI are that it increases the scan time (i.e. by adding TI per slice per b-value/direction), and loses brain signal (i.e. the net longitudinal magnetization M_z for brain tissues does not fully recover to its full value at the TI needed to null CSF). The latter results in lower signal-to-noise ratio (SNR), which must be increased by using more averages and/or more diffusion directions (i.e. SNR is proportional to the square root of the number of averages). FLAIR-DTI is utilized in the remaining chapters to study the fornix because it reduces deleterious partial volume effects that arise due to its location within the ventricles and confounding CSF (Kwong 1991). Partial voluming from CSF occurs because of limitations with voxel size, specifically for voxels near the boundaries of brain tissue and CSF. Since there is not unlimited resolution, voxels near boundaries include both brain tissue and rapid isotropic diffusing CSF, which also contributes to the mean diffusion metrics for that voxel. CSF partial voluming can therefore either be minimized using higher resolution and/or CSF-suppression.

DTI protocols are commonly acquired with single-shot spin-echo-planar imaging (SS-EPI) because the acquisition is quick and reduces artifacts due to subject motion. In SS-EPI, a single excitation pulse is applied, followed by multiple rapidly oscillating gradient echos to acquire an entire slice in a single shot (i.e. samples multiple echos per excitation). Additional 2D slices are acquired by repeating the spin echo diffusion sequence per slice. As an aside, the slice thickness is determined by the slice excitation RF pulse/gradient. The use of SS-EPI to reduce acquisition time is especially needed for diffusion MRI protocols, which can otherwise be quite lengthy due to the application of diffusion gradients that take up additional time (i.e. gradient rise times and time for protons to diffuse). However, acquiring in a single-shot and having a long EPI train of echoes limits the spatial resolution, which is defined by the field-of-view divided by the

matrix (i.e. number of phase encode blips in one axis and number of frequency encode points per echo). Another limitation is that a long echo train increases TE, which leads to signal loss and blurring as the transverse magnetization (M_{xy}) decays during the acquisition. SS-EPI is also accompanied by Eddy current distortions from EPI gradients that are switched on and off rapidly, and the strong diffusion gradients. Eddy currents, or electrical currents, are induced by rapidly changing magnetic fields from imaging gradients (i.e. Faraday's law), which in turn produce time-varying gradients and change the static magnetic field (B_0). Eddy current distortions, and other artifacts from noise, Gibbs ringing, subject motion, and field inhomogeneities can be corrected for using post-processing, which is discussed in Section 2.4. Susceptibility artifacts can also arise, particularly between tissue-air interfaces as a result of differences in magnetic susceptibilities (χ), which alter the static magnetic field (B_0) and Lamor frequency (ω_0). These changes result in spatial mismapping and areas with much higher and lower signal than expected, and distortions.

Encouragingly, shorter acquisition time, less artifacts, and reduced blurring can be achieved using Parallel imaging, and reduces TE due to less data points being acquired, which minimizes SNR loss from T2 relaxation. Parallel imaging can acquire less k-space (i.e. phase encoding steps) by using the data from an array of receiver coils (i.e. standard 64 channel head/neck RF coil has 64 receiver coils). Typically, acquiring less k-space results in less spatial frequencies to construct the image, and subsequent reduced field-of-view and aliasing, however parallel imaging is able to correct for aliasing so that this is not an issue. Specifically, GeneRalized Autocalibrating Partially Parallel Acquisitions (GRAPPA) was used for the DTI protocol in this thesis, which corrects data in the k-space frequency domain before reverse Fourier transform to the image domain. The DTI protocol used in this thesis also did not acquire

full brain coverage, but a "slab" surrounding the fornix region. This reduces the TR and scan time, allowing for the collection of more averages and/or diffusion directions per slice (i.e. increased SNR) because fewer slices are acquired in a given scan time.

1.7.3 Diffusion Tensor Model

The diffusion tensor model can measure the diffusion of water within each voxel (i.e. volume pixel of a MR image) three-dimensionally (Basser 1994), which is important because the diffusion of water in biological tissue will likely not be the same in all directions (i.e. the brain has many fibre directions/orientations). The model describes diffusion tensor, D, which is a symmetric, positively defined matrix that contains (minimum) six diffusion coefficients, each of which measure diffusion along a different principle axis (i.e. x, y, z) or a combination of axes (**Figure 1.9**). Following a mathematical process called eigendecomposition, the diffusion tensor matrix, D, yields three eigenvalues (λ_1, λ_2, λ_3) and three main eigenvectors (ε_1, ε_2, ε_3). The eigenvalues represent magnitude of diffusion (i.e. λ_1 is the diffusion coefficient along/parallel to tracts, and $\lambda_{2,3}$ are the diffusion coefficients across/perpendicular to tracts), and eigenvectors give the direction/axis of diffusion. Together, the eigenvalues and eigenvectors describe a diffusion tensor ellipsoid per each voxel, which may be more or less isotropic/anisotropic. The diffusion coefficient values for each voxel are estimated by applying a minimum of six different diffusion sensitive gradient directions, acquiring each of their DWIs (in addition to the b=0 DWI), and then solving the adapted Stejskal-Tanner equation (Stejskal 1965) [7].

$$[7] \qquad Signal\ Intensity = S_0\, exp(-b_G^T\, D_G)$$

Here, S_0 represents the b0 signal intensity, G is the diffusion sensitive gradient, and D is the diffusion tensor.

Theoretically, more than six diffusion gradient directions could be used and would be able to measure diffusion along more axes, which is especially helpful when there are crossing fibers. Although, a major limitation of the diffusion tensor model is that it assumes just one primary direction or fiber orientation (Tournier 2011) per voxel. Fortunately, for the purpose of this thesis, the fornix is a "stand alone" tract without crossing fibers making the diffusion tensor model appropriate.

$$D = \begin{bmatrix} D_{xx} & D_{xy} & D_{xz} \\ D_{yx} & D_{yy} & D_{yz} \\ D_{zx} & D_{zy} & D_{zz} \end{bmatrix} \qquad \begin{bmatrix} \lambda_1 & 0 & 0 \\ 0 & \lambda_2 & 0 \\ 0 & 0 & \lambda_3 \end{bmatrix} \begin{bmatrix} \varepsilon_{1x} & \varepsilon_{2x} & \varepsilon_{3x} \\ \varepsilon_{1y} & \varepsilon_{2y} & \varepsilon_{3y} \\ \varepsilon_{1z} & \varepsilon_{2z} & \varepsilon_{3z} \end{bmatrix}$$

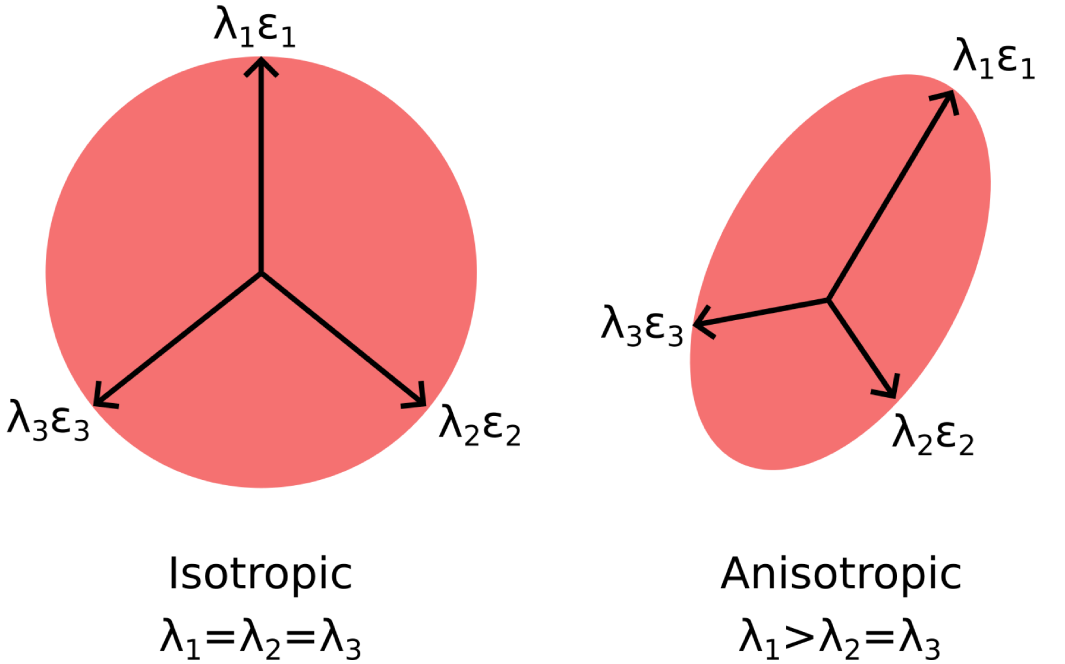

Figure 1.9. Diffusion Tensor Model. Diffusion tensor matrix, D, eigenvalues (λ), and eigenvectors (ε) represented as isotropic and anisotropic diffusion tensor ellipsoids.

1.7.4 DTI Metrics

The diffusion tensor eigenvalues can be used to yield a variety of DTI metrics that may be sensitive to MS pathologies. *Mean Diffusivity (MD)* is derived from equation [5]. MD (mm^2/s) is the average of all three eigenvalues so it represents the overall diffusion of water within a voxel without regard to direction (Concha 2014). Elevated MD can be indicative of more "free" water space due to the loss of membranes (i.e. myelin, axon density) from MS lesions (Filippi 2001, Concha 2014)

$$[5] \qquad MD = \frac{\lambda_1+\lambda_2+\lambda_3}{3}$$

Fractional Anisotropy (FA) is derived from equation [6]. The scalar value of FA for each voxel can vary from 0 (i.e. fully isotropic; the diffusion of water is the same in all directions) to 1 (i.e. fully anisotropic, the diffusion of water is in one direction). The FA value for each voxel of a directionally encoded colour FA map is determined by the primary eigenvector (i.e. fastest diffusion direction) of the voxel, which alters the diffusion ellipsoid (i.e. more isotropic or anisotropic) (Pajevic 1999). Lower FA may be indicative of more "free" water space due to the loss of membranes (i.e. myelin, axon density) from MS lesions (Filippi 2001, Concha 2014).

$$[6] \qquad FA = \sqrt{\frac{1}{2}}\sqrt{\frac{(\lambda_1-\lambda_2)^2+(\lambda_2-\lambda_3)^2+(\lambda_3-\lambda_1)^2}{\sqrt{\lambda_1^2+\lambda_2^2+\lambda_3^2}}}$$

Axial Diffusivity (AD) is denoted by the primary eigenvalue λ_1[7]. AD (mm^2/s) is sensitive to the diffusion of water that is along or parallel to a tract within each voxel, but may be uniquely sensitive to axonal injury (i.e. AD decreases due to axon membrane collapse) or loss (i.e. AD increases due to more extracellular space from MS lesions) (Song 2002, Song 2003, Concha 2006, Klistoner 2018).

$$[7] \qquad AD = \lambda_1$$

Radial Diffusivity (RD) is derived from equation [8]. RD (mm^2/s) is sensitive to the diffusion of water that is across or perpendicular to a tract within each voxel, and may be sensitive to demyelination (i.e. increased diffusion perpendicular axons due to a lack of myelin) (Song 2002, Song 2003, Concha 2006, Klawiter 2011, Klistoner 2018).

$$[8] \qquad RD = \frac{(\lambda_2+\lambda_3)}{2}$$

DTI maps can be constructed (i.e. for MD, FA, AD, and RD) now that the metrics have been calculated for each voxel (**Figure 1.10**).

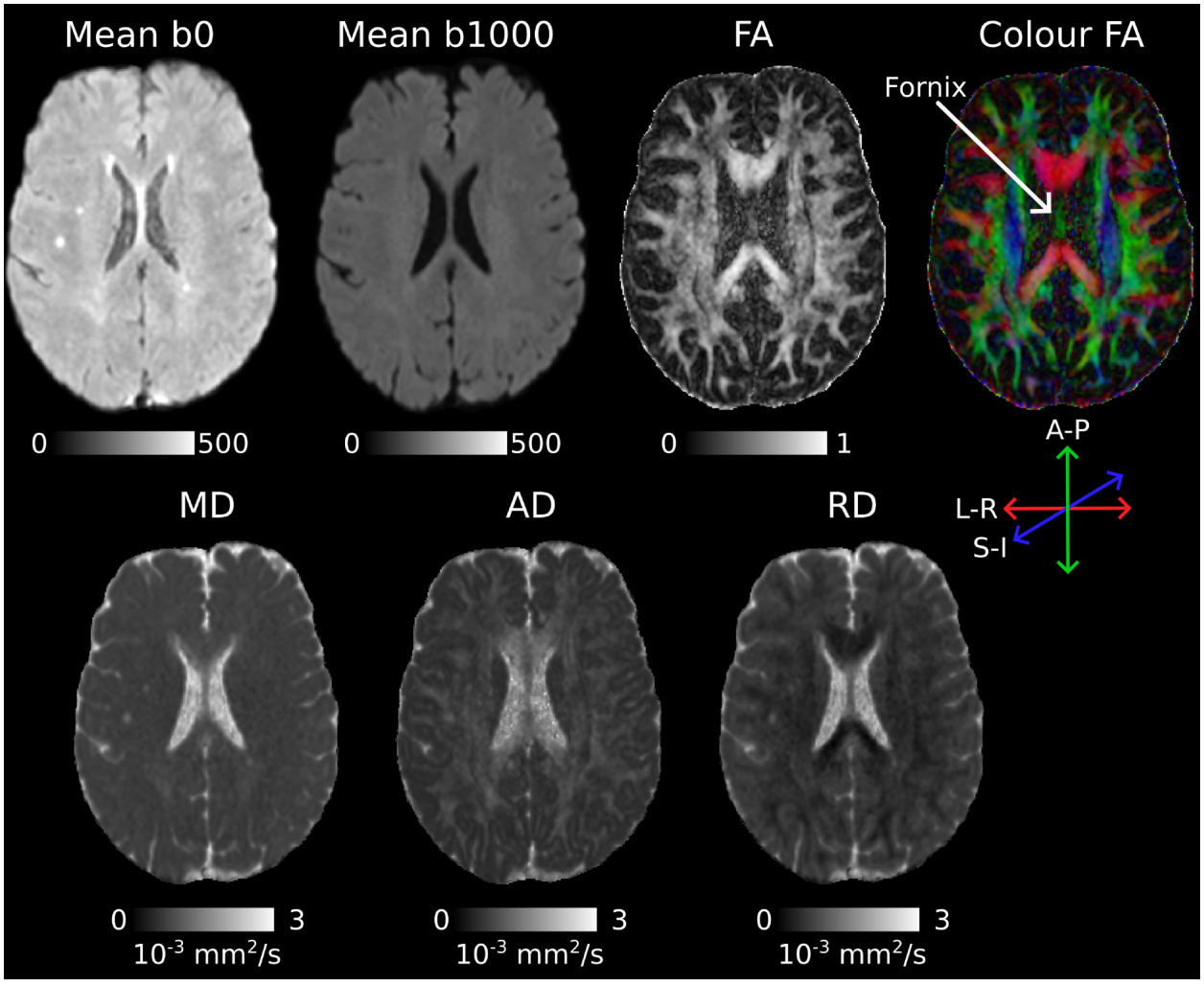

Figure 1.10. DTI Maps. Examples of mean b0 and mean DWI b1000 images, FA, colour FA, MD, AD and RD maps are shown from the FLAIR-DTI protocol. FA highlights anisotropic WM, colour FA shows bright WM tracts colour-coded by fastest diffusion direction (i.e. anterior-poster tracts in green, left-right tracts in red, superior-inferior traits in blue), MD is quite flat across WM and GM, whereas AD and RD better show WM vs GM.

1.7.5 DTI Tractography

Following post-processing, DTI maps may be utilized for DTI tractography in order to further analyze volume and diffusion metrics of individual WM tracts. This involves tracking the fiber orientations (i.e. diffusion ellipsoids) across adjacent voxels using a technique called fiber assignment by continuous tracking (FACT) to obtain a 3D reconstruction of the WM tract (Mori

1999, Tournier 2011). The orientation of the primary eigenvector (ε_1) and associated eigenvalue (λ_1) of each voxel's diffusion ellipsoid represents the dominant fiber orientation within that voxel. The voxels are then connected to adjacent voxels based on the continuation of a similar fiber orientation until there is an abrupt change or certain assigned thresholds are not met (**Figure 1.11**). It is important to note that deterministic tractography was used in the remaining chapters, which assumes only one fiber orientation per voxel (i.e. the primary eigenvector/value from the diffusion tensor model), and utilized thresholds for FA and turning angle between adjacent voxel ellipsoids to determine whether fiber propagation was continued or terminated (thresholds are discussed further in Chapter 2). For example, if a voxel has an FA value below the set threshold or the turning angle between adjacent ellipsoids is too sharp, fiber tracking will terminate (i.e. no longer considered the same streamline or tract). Additionally, the brain was seeded so that only voxels with FA values over a set threshold (i.e. WM) were "seed" regions of interest (ROI), followed by a series of "AND" (i.e. include) and "NOT" (i.e. exclude) ROIs to 3D reconstruct the fornix and eliminate all other unwanted streamlines (see Section 2.4 for an outline of specific steps). As such, tractography requires a deep anatomical understanding of the tracts being analyzed. After 3D reconstruction of the WM tract, volume and average diffusion metrics (i.e. FA, MD, AD, RD) may be obtained from the whole tract.

Tractography has advantages over other diffusion MRI analyses shown in WM like manual ROI placements on 2D slices and voxel-based analyses like TBSS. Tractography can yield a 3D reconstruction of an individual WM tract and therefore output tract volume, and allows for anatomical variation (shape and location) between subjects (i.e. it does not require spatial normalization to a population template brain). Tractography also takes into account directional information in order to distinguish between neighboring tracts (Bach 2014), which

may reduce analysis subjectivity. However, tractography outputs the average diffusion parameters across the entire tract, assuming the same value throughout, which is not the case. Tractography is also limited by set thresholds (i.e. minimum FA, turning angles, tract lengths), which can truncate streamlines prematurely (at MS lesions for example), and therefore requires close observation. There is also user variability, in respect to different preferred processing pipelines and variable understanding of the anatomy of the tract of interest. For example, our lab's previous fornix tractography study in adult MS (Valdés Cabrera 2022) used a larger maximum tract length (500 mm in the previous study) compared to the fornix tractography in this thesis (109 mm), which may have overestimated the fornix in adult MS (included both the fimbria and alveolus) and potentially underestimated the fornix here (included only up to the fimbria). Different tractography algorithms (i.e. deterministic vs probabilistic) further increases variability.

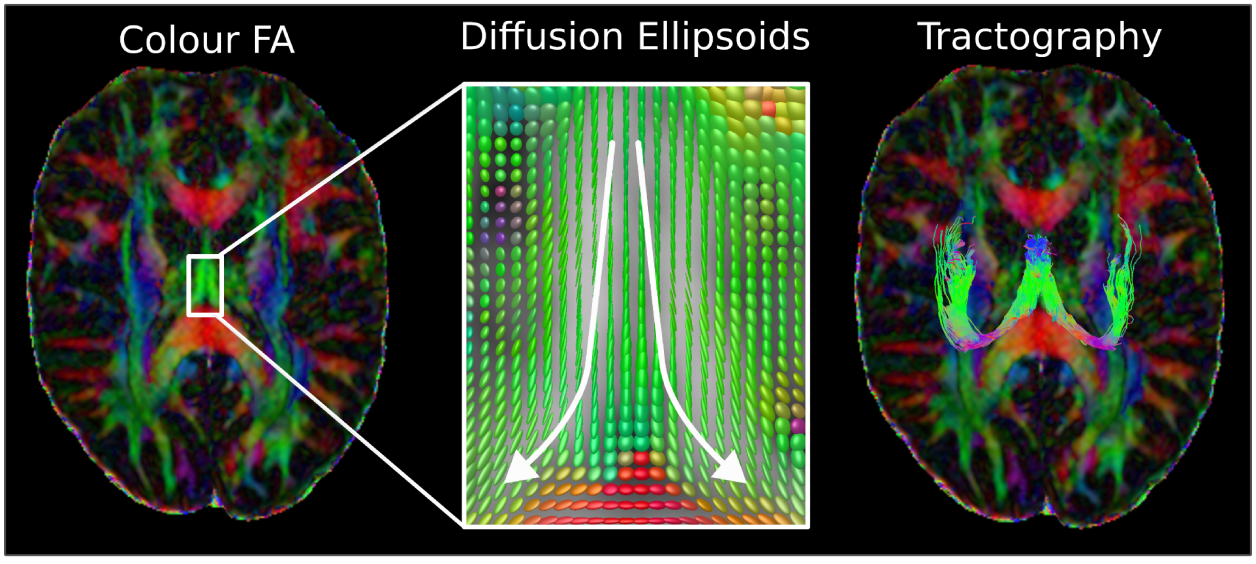

Figure 1.11. Colour FA and Diffusion Ellipsoids (per each voxel) of the fornix. The white box surrounds the fornix in green (anterior-posterior). This is consistent with the zoomed-in diffusion ellipsoids in this region, which are strongly oriented anterior-posterior. Given proper placement of regions of interest (ROIs), a tractography algorithm (i.e. deterministic tractography) will track and 3D reconstruct only fibers that belong to the fornix The white arrows represent two continuous fornix streamlines.

1.8 Thesis Motivation

Quantitative MRI has shown marked volume reductions and abnormal diffusion metrics in pediatric and adult MS NAWM, which are not detectable by conventional MRI and that are associated with physical and cognitive impairments. Although much of the focus has been on major white matter tracts, the fornix has also been implicated in many of the DTI studies mentioned earlier. Previously, our lab improved fornix diffusion tractography by using high-resolution, FLAIR-DTI (Concha 2005), which later showed marked fornix volume/diffusion metric abnormalities that were most affected in MS patients with cognitive impairment, and were greater than losses in other WM and GM volumes in adult MS (Valdés Cabrera 2022). As such, the fornix appears to be an important brain region affected in MS, and also plays an important role in memory and other cognitive functions in healthy aging. However, high-resolution, FLAIR-DTI has not been applied to study the fornix in children/adolescents with POMS, which would provide evidence that the fornix is affected early on in the disease course. Additionally, the fornix has only been studied in MS across ages 32-71 years old compared to controls, not in children/adolescents to elderly subjects, which would provide information about how the fornix is changing over the disease course of MS, relative to the healthy lifespan, especially compared to other total/region brain volumes that have been shown to decline with age in MS.

These applications may improve our understanding of the fornix in regards to its role in disability and disease progression, and the mechanisms of disease in MS. To our knowledge, only one POMS DTI study in children/adolescents mentions the fornix with elevated MD (Blaschek 2013), however it used suboptimal methodology for measuring the fornix and did not report the actual MD value, volume or other diffusion metrics, which is possible using DTI

tractography. Additionally, no studies have analyzed the fornix in MS across the "lifespan" compared to controls (or the healthy lifespan with our lab's improved techniques). It was hypothesized that fornix volume/diffusion metrics in POMS would be affected similarly relative to controls as in the adult MS study using the identical protocol, and that fornix volume/diffusion abnormalities would be shown for MS relative to healthy controls across age.

2. Methods

This chapter provides comprehensive information about the materials and methodologies used in Chapters 3 and 4.

2.1 Participants

This study included 42 participants diagnosed with MS that were recruited from the pediatric neuroinflammatory registry and University of Alberta Neurosciences Clinic, and 103 healthy controls chosen with a similar age/sex distribution from a previous normative study using an identical MRI protocol. There were 16 POMS diagnosed with MS before 18 years of age and 26 AOMS, which together included 34 RRMS, 5 SPMS, 2 PPMS, and 1 benign MS (i.e. RRMS with no attacks or symptoms for several years). The inclusion criteria for the MS cohort was a diagnosis of MS according to the 2017 McDonald criteria. The study excluded those with medical diagnoses other than MS that were expected to impact MRI or cognitive testing or with known clinical relapses at the time of the MRI scan or within 30 days of the study visit. Most (35/42) MS were on disease modifying therapies (rituximab, ocrelizumab, fingolimod, ofatumumab, dimethyl fumarate, interferon beta-1a, and natalizumab), 19/42 MS had diagnosed depression/anxiety and were on various antidepressant medications, and 5/42 MS had diagnosed attention deficit hyperactivity disorder (ADHD) and were taking ADHD medications. All 145 participants provided written informed consent (or parental consent and assent if under 16 years of age) and the study was approved by the University of Alberta Research Ethics Board. It is important to note that the adult MS participants here do not overlap with a previous study from our lab (Valdés Cabrera 2022).

Chapter 3 included 11 child/adolescent POMS (all RRMS) that were recruited from the pediatric neuroinflammatory registry and the University of Alberta Neurosciences Clinic, and 26 healthy controls chosen with a similar age/sex distribution from a previous normative study using an identical MRI protocol. The inclusion criteria for the POMS cohort were as follows: diagnosis of MS according to the 2017 McDonald criteria, disease onset prior to 18 years of age, and under 20 years of age at the time of MRI scan. The exclusion criteria included no POMS participants with medical diagnoses other than MS or with known clinical relapses at the time of the MRI scan or within 30 days of the study visit. All 11 POMS participants were on disease modifying therapies (ocrelizumab, rituximab, and fingolimod). Three POMS participants had diagnosed depression/anxiety and were on various antidepressant medications. Two POMS participants had diagnosed attention deficit hyperactivity disorder (ADHD) and were taking ADHD medications. The demographic and clinical data are summarized in **Table 2.1.**

Chapter 4 included all 42 MS and 103 controls. The demographic and clinical data are summarized in **Table 2.2.**

Table 2.1: Demographics, cognitive/clinical scores, and total lesion volume for age/sex matched controls and POMS with range, mean, and standard deviation.

	Controls (n=26)	**POMS (n=11)**
Sex (M/F)	3/23	1/10
Age (years)	12-20 16.9 +/- 2.2	13 - 19 17.5 +/- 1.9
Time since MS onset (years)	-	1.1 - 8.0 3.2 +/- 2.1
Expanded Disability Status Scale, EDSS	-	0 - 4 1.4 +/- 1.6
Pediatric Fatigue (z-score)	-	-0.3 - 2.2 0.9 +/- 0.9
Beck's Depression Inventory-II, BDI-II	-	3 - 41 14 +/- 13
Symbol Digit Modalities Test, SDMT (z-score)	-	-5.3 - 3.2 -1.1 +/- 2.3
Brief Visuospatial Memory Test-Revised, BVMT-R (total recall) (z-score)	-	-0.5 - 2.6 1.0 +/- 1.1
Total Lesion Volume, TLV (cm^3)	-	0.05 - 51.9 11.7 +/- 15.3

Table 2.2: Demographics, clinical scores, and total lesion volume for age/sex matched controls and MS with range, mean, and standard deviation.

	Controls (n=103)	**MS (n=42)**
Sex (M/F)	27/76	10/32
Age (years)	12 - 65 33 +/- 15	13 - 63 34 +/- 15
Time since MS onset (years)	-	1 - 31 11 +/- 9
Expanded Disability Status Scale, EDSS	-	0.0 - 8.5 3.0 +/- 2.2
Pediatric Fatigue (raw score)	-	12 - 36 23 +/- 8
Modified Fatigue Impact Scale, MFIS	-	9 - 77 43 +/- 18
Beck's Depression Inventory-II, BDI-II	-	1 - 43 15 +/- 11
Symbol Digit Modalities Test, SDMT (raw score)	-	19 - 95 54 +/- 18
Brief Visuospatial Memory Test-Revised, BVMT-R (total recall) (raw score)	-	3 - 34 27 +/- 7
Timed 25-Foot Walk, T25FW (average of 2 trials, seconds)	-	3.1 - 7.8 4.5 +/- 1.1
Nine-Hole Peg Test, 9HPT (average of 4 trials, seconds)	-	16.3 - 43.6 22.8 +/- 5.6
Total Lesion Volume, TLV (cm^3)	-	0.04 - 55.7 12.1 +/- 14.7

EDSS not obtained from one adult RRMS; BDI-II not obtained from one pediatric-onset adult RRMS; BVMT-R not obtained from one adult SPMS; T25FW and 9HPT not obtained from five POMS and 15 adult MS (8 RRMS, 5 SPMS, 2 PPMS)

2.2 Cognitive Assessment

Cognitive and clinical tests were administered by a trained user (author CW) and MS neurologists from the University of Alberta, respectively. Tests included: Expanded Disability Status Scale (EDSS) for overall MS disability, Pediatric Fatigue (Neuro-QOL Item Bank v.2.1) for POMS fatigue, Modified Fatigue Impact Scale (MFIS) for AOMS fatigue, Beck's Depression Inventory-II (BDI-II) for depression, Symbol Digit Modalities Test (SDMT) to measure processing speed, and Brief Visuospatial Memory Test-Revised (BVMT-R) to test visuospatial memory (only total recall score). See Appendix C for the cognitive/clinical test versions used.

Pediatric Fatigue, SDMT, and BVMT-R scores were converted to standardized z-scores in Chapter 3 based on the 2021 Neuro-QOL Scoring Manual (Version 3.0) and pediatric norms (Smerbeck 2011). Cognitive/clinical test scores are summarized in **Table 2.1**

Chapter 4 also included the timed 25-Foot Walk (T25FW) for mobility, and Nine-Hole Peg Test (9HPT) for dexterity, which were implemented partway through the study. Cognitive/clinical test scores are summarized in **Table 2.2**

2.3 MRI Protocol

Participants were scanned on a 3T Siemens Prisma MRI with a 64 channel head/neck RF coil. A whole-brain 3D T1-weighted magnetization-prepared rapid acquisition gradient echo (MPRAGE) was acquired using the following parameters: 0.9 mm isotropic voxels, TR 1800 ms, TE 2.37 ms, and total scan time 3.7 minutes. Whole-brain 3D sampling perfection with application optimized contrasts using different flip angle evolution (SPACE) FLAIR was acquired with 1.2 mm isotropic voxels, TI 1800 ms, TR 5000 ms, TE 385 ms, and total scan time

3.1 minutes. The FLAIR-DTI protocol was the same as used in the previous adult MS study (Valdés Cabrera 2022): 2D SS-EPI, 35 2 mm transverse slices centered for fornix coverage (**Figure 2.1**), 1.2x1.2 mm^2 zero-filled to 0.64x0.64 mm^2 interpolated in-plane resolution, GRAPPA R=2, phase partial Fourier 6/8, TI 2300 ms, TR 9000 ms, TE 70 ms, 5 b=0 and 20 b=1000 s/mm^2, and total scan time 4.2 minutes.

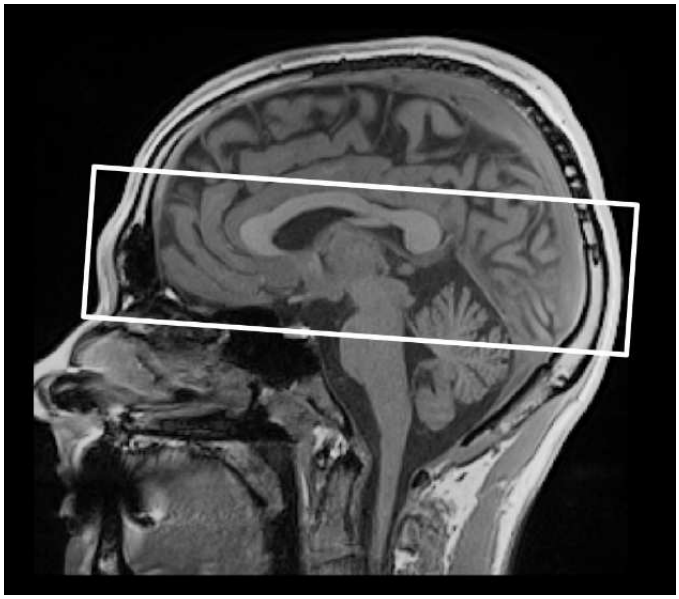

Figure 2.1. Fornix "slab" coverage shown on sagittal MPRAGE. 35 2 mm transverse slices centered for fornix coverage, with the top slice positioned just above the corpus callosum.

The scans below were also acquired in all 42 MS and all 103 controls (except the FLAIR, DIR, and coronal T2), but not analyzed for the purpose of this thesis.

I. HIPPO-DTI slab for hippocampus coverage, acquired over 20 slices with 1 mm^3 isotropic voxels, TR 2900 ms, TE 74 ms, 10 b0 and b=500 s/mm^2 (10 directions, 10 averages), and total scan time 5.5 minutes

II. T2-weighted axial slab for hippocampus coverage, acquired with 0.5x0.5x1 mm^3 voxels, TR 5440 ms, TE 52 ms, and total scan time 4.7 minutes

III. 3D whole-brain DTI, 90 slices acquired with 1.5 mm isotropic voxels (zero-filled in-plane to 0.75x0.75 mm^2), TR 4700 ms, TE 64 ms, 6 b0, 30 b=1000 s/mm^2, 30 b=2000 s/mm2, and total scan time 6 minutes

IV. Whole-brain SPACE Dual Inversion Recovery (DIR), 160 slices acquired with 1.0x1.0x1.2 mm^3 voxels, TR 7500 ms, TE, 327 ms, TI_1 3000 ms, TI_2 450 ms, and total scan time 6.24 minutes

V. T2-weighted Turbo Spin Echo (TSE) coronal slab, 70 slices acquired with 0.5x0.5x1.0 mm^3 voxels, TR 9550 ms, TE 52 ms, and total scan time 7.4 minutes.

Oscillating-gradient spin-echo (OGSE) (TE 108 ms, b400 s/mm^2), Pulsed-gradient spin-echo (PGSE) (TE 90 ms, b400 s/mm^2) and four FWF sequences/scans were also obtained from 32/42 MS partway through the study.

2.4 MRI Analysis

MPRAGE brain volumes and SPACE FLAIR total MS lesion volumes were measured using the volBrain and lesionBrain pipelines, respectively, offered through the online volBrain platform for MRI brain analysis (Manjón 2016, Coupé 2018). The volBrain pipeline denoises MPRAGE images using a non-local means (NLM) filter, corrects for inhomogeneity and registers images to the Montreal Neurological Institute (MNI) space, normalizes image intensity, and then performs non-local intracranial extraction (NICE) to yield intracranial cavity (ICC) masks (i.e. WM, GM, CSF) (Manjón 2016). Mean intensity values are estimated for each tissue, followed by a non-local automatic brain hemispheric segmentation (NA2BS) that segments WM and GM into five regions (i.e. left and right cerebrum, left and right cerebellum, brainstem), and

then a non-local subcortical structure segmentation. The volBrain pipeline yielded segmented total and region brain volumes (cm^3) including: WM, GM, CSF, total brain volume (TBV), cerebrum (total, WM, GM), cerebellum (total, WM, GM), lateral ventricles, caudate, putamen, thalamus, globus pallidus, hippocampus, and amygdala (**Figure 2.2**)

The lesionBrain pipeline processes MPRAGE images as described for the volBrain pipeline (above), but only segments ICC masks, brainstem, cerebellum, and lateral ventricles (Coupé 2018). FLAIR images are denoised using a NLM filter, corrected for inhomogeneity, and normalized for image intensity. Mean and standard deviation GM FLAIR image intensities as well as a MNI lesion atlas are used to estimate lesion thresholds that identify lesion candidates, which are segmented/classified using a rotation-invariant multicontrast version of the NLM, patch-wise NLM, and patch-based ensemble corrector (PEC) for error correction. The lesionBrain pipeline yields segmented lesion location and total lesion volume (TLV) in cm^3. TLV mean values and ranges are shown in **Table 2.1** and **Table 2.2**.

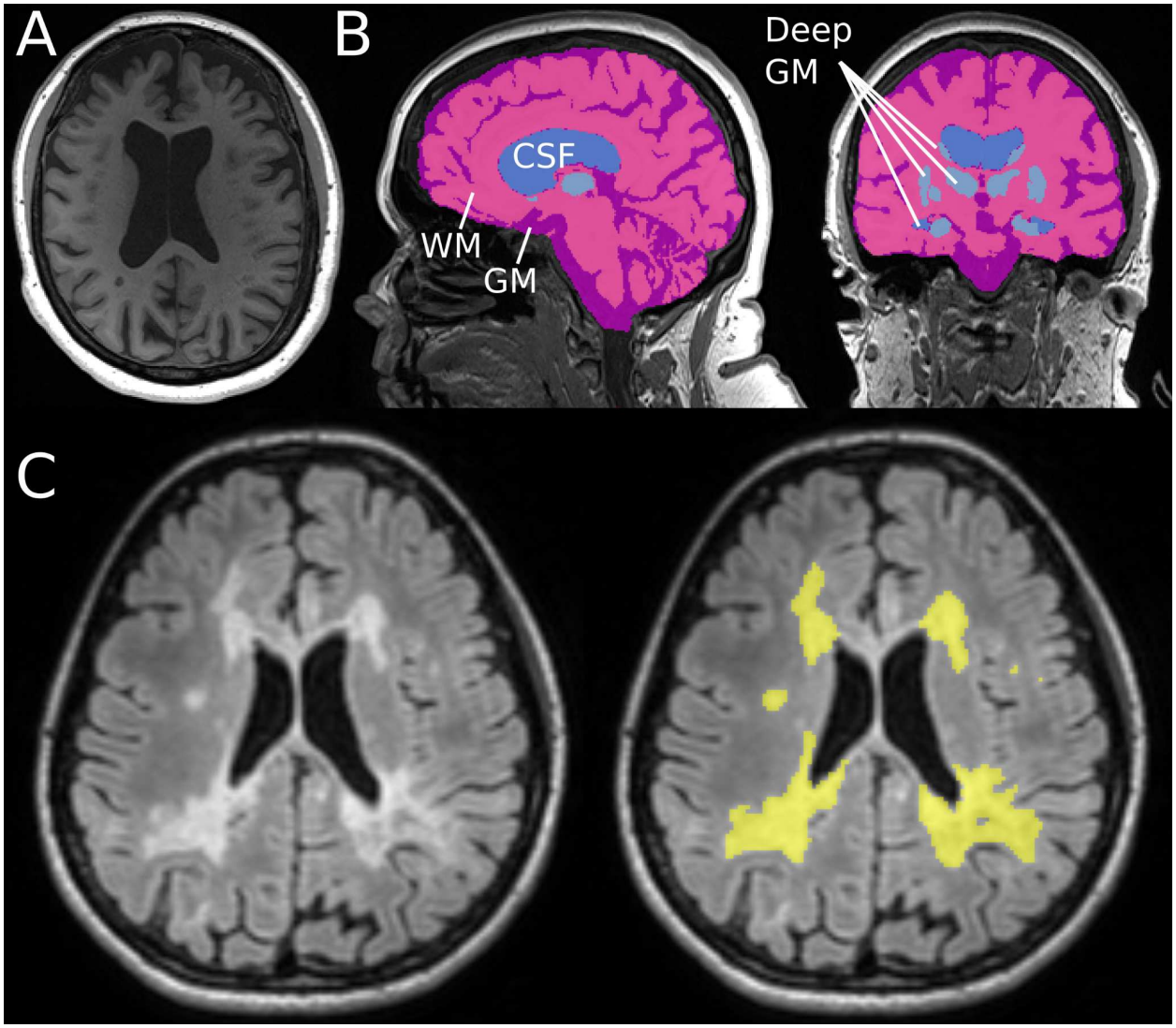

Figure 2.2. volBrain and lesionBrain outputs. (A) Axial MPRAGE submitted to volBrain and (B) WM, GM, CSF and deep GM segmentations from volBrain of 63 year old female AOMS, (C) Example of FLAIR scan showing periventricular lesions (left) and lesionBrain lesion segmentations (right) from 19 year old female POMS.

DTI processing included masking, performed in FSL (v.6.0) (Smith 2002, Jenkinson 2012), as well as denoising (Veraart 2016), Gibbs ringing (Kellner 2016), eddy current and motion (Andersson 2015), bias field correction (Tustison 2010), and tensor fitting (Basser 1994a, Basser 1994b, Westin 1997, Veraart 2013), performed in MRtrix3 (v.2.0) (Tournier 2019).

Deterministic tractography (Mori 1999) of the fornix was performed in MRtrix3 similar to previously published lab protocols (Valdés Cabrera 2022) using: FA threshold 0.15, maximum turning angle 65^{o}, step size 0.64 mm, minimum fiber length 10 mm, and maximum fiber length of 109 mm (i.e. MRtrix3 default, geometric mean of interpolated voxel size times 100). ROIs were placed as follows (**Figure 2.3**): coronal AND ROI in the fornix body (**Figure 2.3A**), axial NOT ROI to remove tracts superior the fornix (**Figure 2.3B**), coronal NOT ROI to remove tracts anterior the fornix columns (**Figure 2.3C**), coronal NOT ROI to remove tracts posterior the fornix crura (**Figure 2.3D**), other NOT ROIs as needed to remove all remaining unwanted streamlines not attributable to the fornix. The final tract (**Figure 2.4**) yielded the whole fornix volume, as well as average FA, MD, AD and RD with left and right sides combined to limit comparisons. There were no indications of left/right differences in MS or controls. The intraclass correlation coefficient (ICC) (used to measure intra-rater reliability) for whole fornix tract volume was 0.97 as measured in four subjects (two controls and two MS).

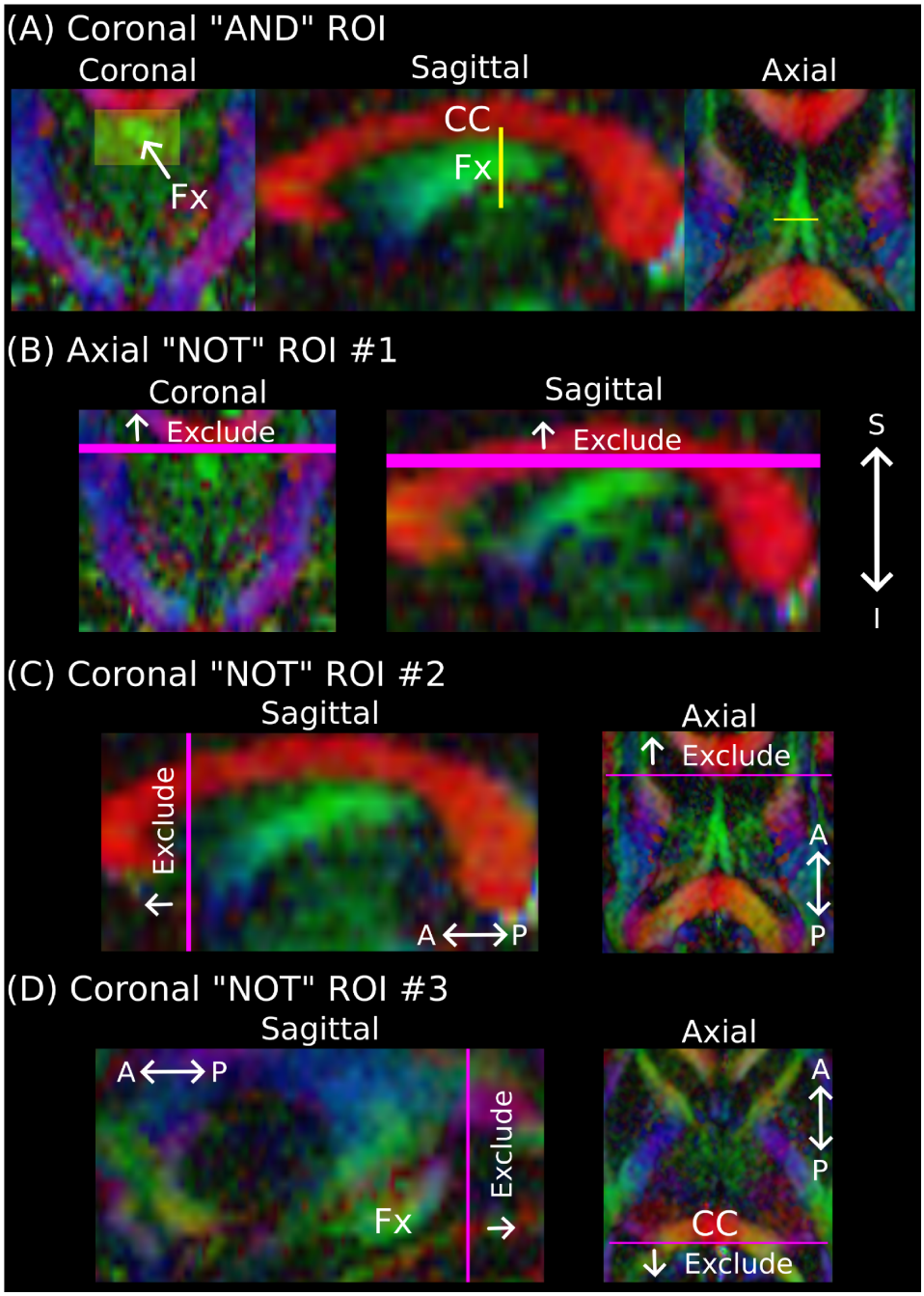

Figure 2.3. Fornix Tractography ROIs displayed on colour FA map. (A) Coronal "AND" ROI (yellow) to surround the fornix (fx) body in green to include it, (B) Axial "NOT" ROI (pink) to exclude tracts superior to the fornix including the corpus callosum (CC) in red (i.e. ROI covers entire axial slice above fornix, not shown), (C) Coronal "NOT" ROI (pink) to exclude tracts anterior to the fornix (i.e. ROI covers coronal slice directly before the fornix, not shown), and (D) Coronal "NOT" ROI (pink) to exclude tracts posterior to the fornix (i.e. ROI covers coronal slice directly after the fornix, not shown). Note that the superior-inferior axis is denoted by S-I, and the anterior-posterior axis is denoted by A-P.

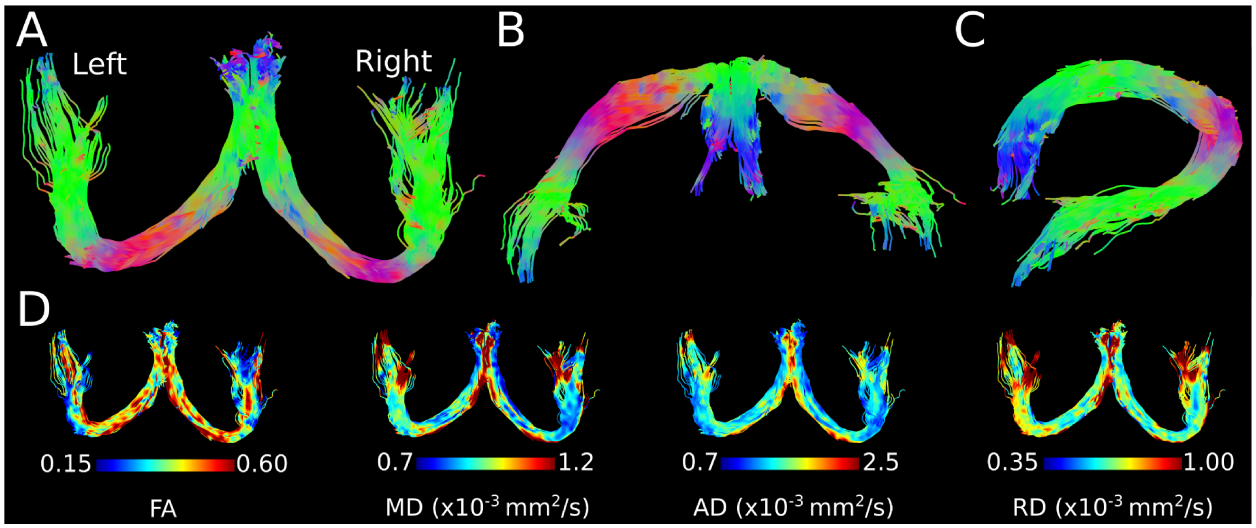

Figure 2.4. Example of the whole fornix tractography in a 19 year old male healthy control. Fornix shown in the (A) axial, (B) coronal and (C) sagittal plane colour coded by direction (i.e. anterior-posterior in green; superior-inferior in blue; left-right in red). (D) Fornix shown in the axial plane colour coded by FA, MD, AD, and RD, respectively. Note that the colour scales differ between MD, AD, and RD.

3. Disproportional Smaller Fornix with Altered Microstructure in Pediatric Multiple Sclerosis Shown by High-Resolution Fluid-Suppressed Diffusion Tractography[1]

3.1 Abstract

Background: Diffusion tensor imaging (DTI) in adults with multiple sclerosis (MS) has identified marked volume and diffusion abnormalities of the fornix, the main white matter (WM) output tract of the hippocampus.

Objective: To determine if the fornix is affected in pediatric-onset MS (POMS) using the same DTI protocols used in adult-onset MS (AOMS), which would suggest its early involvement in the disease course.

Methods: High-resolution, fluid-suppressed diffusion tractography was used to identify the fornix in 11 POMS patients (13-19 years old) and 26 controls. Fornix volume and diffusion metrics were compared between groups and with other total/regional brain volumes, and then correlated with cognitive/clinical scores.

Results: POMS showed lower fornix volumes (-26%) compared to controls, which was greater than proportional losses in total and other regional brain volumes. Notably, the hippocampus volume was not lower in POMS. DTI yielded lower fractional anisotropy (-7%) and higher mean

[1] A version of Chapter 3 of this thesis was presented at the 2024 International Society for Magnetic Resonance in Medicine (ISMRM) Annual Meeting in Singapore as Weber C, Wilbur C, Beaulieu C "High-resolution Fluid-Suppressed Diffusion Tractography Shows Altered Fornix Volume and Diffusion Metrics in Pediatric Multiple Sclerosis" (Abstract #0117). Chapter 3 of this thesis has been submitted for publication as Weber C, Wilbur C, Blevins G, Beaulieu C "Disproportional Smaller Fornix with Altered Microstructure in Pediatric Multiple Sclerosis Shown by High-Resolution Fluid-Suppressed Diffusion Tractography."

(12%), axial (7%), and radial (16%) diffusivities in POMS. There were no significant correlations between fornix volume/diffusion metrics and cognitive/clinical scores.

Conclusion: Diffusion tractography showed marked injury to the fornix in POMS that precedes injury to connected gray matter such as hippocampus, implicating the fornix as an early brain region affected in MS.

3.2 Introduction

Pediatric-onset multiple sclerosis (POMS) accounts for up to 5% of MS cases and is characterized by disease onset and high clinical and radiographic disease activity during childhood and adolescence (Bigi 2012) It was shown that within just 2 years of MS onset, approximately 30% of children and adolescents with MS become cognitively impaired. Like adult-onset MS (AOMS), POMS has shown widespread gray matter (GM) atrophy across most cortical and subcortical regions that appear to worsen over time (De Meo 2019). Early and disproportionate thalamic atrophy has also been reported in POMS, particularly at the ventricular interface, presumably due to soluble MS inflammatory factors in the cerebrospinal fluid (CSF) (Fadda 2019). Thalamic and other GM atrophy in POMS have been shown to correlate with various measures of disability (i.e. Expanded Disability Status Scale, EDSS) and cognition (i.e. episodic memory performance) (De Meo 2019, Fabri 2021). POMS also showed deviations from sex- and age-expected developmental trajectories of hippocampus volume (De Meo 2019) Other POMS studies have shown hippocampal atrophy relative to controls, but there is inconsistency on whether it is associated with cognitive impairment (Rocca 2016a, Fabri 2021).

Beyond GM, cognitive impairment in MS may result from injury to normal-appearing WM (NAWM) from demyelination and axonal loss leading to disconnections between cortical and subcortical structures (Dineen 2009). Diffusion tensor imaging (DTI) can detect changes indicative of demyelination and/or axonal injury in NAWM, as well as virtually identify WM tracts with diffusion tractography. DTI has shown reduced tract volumes and altered diffusion metrics in NAWM in adults with MS compared to controls, which are associated with physical and cognitive impairment, such as the fornix which is the main efferent tract of the hippocampus (Fink 2010, Syc 2013, Kern 2015, Welton 2015, Keser 2017, Huang 2018, Valdés Cabrera 2020) The fornix plays an important role in episodic memory and other cognitive functions (Douet 2014a). The fornix is a small, curved WM tract located within the lateral ventricles making it prone to diffusion tractography errors due to partial volume effects from rapid, isotropic diffusing CSF, which contributes to the diffusion parameters per voxel; however, tractography and output diffusion metrics can be improved using high-resolution fluid-attenuated inversion recovery (FLAIR) DTI, which suppresses the confounding CSF (Concha 2005). FLAIR-DTI has shown marked volume and diffusion abnormalities of the fornix in adults with MS compared to controls, including lower tract volume and fractional anisotropy (FA) and higher mean (MD), axial (AD), and radial (RD) diffusivities, which were most affected in those with cognitive impairment and greater than losses in other WM and GM volumes (Valdés Cabrera 2022).

DTI metrics are altered in POMS in most NAWM, including major tracts like the corpus callosum, posterior limb of the internal capsule, cerebral peduncle, and long association fibers (i.e. superior longitudinal, inferior fronto-occipital, and uncinate fasciculus) (Vishwas 2013). Relative to controls, DTI metrics in POMS NAWM appear to worsen over time and fail to reach age-expected maturation (Longoni 2017). Additionally, these abnormal DTI metrics are apparent

even in very early-onset POMS (<12 years of age), which may suggest early NAWM injury in MS (Rocca 2016b). However, there is only one POMS DTI study that has mentioned the fornix region (Blaschek 2013), namely reporting elevated MD, but it used low spatial resolution DTI protocols (voxel volume > 12 mm^3) and a voxel-based analysis not ideal for measuring the fornix and which does not yield tract volume (Bach 2014). FLAIR-DTI tractography has not been applied to study the fornix in POMS, and comparison to adults with MS previously studied using the exact same protocol would examine whether it is involved early in the disease course of MS.

The purpose of this study was to: (i) determine if the fornix (volume and diffusion metrics) is affected in POMS using CSF-suppressed, high-resolution FLAIR-DTI tractography, (ii) evaluate other brain volumes (e.g. hippocampus) to determine if fornix injury precedes GM atrophy, and (iii) assess correlations between fornix volume/diffusion metrics, and clinical disability/cognitive function.

3.3 Materials and Methods

3.3.1 Participants

This study was approved by the University of Alberta Human Research Ethics Board. All 37 participants provided written informed consent (or parental consent and assent if under 16 years of age) including 11 diagnosed with relapsing-remitting POMS that were recruited from the pediatric neuroinflammatory registry and the University of Alberta Neurosciences Clinic, and 26 healthy controls chosen with a similar age/sex distribution from a previous normative study using an identical MRI protocol. The inclusion criteria for the POMS cohort were as follows: diagnosis of MS according to the 2017 McDonald criteria, disease onset prior to 18 years of age,

and under 20 years of age at the time of MRI scan. The exclusion criteria included no POMS participants with medical diagnoses other than MS or with known clinical relapses at the time of the MRI scan or within 30 days of the study visit. All 11 POMS participants were on disease modifying therapies (ocrelizumab, rituximab, and fingolimod). Three POMS participants had diagnosed depression/anxiety and were on various antidepressant medications. Two POMS participants had diagnosed attention deficit hyperactivity disorder (ADHD) and were taking ADHD medications. The demographic and clinical data are summarized in **Table 3.1.**

3.3.2 Cognitive Assessment

Cognitive and clinical tests were administered by a trained user and MS neurologists from the University of Alberta, respectively. Tests included: Expanded Disability Status Scale (EDSS) for overall MS disability, Pediatric Fatigue (Neuro-QOL Item Bank v.2.1) for fatigue, Beck's Depression Inventory-II (BDI-II) for depression, Symbol Digit Modalities Test (SDMT) to measure processing speed, and Brief Visuospatial Memory Test-Revised (BVMT-R) to test visuospatial memory (only total recall score). Pediatric Fatigue, SDMT, and BVMT-R scores were converted to standardized z-scores based on the 2021 Neuro-QOL Scoring Manual (Version 3.0) and pediatric norms (Smerbeck 2011). Cognitive/clinical test scores are summarized in **Table 3.1.**

Table 3.1: Demographics, cognitive/clinical scores, and total lesion volume for age/sex matched controls and POMS with range, mean, and standard deviation.

	Controls (n=26)	**POMS (n=11)**
Sex (M/F)	3/23	1/10
Age (years)	12-20 16.9 +/- 2.2	13 - 19 17.5 +/- 1.9
Time since MS onset (years)	-	1.1 - 8.0 3.2 +/- 2.1
Expanded Disability Status Scale, EDSS	-	0 - 4 1.4 +/- 1.6
Pediatric Fatigue (z-score)	-	-0.3 - 2.2 0.9 +/- 0.9
Beck's Depression Inventory-II, BDI-II	-	3 - 41 14 +/- 13
Symbol Digit Modalities Test, SDMT (z-score)	-	-5.3 - 3.2 -1.1 +/- 2.3
Brief Visuospatial Memory Test-Revised, BVMT-R (total recall) (z-score)	-	-0.5 - 2.6 1.0 +/- 1.1
Total Lesion Volume, TLV (cm^3)	-	0.05 - 51.9 11.7 +/- 15.3

3.3.3 MRI Protocol

Participants were scanned on a 3T Siemens Prisma MRI with a 64-channel head/neck radiofrequency coil. A whole-brain 3D T1-weighted magnetization-prepared rapid acquisition gradient echo (MPRAGE) was acquired using the following parameters: 0.9 mm isotropic voxels, TR 1800 ms, TE 2.37 ms, and total scan time 3.4 minutes. Whole-brain 3D sampling perfection with application optimized contrasts using different flip angle evolution (SPACE) FLAIR was acquired with 1.2 mm isotropic voxels, TI 1800 ms, TR 5000 ms, TE 385 ms, and total scan time 3.1 minutes. The FLAIR-DTI protocol was the same as used in a previous adult MS study here (Valdés Cabrera 2022): 2D single-shot echo-planar imaging, 35 2 mm transverse slices centered for fornix coverage, 1.2x1.2 mm^2 zero-filled to 0.64x0.64 mm^2 in-plane resolution, GRAPPA R=2, phase partial Fourier 6/8, TI 2300 ms, TR 9000 ms, TE 70 ms, 5 b=0 and 20 b=1000 s/mm^2, and total scan time 4.1 minutes.

3.3.4 MRI Analysis

MPRAGE brain volumes and SPACE FLAIR total MS lesion volumes were measured using the volBrain and lesionBrain pipelines, respectively, offered through the online volBrain platform for MRI brain analysis (Manjón 2016, Coupé 2018). The volBrain pipeline yielded segmented total and regional brain volumes including: WM, GM, CSF, cerebrum (total, WM, GM), cerebellum (total, WM, GM), lateral ventricles, caudate, putamen, thalamus, globus pallidus, hippocampus, and amygdala. Left and right hemispheres were combined to limit comparisons and yielded 16 volumes per participant. The lesionBrain pipeline yielded segmented total lesion volume (TLV).

DTI processing was performed in MRtrix3 (v.2.0) including denoising, Gibbs ringing, eddy current and motion, bias field correction, and tensor fitting (Tournier 2019). Deterministic tractography of the fornix was performed in MRtrix3 similar to previously published lab protocols using (Valdés Cabrera 2022): FA threshold 0.15, maximum turning angle 65^{o}, step size 0.64 mm, minimum fiber length 10 mm, and maximum fiber length of 109 mm (i.e. MRtrix3 default, geometric mean of interpolated voxel size times 100). Regions of interest (ROIs) were placed as follows: coronal AND ROI in the fornix body, axial NOT ROI to remove tracts superior to the fornix, coronal NOT ROI to remove tracts anterior to the fornix columns, coronal NOT ROI to remove tracts posterior to the fornix crura, and other NOT ROIs as needed to remove all remaining streamlines not attributable to the fornix. This tract yielded the whole fornix volume, as well as average FA, MD, AD and RD across left and right sides.

3.3.5 Statistical Analysis

Fornix volume, FA, MD, AD and RD for POMS and controls were tested for normality, and then metrics were assessed with two-sample independent t-tests to test for differences between POMS and controls. Regional brain volumes for POMS and controls were also tested for normality and then evaluated using two-sample independent t-tests to test for group differences. Pearson correlations were used to assess linear relationships between fornix volume/diffusion metrics and clinical/cognitive scores, i.e. time since MS onset, EDSS, TLV, Pediatric Fatigue, BDI-II, SDMT, and BVMT-R. Multiple comparisons (FDR) were conducted for group comparisons and Pearson correlations; FDR corrected p-values are presented (*$p<0.05$).

3.4 Results

CSF-suppressed, high-resolution FLAIR-DTI tractography depicted the full fornix in all 11 POMS and 26 controls. Fornix tractography showed visibly thinner fornix with bilateral regions of lower FA and elevated diffusivities (MD, AD, and particularly RD) in POMS relative to controls (**Figure 3.1**). These tractography observations were similar across all 11 POMS fornix and 11 representative age/sex matched controls, as shown on the tracts color-coded for MD (**Figure 3.2**).

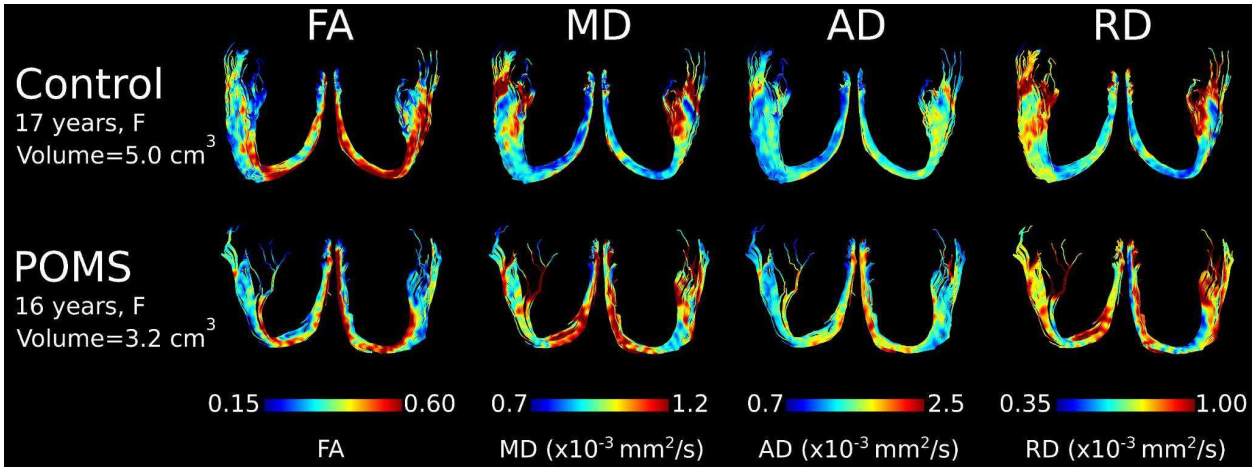

Figure 3.1: Examples of CSF-suppressed, high-resolution FLAIR-DTI fornix tractography (as seen from superior view) colour-coded by FA, MD, AD and RD in a 17 year old female control and a 16 year old POMS participant. In this case, the POMS fornix appears thinner with markedly smaller volume (-36%) and shows bilateral regions with lower FA (-9%), and higher MD (14%), AD (9%), and RD (18%).

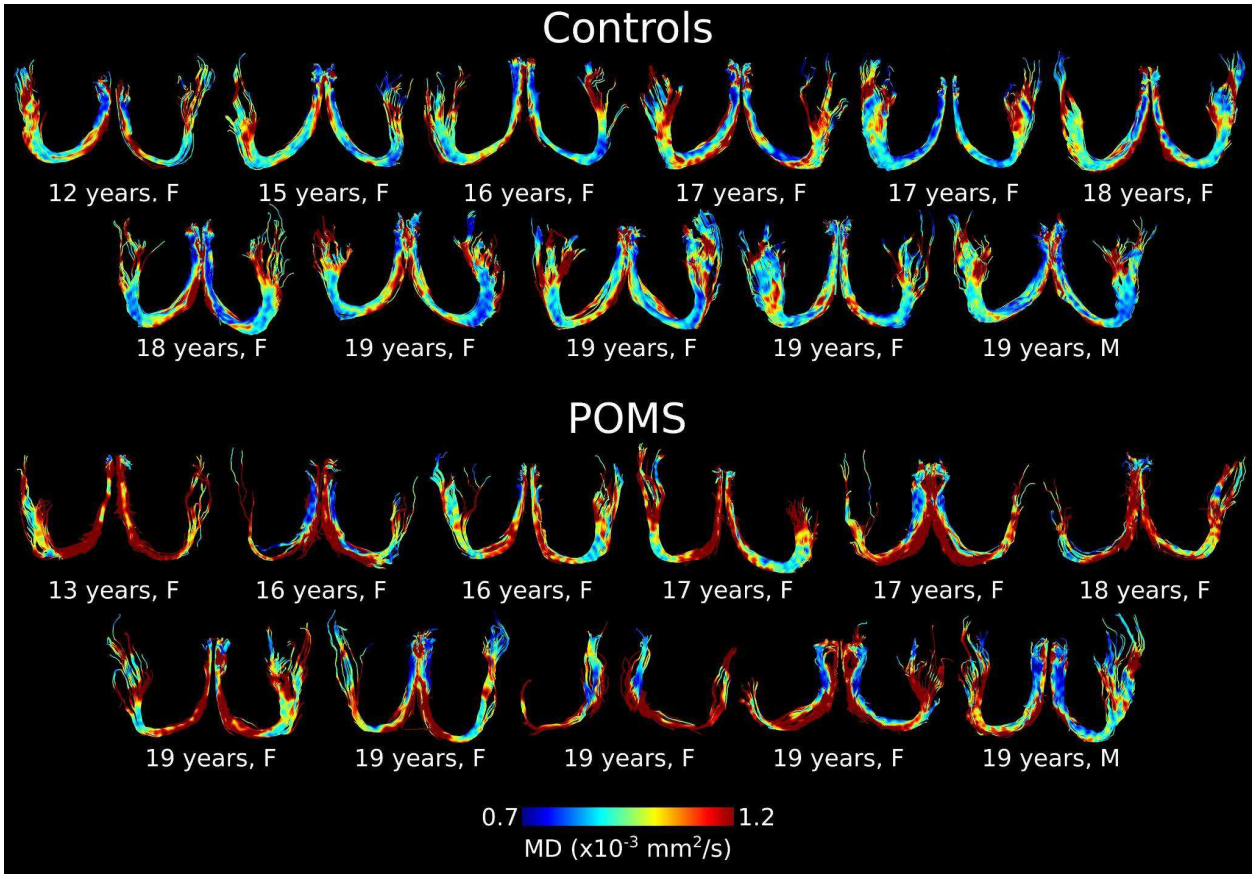

Figure 3.2: Examples of CSF-suppressed, high-resolution FLAIR-DTI fornix tractography (as seen from superior view) colour-coded by MD in 11 representative age/sex matched controls and all 11 POMS, ordered by age. Fornix tractography depicted the full fornix in all, but the fornix in POMS appeared thinner compared to controls, and showed bilateral regions with higher MD.

Relative to controls, the POMS had a fornix with 26% lower volume (4.6 +/- 1.1 vs 3.4 +/- 0.9 cm^3, p=0.003), 7% lower FA (0.43 +/- 0.02 vs 0.40 +/- 0.03, p<0.001), 12% higher MD (1.06 +/- 0.05 vs 1.19 +/- 0.07 $x10^{-3}$ mm^2/s, p<0.001), 7% higher AD (1.61 +/- 0.06 vs 1.72 +/- 0.08 $x10^{-3}$ mm^2/s, p<0.001), and 16% higher RD (0.79 +/- 0.05 vs 0.92 +/- 0.08 $x10^{-3}$ mm^2/s, p<0.001) **(Figure 3.3)**. In contrast, hippocampus volume was not different between POMS and controls (p=0.551).

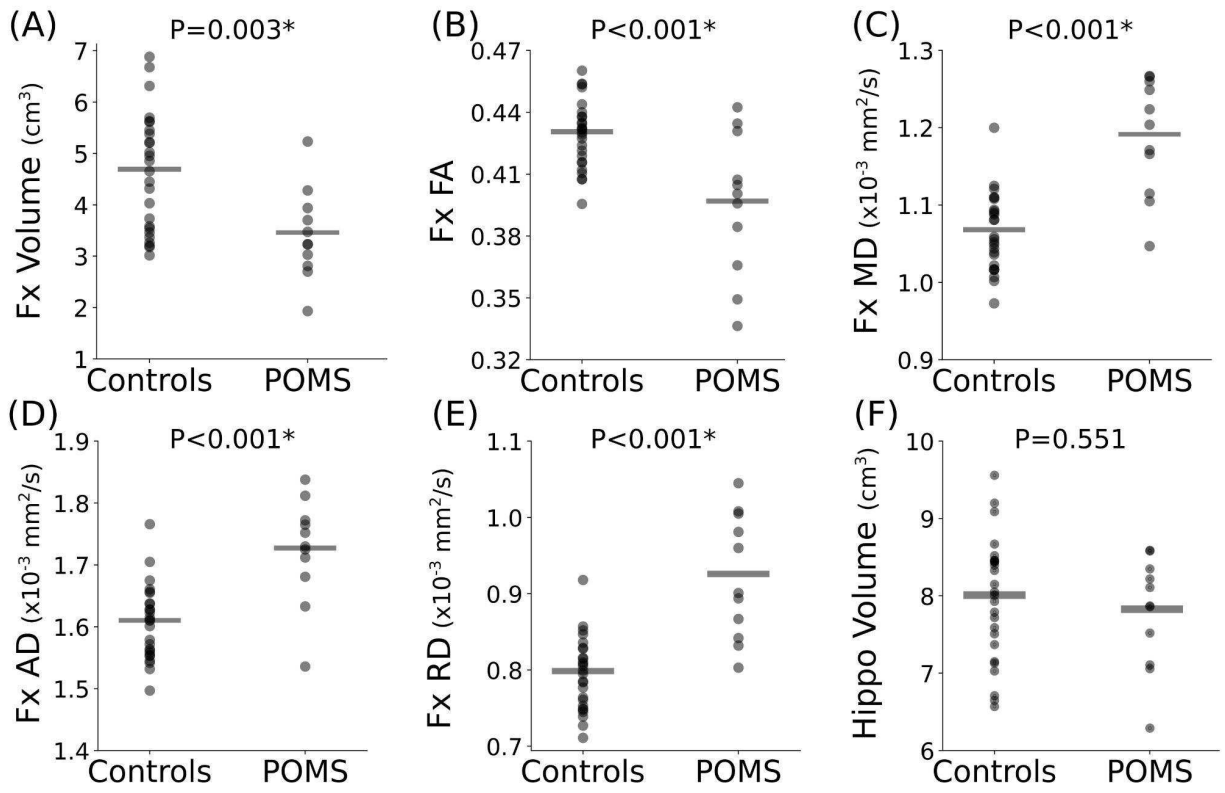

Figure 3.3: Group comparisons of controls (n=26) and POMS (n=11) are shown for fornix (Fx) (A) volume, (B) FA, (C) MD, (D) AD and (E) RD as well as (F) hippocampus (hippo) volume. POMS showed a smaller volume (-26%) compared to controls as the largest change in the fornix, in addition to significant differences in FA (-7% lower), MD (12% higher), AD (7% higher), and RD (16% higher). Hippocampus volume was not significantly different between groups.

Relative to controls, POMS had many volume differences with the greatest proportional changes in the lateral ventricles (+56%) and CSF (+41%) volumes (**Table 3.2**). For brain subregions, the greatest volume losses in order were the thalamus (-23%), cerebellum WM (-23%), total WM (-17%), globus pallidus (-16%), cerebrum WM (-16%), putamen (-12%), total cerebellum (-9%), and then total cerebrum (-8%). These differences were not as great as the fornix which was proportionally smaller (-26%). Notably, there were no differences in the volumes of other GM, including total GM, cerebrum GM (i.e. cortex), cerebellum GM, caudate, or amygdala.

Table 3.2: Total/regional left + right WM/GM volumes (cm^3) derived from the 3D T1-weighted images with group comparisons for age/sex matched controls versus POMS with mean, standard deviation, percentage difference, and FDR corrected p-values (*p<0.05; n.s. is non-significant).

Volumes (cm^3)	**Controls (n=26)**	**POMS (n=11)**	**Difference (%)**	
Lateral Ventricles	9.4 +/- 6.0	14.7 +/- 5.3	+56	p=0.025*
CSF	142 +/- 36	200 +/- 52	+41	p=0.001*
Thalamus	13.1 +/- 1.0	10.1 +/- 2.0	-23	p<0.001*
WM (total)	538 +/- 47	448 +/- 84	-17	p=0.001*
Globus Pallidus	2.5+/- 0.3	2.1 +/- 0.4	-16	p=0.008*
Putamen	9.3 +/- 0.9	8.2 +/- 1.1	-12	p=0.005*
Cerebellum WM GM	149 +/- 16 40 +/- 6 110 +/- 14	135 +/- 16 31 +/- 8 104 +/- 12	-9 -23 n.s.	p=0.025* p=0.003* p=0.302
Cerebrum WM GM (cortex)	1135 +/- 81 478 +/- 41 657 +/- 50	1046 +/- 111 400 +/- 73 647 +/- 45	-8 -16 n.s.	p=0.022* p=0.001* p=0.559
GM (total)	770 +/- 60	755 +/- 47	n.s.	p=0.551
Caudate	8.2 +/- 1.0	7.5 +/- 1.3	n.s.	p=0.094
Hippocampus	8.0 +/- 0.8	7.8 +/- 0.7	n.s.	p=0.551
Amygdala	1.6 +/- 0.3	1.6 +/- 0.3	n.s.	p=0.551

Within the POMS cohort, Pearson correlations (uncorrected) were only found for SDMT vs fornix MD (R=-0.60, p=0.049), SDMT vs fornix RD (R=-0.61, p=0.048), and TLV vs fornix FA (R=-0.63, p=0.040); however, none were significant after FDR-correction. There were also no significant correlations between fornix volume or diffusion metrics and age, time since MS onset, EDSS, Pediatric Fatigue, BDI-II, or BVMT-R.

3.5 Discussion

High-resolution FLAIR-DTI tractography enabled the virtual identification and quantification of the fornix in POMS (age range of 13-19 years), which showed markedly lower volume that was affected more than any other brain region assessed in this study, as well as diffusion metric differences of FA, MD, AD and RD, compared to controls, indicative of micro-structural abnormalities. A previous POMS DTI study of 12-17 year olds identified elevated MD in the fornix, amongst many white matter regions, using a whole brain white matter voxel-based skeletonized approach, but this was on low spatial resolution diffusion images acquired without CSF suppression (susceptible to partial volume effects) and the actual MD values were not reported, nor was the fornix volume or other diffusion metrics such as FA, AD, and RD (Blaschek 2013). Minimizing the effects of CSF partial volume by smaller voxels (volume of 2.9 mm^3) and CSF suppression (using inversion recovery FLAIR preparation) is important to not attribute changes of diffusion properties to merely partial volume effects in a smaller fornix (Vos 2011). Here, the largest percent change of the diffusion metrics in the fornix was a 16% larger RD that could be interpreted as demyelination (Song 2002, Klawiter 2011); however, axonal loss (i.e. lower density) leading to a markedly smaller fornix is also possible. A

potential injury mechanism is that the thin fornix is bathed in CSF, which has been shown to contain MS inflammatory immunoglobulins in POMS (McKay 2021).

The large 26% volume percent reduction of the fornix in POMS is in exact agreement with the 26% volume reduction found in our cross-sectional adult MS study (age range of 32-70 years) that used the same FLAIR-DTI acquisition protocol (Valdés Cabrera 2022). Further, POMS fornix DTI metrics were similarly affected relative to controls as in the previous adult MS study: POMS FA -7% vs AOMS -7%, MD +12% vs +9%, AD +7% vs +6%, and RD +16% vs +12%. The similarly affected fornix volume and diffusion metrics regardless of the differences in average disease durations (i.e. 3 years for POMS here versus 15 years in the adult MS study) (Valdés Cabrera 2022) and lower disease burden of disability in POMS, suggests that the fornix is affected early on in the disease course of MS and that fornix injury is not necessarily progressive, although this assessment would require longitudinal scans rather than the cross-sectional cohorts as in our two studies. However, this hypothesis is further supported by the presence of inflammatory cytokines in CSF early on in the disease course of adult MS, which could disproportionately affect the fornix early on (Pardini 2021). POMS were all relapsing-remitting MS in the current study as well as the majority (35/43 MS participants) in the adult study (Valdés Cabrera 2022). However, the prior adult MS FLAIR-DTI study showed far greater fornix changes in volume and all diffusion metrics in those with cognitive impairment, whereas those without cognitive impairment showed significant, albeit less changes, of lower volume and higher MD/RD with no significant changes in FA or AD (Valdés Cabrera 2022). The POMS cohort here showed no FDR-corrected significant correlations of the fornix parameters versus cognitive (or clinical) scores, likely due to the small sample size. Further, POMS with cognitive impairment according to the criteria used in the previous adult MS study (i.e. SDMT

z-scores below -1.67 standard deviations (SD) and/or BVMT-R z-scores below -1.17 SD) (Valdés Cabrera 2022) and without cognitive impairment showed similar abnormal fornix volume/diffusion metric differences relative to controls. Encouragingly, the non multiple comparison corrected negative correlations of SDMT with fornix MD and RD, and total lesion volume with fornix FA, agree with the prior adult MS study (Valdés Cabrera 2022). Other adult MS DTI studies have also shown abnormal fornix metrics with some reports of relationships to cognitive impairment, including reduced FA, and elevated MD, AD, and RD (Fink 2010, Syc 2013, Kern 2015, Welton 2015, Keser 2017).

The fornix is the primary efferent tract of the hippocampus, yet a key observation here is that the hippocampus volume was not different in POMS than controls. This would suggest that the fornix abnormalities are not the result of Wallerian degeneration from neuronal death in the hippocampus, but rather that the fornix may be directly affected by adjacent CSF factors as mentioned earlier. This is consistent with the hypothesis that WM injury precedes injury to connecting GM in MS (Bodini 2016). Our previous adult MS study showed no differences in hippocampus volume (as measured using automated segmentation software on 3D T1-weighted scans) either, although FA, MD, and RD were abnormal in the hippocampus of cognitively impaired adult MS participants (Valdés Cabrera 2022). However, a follow-up study on the same adult MS cohort showed a 14% smaller hippocampus volume as measured by manual segmentation on 1 mm isotropic DTI scans, with no reduction of hippocampus volume in the cognitively unimpaired group although both groups had elevated MD in the hippocampus suggestive of microstructural alterations (Valdés Cabrera 2023). There are discrepancies in POMS with hippocampus reported as being smaller or no different than controls, which may be due to a shorter preclinical disease activity or differences in the disease process (i.e. absence of

progressive MS) compared to adult MS (Fabri 2021, Rocca 2016a, Fuentes 2012). Our observations of greatly enlarged lateral ventricles (+56%) and CSF volume (+41%) as well as smaller volumes of thalamus (-23%), total white matter (-17%), globus pallidus (-16%), putamen (-12%), and total cerebellum (-9%) in POMS are consistent with previous work (Aubert-Broche 2011, Bartels 2019, De Meo 2019, Fadda 2019). The thalamus volume is affected nearly as much as the fornix volume, presumably due to the thalamus being located adjacent to the CSF as well (Fadda 2019). Interestingly, there was no difference in total GM volume between groups, which may suggest that brain volume losses in POMS are driven by WM atrophy (Bartels 2019).

There were several limitations in this study. The sample size of 11 POMS in this single site study was a result of the small local clinical population and the focus on scans under 20 years of age. A larger sample would have been beneficial to assess correlations between fornix volume/diffusion metrics and clinical disability and cognitive function. There was only one male in the 11 POMS participants limiting the analysis of sex effects. The fornix volume/diffusion metrics can depend on the tractography algorithm/parameters between studies although the same methods were used for all POMS and controls here. This study was focused on one key tract of interest, the fornix, but it would be useful to examine other WM tracts in the same cohort. The FLAIR-DTI has limited brain coverage (70 mm coverage by 35 slices 2 mm thick) as it was developed for the fornix, but future analyses of this POMS cohort will include whole brain multi-shell diffusion MRI analysis of other white matter tracts as well as high resolution (1 mm isotropic) DTI of the hippocampus, the latter as performed in our previous adult MS study (Valdés Cabrera 2023).

Diffusion MRI findings in POMS provide evidence that there is early involvement of the fornix in the disease course of MS, which precedes injury to connecting GM, and is likely related

to its location within the ventricles leading to exposure to soluble inflammatory factors in CSF. These results suggest that the microstructural integrity of the fornix may be an early hallmark of MS and that the fornix should not be overlooked in future work examining MS pathology.

4. High-Resolution Fluid-Suppressed Diffusion Tractography of the Fornix Across the Healthy Lifespan and Deviations in Multiple Sclerosis

4.1 Abstract

Background: Microstructural changes of the fornix, which is the main efferent white matter (WM) tract of the hippocampus and part of the limbic system, have been identified using diffusion tensor imaging (DTI) across the healthy lifespan, and in children and adults with multiple sclerosis (MS), separately.

Objective: To analyze fornix microstructure changes in MS compared to healthy controls across age using improved fornix DTI tractography.

Methods: High-resolution, fluid-suppressed diffusion tractography was used to identify and quantify the fornix in 42 MS patients and 103 healthy controls (12-65 years). Fornix volume and diffusion metrics of MS participants were compared to controls across age.

Results: Control fornix volume increased until 33 years and then declined, fractional anisotropy (FA) showed no age relationship, and mean (MD), axial (AD) and radial diffusivity (RD) decreased until 33, 30 and 32 years, respectively, and then increased with age. MS fornix volume and FA followed similar trends, but remained below controls, and MD, AD, and RD did not show age relationships, but deviated above controls across age.

Conclusion: Diffusion tractography showed early deviations in fornix volume and diffusion metrics in MS compared to controls that stayed consistent across aging, suggesting it is an early and consistent target of injury in MS.

4.2 Introduction

The fornix is the main efferent white matter (WM) tract of the hippocampus and is part of the limbic system, which is responsible for aspects of memory and cognition (Douet 2014a). Fornix microstructure changes, identified using diffusion tensor imaging (DTI), have commonly been studied in relation to episodic memory deficits, as shown in healthy controls (Rudebeck 2009), mild cognitive impairment (Metzler-Baddeley 2012) and neurodegenerative/ neuroinflammatory diseases, such as multiple sclerosis (MS) (Dineen 2012, Koenig 2013). However, lower fornix fractional anisotropy (FA) and higher radial diffusivity (RD) have also been implicated in poorer overall cognitive function in MS (Keser 2017). Similarly, fornix volume and axial diffusivity (AD) were predictive of cognitive decline in healthy elderly controls (Fletcher 2013).

Despite fornix findings of relationships to memory and cognition in healthy controls and MS, only a few DTI studies have examined fornix microstructure changes across age, and children/adolescents are often excluded. Only one fornix DTI tractography study has examined fornix volume and diffusion metrics across the healthy lifespan, including very young children up to elderly subjects (5-83 years) (Lebel 2012). Fornix volume and FA showed inverted U-shaped curves, while mean (MD), radial (RD) and axial diffusivity (AD) showed U-shaped curves across age, with peaks and minimums around 20 years, respectively. Tract-based spatial statistics and region-of-interest studies found similar trends across healthy children/adolescents

and young adults for fornix AD and RD in 8-28 year olds, but showed that fornix volume peaked earlier around 13 years (Simmonds 2014), and fornix FA around 15 years in a study of 3-20 year olds (Douet 2014b). Other DTI tractography studies of the fornix in healthy controls have primarily spanned young adults to elderly subjects (~20-80 years old), and have revealed both decreasing fornix volume and FA (Stadlbauer 2008, Michielse 2010, Jang 2011, Sasson 2013) and no changes in FA (Sullivan 2010), as well as increasing (Stadlbauer 2008, Sullivan 2010, Jang 2011, Sasson 2013) and decreasing fornix diffusivities with age (Michielse 2010). Recently, DTI tractography also showed negative and positive quadratic relationships between age and fornix FA and MD in 20-94 year olds, which decreased and increased after 20 years of age, respectively (Foster 2019). However, none of these studies used cerebrospinal fluid (CSF) suppression, which is important to not attribute changes in diffusion properties to partial volume effects from rapid, isotropic diffusing CSF, since the small fornix is located in the ventricles (Concha 2005, Vos 2011). The only fornix DTI study across the healthy lifespan also used low spatial resolution (3 mm thick slices) and was acquired on a 1.5T scanner (Lebel 2012), which makes the fornix more prone to effects from CSF partial volume.

Fornix DTI has also been used to study fornix microstructure changes in MS, albeit in children and adults with multiple sclerosis (MS), separately. Only one voxel-based analysis, showed the fornix with elevated MD in children with MS, but the study did not report the actual MD value, other diffusion metrics, or output volume (Blaschek 2013). Fornix tractography in adults with MS showed smaller fornix volume with reduced FA, and elevated MD, AD, and RD, compared to controls (Valdés Cabrera 2020), and lower FA and higher MD and RD that were related to poorer auditory processing and greater cognitive impairment (Syc 2013, Keser 2017). Fluid-attenuated inversion recovery (FLAIR) DTI tractography, which suppressed CSF and

improved fornix volume and diffusion metrics has since been applied to study the fornix in children/adolescents with MS (Chapter 3) and adult MS (Valdés Cabrera 2022). FLAIR-DTI showed marked fornix volume reductions and diffusion abnormalities in children/adolescents and adults with MS, which were greater than other total/regional brain volume losses. FLAIR-DTI in adult MS also showed that fornix volume/diffusion metrics were most affected in cognitively impaired MS. Additionally, fornix volume/diffusion metric age relationships were only assessed in MS participants spanning 32-71 years old, although fornix volume showed a negative linear relationship, FA showed no relationship, and MD, AD and RD showed positive linear relationships with age. Tractography can output tract volume, as well as diffusion metrics indicative of microstructural fornix integrity, however it has not been applied to study fornix microstructure changes across the MS "lifespan", particularly in very young children and adolescents up to elderly subjects, relative to healthy controls, which is needed to determine if there are age-related fornix changes (i.e. injury) in the disease course of MS.

The purpose of this study was to: (i) assess fornix changes (i.e. volume and diffusion metrics) versus age across the "lifespan" in healthy controls using improved CSF-suppressed, high-resolution FLAIR-DTI tractography, (ii) compare fornix changes in MS across the same age range to healthy control age trajectories, and (iii) examine how fornix volume changes in MS compare to age trajectories of other total/regional brain volumes.

4.3 Materials and Methods

4.3.1 Participants

This study was approved by the University of Alberta Human Research Ethics Board. All 145 participants provided written informed consent (or parental consent and assent if under 16

years of age), including 42 diagnosed with MS that were recruited from the pediatric neuroinflammatory registry and University of Alberta Neurosciences Clinic, and 103 healthy controls chosen with a similar age/sex distribution from a previous local normative study using an identical MRI protocol. There were 16 pediatric-onset MS (POMS) diagnosed with MS before 18 years of age and 26 adult-onset MS (AOMS), which together included 34 relapsing-remitting MS (RRMS), 5 secondary progressive MS (SPMS), 2 primary progressive MS (PPMS), and 1 benign MS. The inclusion criteria for the MS cohort was a diagnosis of MS according to the 2017 McDonald criteria. The exclusion criteria included no MS participants with medical diagnoses other than MS or with known clinical relapses at the time of the MRI scan or within 30 days of the study visit. Most (35/42) MS were on disease modifying therapies (rituximab, ocrelizumab, fingolimod, ofatumumab, dimethyl fumarate, interferon beta-1a, and natalizumab), 19/42 MS had diagnosed depression/anxiety and were on various antidepressant medications, and 5/42 MS had diagnosed attention deficit hyperactivity disorder (ADHD) and were taking ADHD medications. Demographic and clinical data are summarized in **Table 4.1**.

Table 4.1: Demographics, clinical scores, and total lesion volume for age/sex matched controls and MS with range, mean, and standard deviation.

	Controls (n=103)	**MS (n=42)**
Sex (M/F)	27/76	10/32
Age (years)	12 - 65 33 +/- 15	13 - 63 34 +/- 15
Time since MS onset (years)	-	1 - 31 11 +/- 9
Expanded Disability Status Scale, EDSS	-	0.0 - 8.5 3.0 +/- 2.2
Pediatric Fatigue (raw score)	-	12 - 36 23 +/- 8
Modified Fatigue Impact Scale, MFIS	-	9 - 77 43 +/- 18
Beck's Depression Inventory-II, BDI-II	-	1 - 43 15 +/- 11
Symbol Digit Modalities Test, SDMT (raw score)	-	19 - 95 54 +/- 18
Brief Visuospatial Memory Test-Revised, BVMT-R (total recall) (raw score)	-	3 - 34 27 +/- 7
Timed 25-Foot Walk, T25FW (average of 2 trials, seconds)	-	3.1 - 7.8 4.5 +/- 1.1
Nine-Hole Peg Test, 9HPT (average of 4 trials, seconds)	-	16.3 - 43.6 22.8 +/- 5.6
Total Lesion Volume, TLV (cm^3)	-	0.04 - 55.7 12.1 +/- 14.7

EDSS not obtained from one adult RRMS; BDI-II not obtained from one pediatric-onset adult RRMS; BVMT-R not obtained from one adult SPMS; T25FW and 9HPT not obtained from five POMS and 15 adult MS (8 RRMS, 5 SPMS, 2 PPMS)

4.3.2 Cognitive Testing

Cognitive and clinical tests were administered by a trained user and MS neurologists from the University of Alberta, respectively. Tests included: Expanded Disability Status Scale (EDSS) for overall MS disability, Pediatric Fatigue (Neuro-QOL Item Bank v.2.1) for POMS fatigue, Modified Fatigue Impact Scale (MFIS) for AOMS fatigue, Beck's Depression Inventory-II (BDI-II) for depression, Symbol Digit Modalities Test (SDMT) to measure processing speed, Brief Visuospatial Memory Test-Revised (BVMT-R) to test visuospatial memory (only total recall score), Timed 25-Foot Walk (T25FW) for mobility, and Nine-Hole Peg Test (9HPT) for dexterity. Cognitive/clinical test scores are summarized in **Table 4.1**.

4.3.3 MRI Protocol

Participants were scanned on a 3T Siemens Prisma MRI with a 64 channel head/neck radiofrequency coil. A whole-brain 3D T1-weighted magnetization-prepared rapid acquisition gradient echo (MPRAGE) was acquired using the following parameters: 0.9 mm isotropic voxels, TR 1800 ms, TE 2.37 ms, and total scan time 3.7 minutes. Whole-brain 3D sampling perfection with application optimized contrasts using different flip angle evolution (SPACE) FLAIR was acquired with 1.2 mm isotropic voxels, TI 1800 ms, TR 5000 ms, TE 385 ms, and total scan time 3.1 minutes. The FLAIR-DTI protocol was the same as used in a previous adult MS study here (Valdés Cabrera 2022): 2D single-shot echo-planar imaging, 35 2 mm transverse slices centered for fornix coverage, 1.2x1.2 mm^2 zero-filled to 0.64x0.64 mm^2 in-plane resolution, GRAPPA R=2, phase partial Fourier 6/8, TI 2300 ms, TR 9000 ms, TE 70 ms, 5 b=0 and 20 b=1000 s/mm^2, and total scan time 4.2 minutes.

4.3.4 MRI Analysis

MPRAGE brain volumes and SPACE FLAIR total MS lesion volumes were measured using the volBrain and lesionBrain pipelines, respectively, offered through the online volBrain platform for MRI brain analysis (Manjón 2016, Coupé 2018). The volBrain pipeline yielded segmented total and regional brain volumes including: WM, gray matter (GM), total brain volume (TBV), CSF, cerebellum (total, WM, GM), lateral ventricles, caudate, putamen, globus pallidus, thalamus, hippocampus, and amygdala. Left and right hemispheres were combined to limit comparisons and yielded 14 volumes per participant. The lesionBrain pipeline yielded segmented total lesion volume (TLV).

DTI processing was performed in MRTrix3 (v.2.0) including denoising, Gibbs ringing, eddy current and motion, bias field correction, and tensor fitting (Tournier 2019). Deterministic tractography of the fornix was performed in MRtrix3 similar to previously published lab protocols (Valdés Cabrera 2022) using: FA threshold 0.15, maximum turning angle 65^{o}, step size 0.64 mm, minimum fiber length 10 mm, and maximum fiber length of 109 mm (i.e. MRtrix3 default, geometric mean of interpolated voxel size times 100). Regions of interest (ROIs) were placed as follows: coronal AND ROI in the fornix body, axial NOT ROI to remove tracts superior to the fornix, coronal NOT ROI to remove tracts anterior to the fornix columns, coronal NOT ROI to remove tracts posterior to the fornix crura, and other NOT ROIs as needed to remove all remaining streamlines not attributable to the fornix. This tract yielded the whole fornix volume, as well as average FA, MD, AD and RD across left and right sides.

4.3.5 Statistical Analysis and Curve Fitting

Fornix volume, FA, MD, AD and RD, and total/regional brain volumes for controls and MS participants were tested for normality, and then metrics were assessed with Mann-Whitney U tests to test for group differences. False discovery rate (FDR) corrected p-values are reported (*$p<0.05$).

Fornix volume, FA, MD, AD and RD, and total/regional brain volumes for MS and controls were each fit versus age to linear, Poisson, or quadratic models based on best fit, which was determined by comparing the Akaike Information Criterion (AIC) values of each model and selecting the model with the lowest AIC value (Virtanen 2020). If AIC values were within two units of each other, models were considered equally fit, and the simplest model was chosen (i.e. model with the fewest parameters) (Burnham and Anderson 2002). Only significant fits ($p<0.05$) are shown.

4.4 Results

CSF-suppressed, high-resolution FLAIR-DTI tractography depicted the full fornix in all 103 controls and 42 MS participants (see **Figure 4.1** for 42 representative age/sex matched control fornix and **Figure 4.2** for all 42 MS fornix, colour-coded by MD).

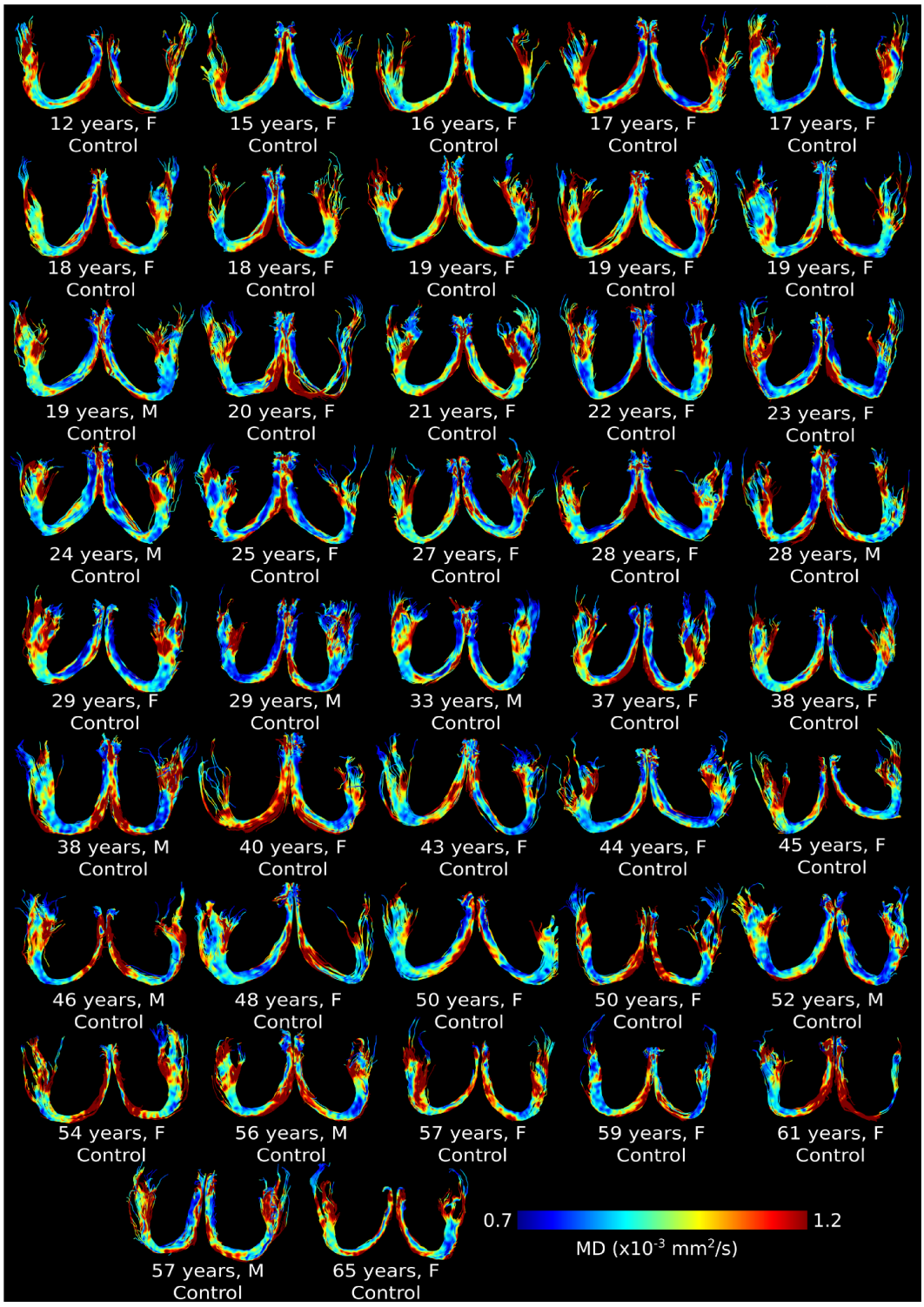

Figure 4.1: Example of CSF-suppressed, high-resolution FLAIR-DTI fornix tractography (as seen from superior view) colour-coded by MD in 42 representative age/sex matched controls, ordered by age. Fornix tractography depicted the full fornix in all and showed bilateral regions with higher MD after the fourth decade of life.

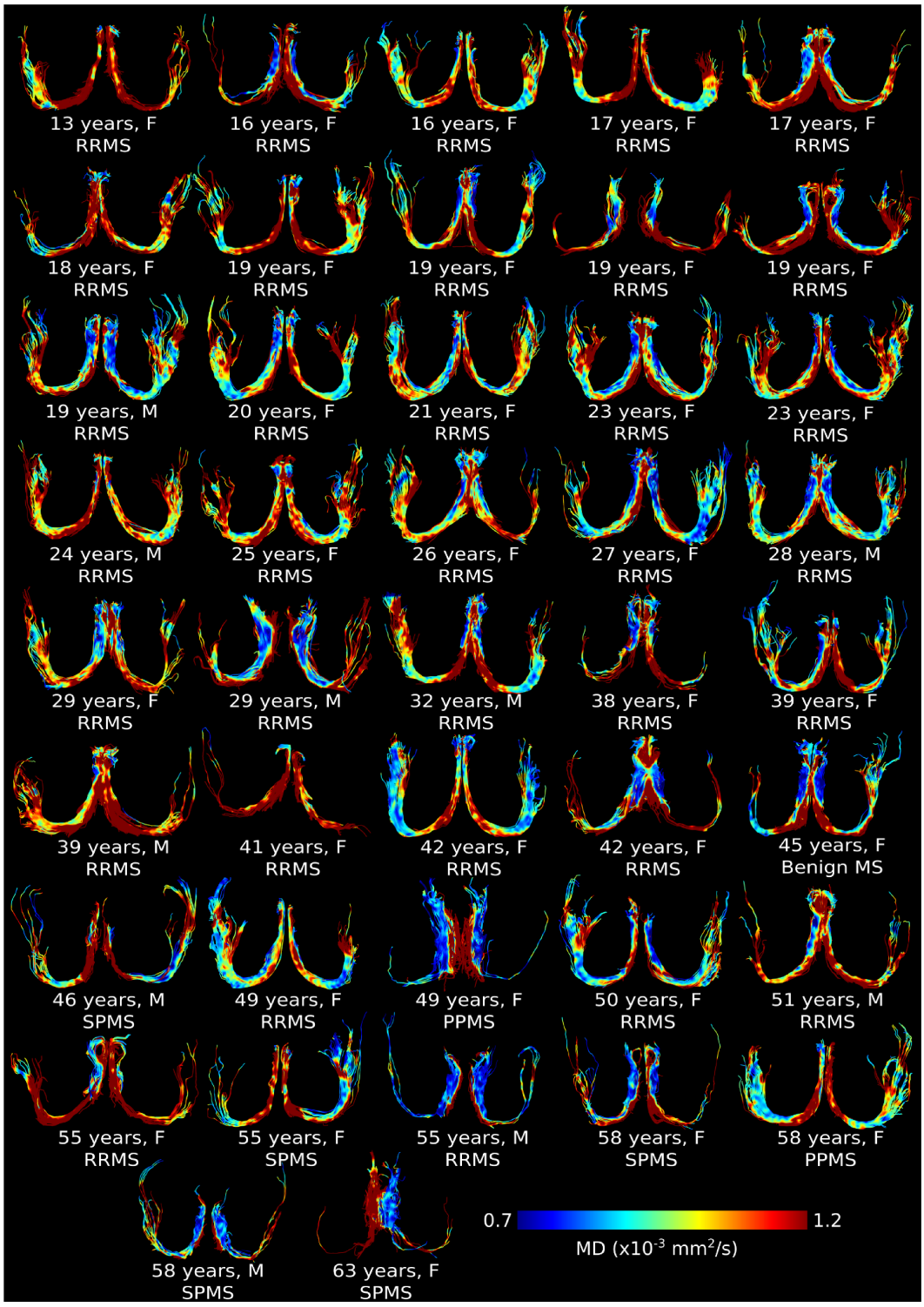

Figure 4.2: Example of CSF-suppressed, high-resolution FLAIR-DTI fornix tractography (as seen from superior view) colour-coded by MD in all 42 MS, ordered by age. Fornix tractography depicted the full fornix in all, but it appeared thinner and showed bilateral regions with higher MD at most ages, especially for progressive MS.

Averaged over all ages relative to controls, MS fornix were 29% smaller (5.2 +/- 1.1 vs 3.7 +/- 0.9 cm^3, p<0.001), with 7% lower FA (0.43 +/- 0.02 vs 0.40 +/- 0.03, p<0.001), 10% higher MD (1.05 +/- 0.06 vs 1.15 +/- 0.09 $x10^{-3}$ mm^2/s, p<0.001), 6% higher AD (1.58 +/- 0.08 vs 1.67 +/- 0.11 $x10^{-3}$ mm^2/s, p<0.001), and 13% higher RD (0.79 +/- 0.06 vs 0.89 +/- 0.09 $x10^{-3}$ mm^2/s, p<0.001) (**Figure 4.3**). MS had the greatest proportional volume differences compared to controls in the lateral ventricles (+81%) and CSF (+28%). For other total/regional brain volumes, the greatest volume losses in order were thalamus (-21%), cerebellum WM (-18%), total WM (-14%), globus pallidus (-13%), putamen (-12%), caudate (-9%), TBV (-8%), total cerebellum (-7%), amygdala (-6%) and hippocampus (-5%). These differences were not as great as the fornix (-29%). Notably, there were no differences in total GM or cerebellum GM volumes (**Table 4.2**).

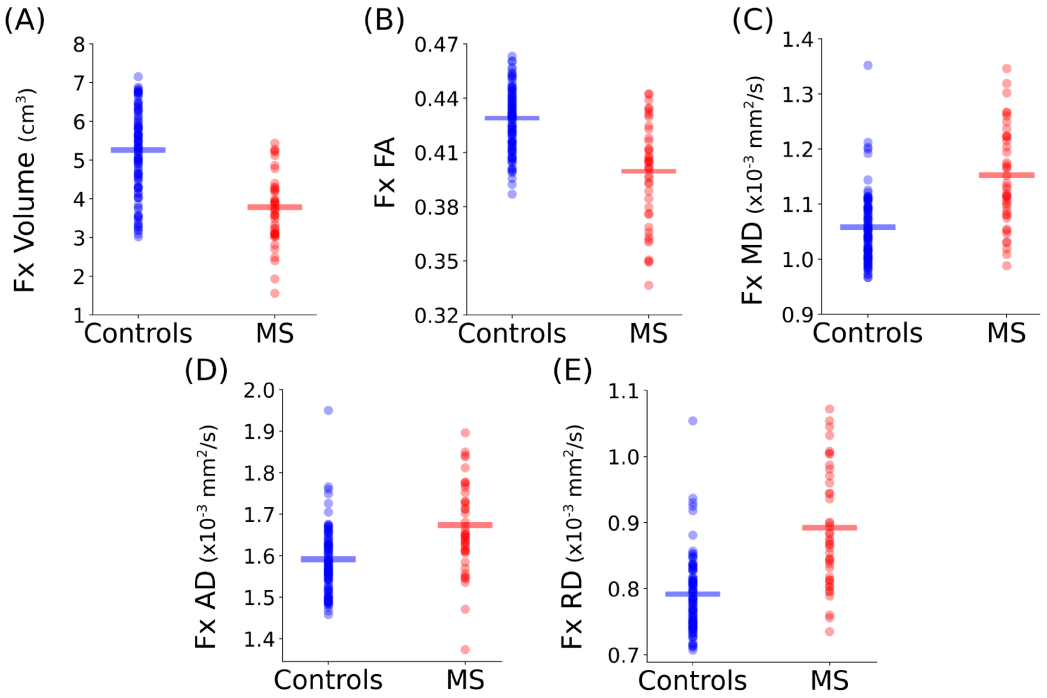

Figure 4.3: Group comparisons of controls (n=103) and MS (n=42) are shown for fornix (Fx) (A) volume, (B) FA, (C) MD, (D) AD and (E) RD. MS fornix showed a smaller volume (-29%) compared to controls as the largest change in the fornix, in addition to significant differences in FA (7% lower), MD (10% higher), AD (6% higher), and RD (13% higher).

Table 4.2: Total/regional left + right WM/GM volumes (cm^3) and fornix volume/diffusion metrics with group comparisons for age/sex matched controls versus MS with mean +/- SD, ordered from greatest positive percentage changes and then greatest negative percentage changes, FDR corrected; *p<0.05; n.s. is non-significant.

Volumes (cm^3)	**Controls (n=103)**	**MS (n=42)**	**Difference (%)**	
Lateral Ventricles	11.3 +/- 6.5	20.4 +/- 14.7	+81	p=0.002*
CSF	174 +/- 48	223 +/- 75	+28	p=0.001*
Fornix	5.2 +/- 1.1	3.7 +/- 0.9	-29	p<0.001*
Thalamus	12.6 +/- 1.2	10.0 +/- 2.0	-21	p=0.002*
WM (total)	546 +/- 58	471 +/- 84	-14	p=0.002*
Globus Pallidus	2.4 +/- 0.3	2.1 +/- 0.4	-13	p=0.001*
Putamen	8.9 +/- 0.9	7.8 +/- 1.3	-12	p=0.002*
Caudate	7.6 +/- 1.0	6.9 +/- 1.1	-9	p=0.001*
TBV	1281 +/- 111	1183 +/- 137	-8	p=0.001*
Cerebellum WM GM	144 +/- 14 38 +/- 7 106 +/- 13	134 +/- 20 31 +/- 8 103 +/- 15	-7 -18 n.s.	p=0.017* p=0.002* p=0.542
Amygdala	1.7 +/- 0.2	1.6 +/- 0.2	-6	p=0.004*
Hippocampus	8.1 +/- 0.8	7.7 +/- 1.0	-5	p=0.019*
GM (total)	735 +/- 76	713 +/- 73	n.s.	p=0.148

Poisson curves fit control and MS fornix volume (R^2=0.45, p<0.001 and R^2=0.27, p=0.024, respectively) (**Figure 4.4A**), both of which became larger from 12 and 13 years until peaking at 33 and 29 years of age with increases of 80% and 56%, respectively, and then became smaller with age towards 62-65 years at a slower rate than the upswing ending up with volumes similar to that at 12 years of age. Notably, the fornix volume of the MS group remained below

controls across all ages. Control and MS fornix FA did not show any significant age relationships, but ~1/3 of the MS participants had FA below all controls across the full age span and the majority were below the mean of the controls (**Figure 4.4B).** Control fornix MD (quadratic, R^2=0.20, p<0.001, **Figure 4.4C**), AD (Poisson, R^2=0.22, p<0.001, **Figure 4.4D**) and RD (quadratic, R^2=0.18, p=0.001, **Figure 4.4E**) followed similar trends with age where they decreased until 33, 30, and 32 years of age, respectively, and then increased to a greater extent with aging. In contrast, fornix MD, AD and RD in MS participants did not show significant age relationships, but most were larger than the control mean across all ages from 12 to 62 years.

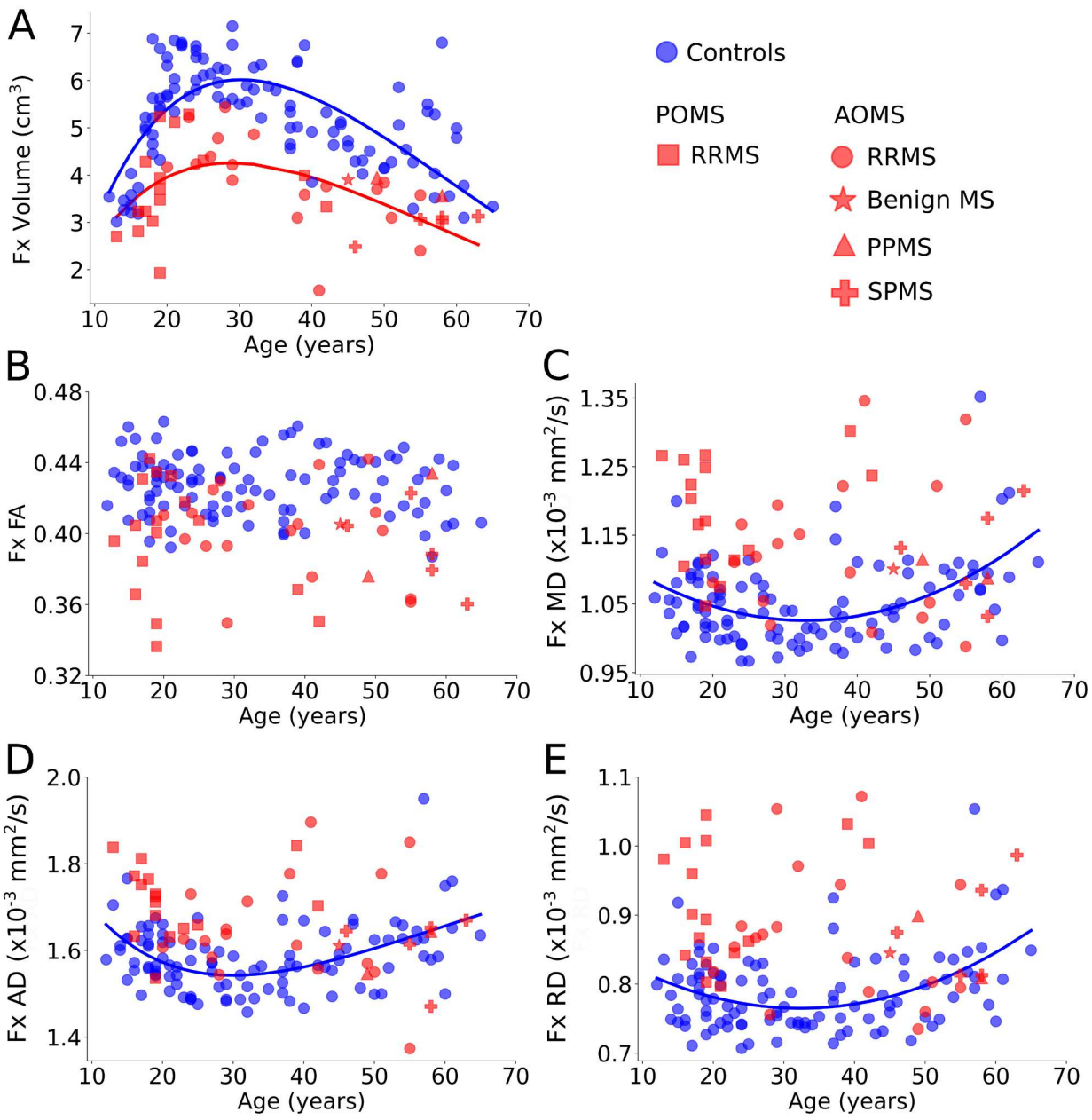

Figure 4.4: Fornix (Fx) (A) volume, (B) FA, (C) MD, (D) AD and (E) RD shown vs age for controls (n=103) and MS (n=42). Fornix volume in MS followed a Poisson curve similar to controls, but peaked earlier (29 vs 33 years) and remained below controls across all ages. Control fornix FA showed no age relationships, whereas MD, AD and RD showed similar curves with age (minimums at 33, 30, and 32 years, respectively), although no age relationships were shown for MS fornix diffusion metrics, which remained below (i.e. FA) and above (i.e. MD, AD, and RD) controls at all ages.

Volumetric analysis of the MPRAGE T1-weighted data showed negative linear correlations with age in the MS participants for TBV (R^2=0.10, p=0.046) (**Figure 4.5C**), total GM (R^2=0.36, p<0.001) (but not total WM) (**Figure 4.5D and E**), total cerebellum (R^2=0.09, p=0.049) (**Figure 4.5F)**, and cerebellum GM (R^2=0.12, p=0.026) (but not cerebellum WM) (**Figure 4.5G and H**). In contrast, the controls only showed a negative linear correlation with age in the total GM (R^2=0.10, p<0.001) (**Figure 4.5E)**, but the slope was not as steep as in MS. However, total GM and cerebellum GM were not significantly different in MS as a group (**Table 4.2**). Although total WM and cerebellum WM did not show age correlations, ~1/3 of the MS participants had smaller volumes than controls spanning the full age range. Groups yielded positive correlations with age for both CSF (MS R^2=0.32, p<0.001 vs control R^2=0.36, p<0.001) and lateral ventricle volumes (MS R^2=0.32, p<0.001 vs control R^2=0.27, p<0.001), but the MS group showed larger volumes over all ages (**Figure 4.5A and B**).

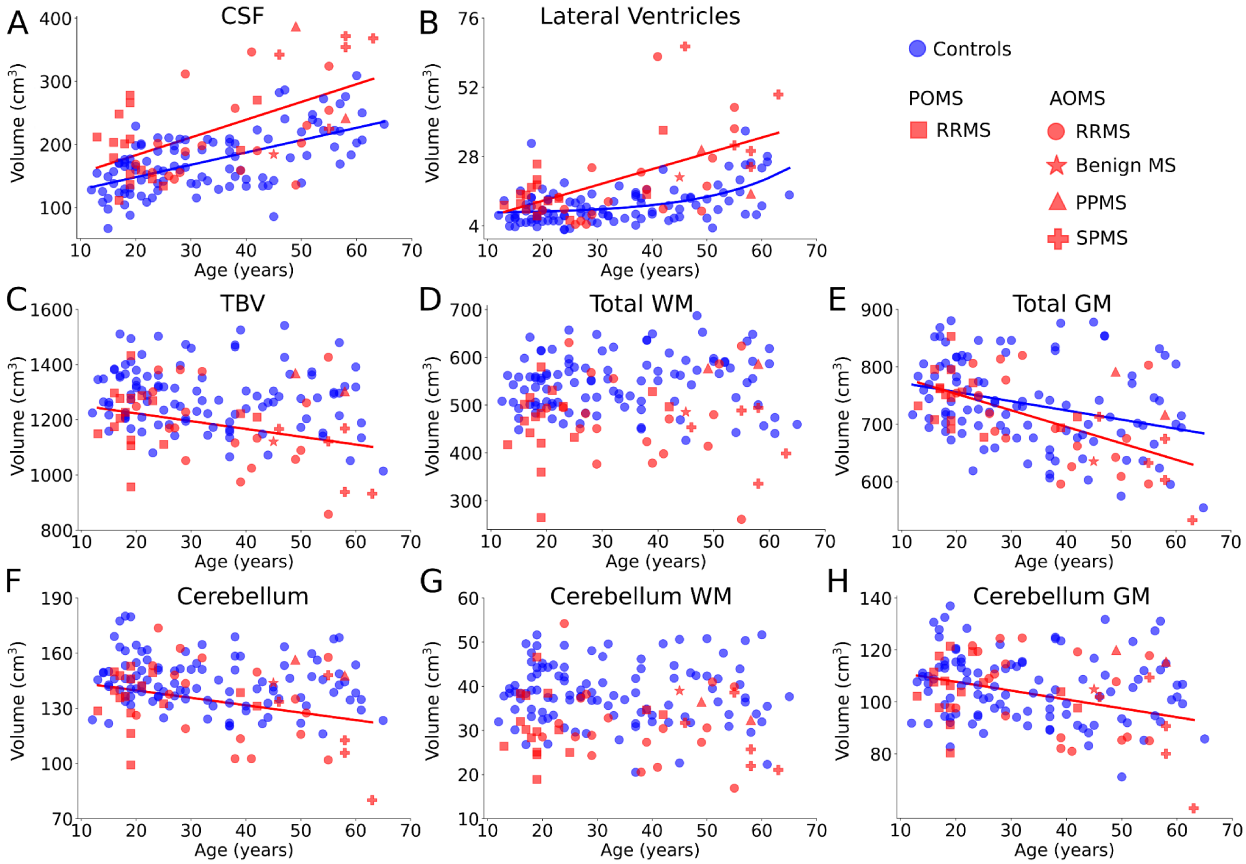

Figure 4.5: (A) CSF, (B) lateral ventricles, (C) TBV, (D) total WM, (E) total GM, (F) cerebellum, (G) cerebellum WM and (H) cerebellum GM volume shown vs age for controls (n=103) and MS (n=42). Control and MS CSF and lateral ventricle volumes showed positive relationships with age, with steeper slopes for MS. The control and MS total GM showed negative relationships with age, with a steeper slope for MS. MS TBV, cerebellum, and cerebellum GM showed negative age relationships. Neither total WM or cerebellum WM showed age relationships in either group, although WM volumes were smaller in a significant proportion of MS across all ages.

For deep GM volumes, control (R^2=0.18, p<0.001) and MS (R^2=0.20, p=0.003) caudate volumes (**Figure 4.6A**), control (R^2=0.15, p<0.001) and MS (R^2=0.21, p=0.002) putamen volumes (**Figure 4.6B**), control globus pallidus volume (R^2=0.09, p=0.002) (**Figure 4.6C**), and control thalamus volume (R^2=0.15, p<0.001) (**Figure 4.6D**) fit negative linear trends versus age. This means the age relationships in MS were lost for globus pallidus and thalamus, presumably due to marked volume reductions at all ages. The caudate and putamen linear fits were offset to

lower values in MS over the entire age span. Interestingly, MS hippocampus volume fit a quadratic curve (R^2=0.23, p=0.014), which started to decline after 32 years of age (**Figure 4.6E**), whereas there was no age relationship in the control hippocampus. Control amygdala volume showed a weak, positive linear relationship with age (R^2=0.07, p=0.006) (**Figure 4.6F**). There was much overlap in the volumes of hippocampus and amygdala between MS and controls.

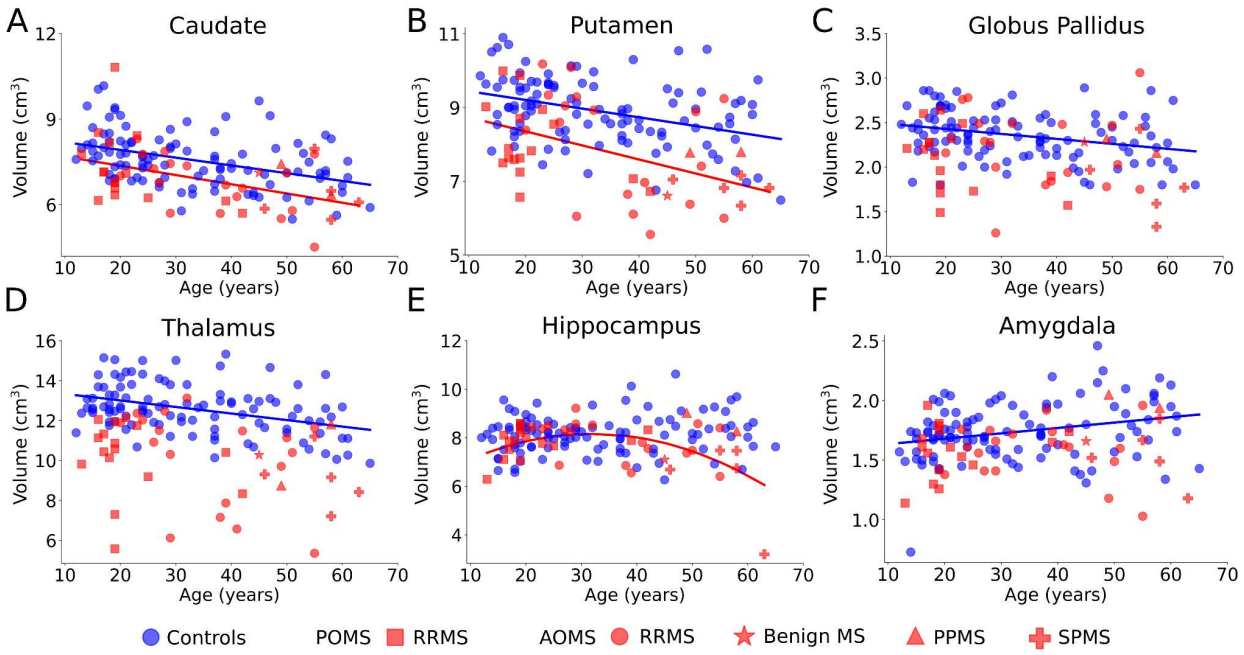

Figure 4.6: (A) Caudate, (B) putamen, (C) globus pallidus, (D) thalamus, (E) hippocampus and (F) amygdala deep GM volumes shown vs age for controls (n=103) and MS (n=42), which showed lower offset age correlations in MS for the caudate and putamen, while the age relationship was lost for globus pallidus and thalamus in MS, presumably due to marked volume reductions at all ages. Most (4/6) deep GM volumes in controls showed negative age relationships as expected.

4.5 Discussion

High-resolution FLAIR-DTI tractography enabled the virtual identification and quantification of MS fornix across age (13-63 years), compared to controls. Relative to controls, MS fornix were smaller and proportionally more affected than any other WM or GM brain volume losses assessed in this study, and showed diffusion metric abnormalities of FA, MD, AD,

and RD. Fornix volume/diffusion metrics were similarly affected relative to controls as in the previous cross-sectional adult MS study with no overlapping patient scans, which used the same FLAIR-DTI tractography protocol (Valdés Cabrera 2022): this study MS volume -29% vs adult MS study -26%, FA -7% vs -7%, MD +10% vs +9%, AD +6% vs +6%, and RD +13% vs +12%. Importantly, the above results were similar regardless of the different DTI post-processing softwares used in either study. The largest percent change in diffusion metrics of fornix RD, over AD, suggests that injury may be largely from demyelination in the fornix (Song 2002, Klawiter 2011).

Other total/regional brain volume group comparisons between MS and controls, including larger lateral ventricles (+81%) and CSF volume (+28%), and smaller thalamus (-21%), cerebellum WM (-18%), total WM (-14%), globus pallidus (-13%), putamen (-12%), caudate (-9%), TBV (-8%), cerebellum (-7%), amygdala (-6%), and hippocampus (-5%) volumes in MS, with no differences in cerebellum GM or total GM, are consistent with previous studies (Aubert-Broche 2011, Eshaghi 2018, Bartels 2019, De Meo 2019). Notably, the fornix showed the greatest proportional volume loss compared to other WM and GM brain regions assessed in this study, which may be attributed to its location within CSF containing soluble MS inflammatory factors early on in the disease course (Pardini 2021).

Similar fornix vs age relationships were shown for controls in this study as in previous fornix DTI studies. Control fornix volume followed a similar inverted U-shaped curve as the previous studies in 5-83 (Lebel 2012) and 8-28 year old controls (Simmonds 2014), although fornix volume peaked later here at 33 years old, compared to 20 and 13 years old in the earlier studies, respectively, which may reflect denser sampling of younger ages in the previous studies and/or later maturation of the fornix in healthy aging revealed in this study through improved

FLAIR-DTI tractography. Fornix FA showed no changes across age, which is consistent with one previous fornix tractography study in 20-81 year old controls (Sullivan 2010), and suggests that AD and RD are changing similarly with age. Although, fornix DTI in 5-83 (Lebel 2012) and 3-20 year old controls (Douet 2014b) showed inverted U-shaped curves for FA with age, which peaked at 20 and 15 years old, respectively, as well as negative FA relationships with age in 20-94 (Foster 2019) and ~20-80 year old controls (Stadlbauer 2008, Michielse 2010, Jang 2011, Sasson 2013), so the reason there were no age relationships found here may be due to the fact that very young (under 12 years) and elderly (above 65 years) controls were missing from the current study and drive fornix FA age relationships in controls. Notably, none of the studies mentioned above used CSF-suppression, so their findings may reflect partial voluming from CSF that increases with age (Lebel 2012). Control fornix MD, AD and RD all followed similar U-shaped trends as previously reported in fornix DTI across 5-83 (Lebel 2012) and 8-28 year old controls (Simmonds 2014), however later minimum values were reported here (33, 30 and 32 years, respectively, vs 20 years). Additionally, the later minimum value shown for fornix MD in this study is comparable with the minimum MD values reported for other larger WM tracts not affected by CSF (notably the corpus callosum, corticospinal tract, uncinate, superior fronto-occipital, and superior longitudinal fasciculus) from the previous study in 5-83 year olds, which used thick slices and no CSF-suppression (Lebel 2012). Fornix MD and RD also showed positive relationships with age in 32-70 year old controls, which is consistent with the findings here (Valdés Cabrera 2022),

MS fornix volume followed a similar inverted curve as controls in this study, but MS peaked earlier at 29 years, showed a smaller proportional increase (56% vs 80%), and remained below controls across all ages, providing evidence that fornix volume is affected early on in the

disease course and that fornix injury is not progressive, although this would require longitudinal scans. Notably, the decline in fornix volume after 29 years old is consistent with the negative relationship shown for fornix volume in adult MS spanning 32-71 years old (Valdés Cabrera 2022). Similar to controls, MS fornix FA did not show changes with age, similar to adults with MS spanning 32-71 years old (Valdés Cabrera 2022), but the majority of MS were below the mean FA of controls across all ages (**Figure 4.3**), which may reflect early and persistent MS injury from lesions and/or demyelination (Filippi 2001). Unlike MS fornix volume, there was still notable overlap between controls and MS for fornix FA. None of the MS fornix diffusivities (MD, AD or RD) showed age relationships, however they all deviated above controls across all ages, with minimal overlap between MS and controls, especially fornix RD, which provides evidence for early fornix injury from demyelination (Song 2002, Klawiter 2011). However, axonal loss (i.e. lower density) is also possible and would explain the markedly smaller fornix volume shown for MS compared to controls. Presumably, pathological effects on fornix diffusion metrics (FA and diffusivities) in MS overwhelmed expected age relationships (shown in controls). Fornix diffusivities previously showed positive linear trends in adult MS spanning 32-71 years of age (Valdés Cabrera 2022), so expected age relationships may have been primarily overwhelmed by pathological effects at younger ages (under 32 years old). MS fornix volume and diffusion metrics exhibited changes indicative of MS injury across all ages (13-63 years), which suggests that the fornix is an early and consistent target of injury in MS. Notably, these changes were even similar between POMS (13-19 years) and progressive MS (46-63 years), providing further evidence for early, not progressive, fornix injury in MS, which is likely due to its location within the ventricles and exposure to soluble MS inflammatory factors in CSF (Pardini 2021). Although, there were small sample sizes for either group (n=11 POMS and n=7

progressive MS). These findings agree with a longitudinal fixel-based analysis in 20 WM tracts of interest (using a DTI-based WM atlas, including the fornix) in all MS subtypes (mean age of 48 years), which did not show diffusion changes of the fornix over five years (Koubiyr 2024). Diffusion changes were, however, shown over time for other WM tracts, namely the corticospinal tract, cingulum, and superior longitudinal fasciculus. Fornix volume/diffusion metrics appear also worse in two later adult POMS subjects (39 and 42 years old) relative to controls than other AOMS in the same age range, however future work is needed to determine whether these findings persist in larger sample sizes.

For total/regional brain volumes in controls, the positive relationships shown for CSF and lateral ventricles, and negative relationship shown for total GM with age are in agreement with previous work (Good 2001, Michielse 2010, Lebel 2012, Narvacan 2017, Treit 2022). There were also negative linear (and Poisson) relationships shown for TBV and total WM with age in controls in the previous studies, but very young (under 12 years) and elderly (above 65 years) controls were included in those studies (missing in this study) and may have driven age relationships. However, TBV and total WM also showed no changes with age in a female-only cohort of controls (Good 2001), which reflects the female majority of controls used in this study. For MS, increasing CSF and lateral ventricle volumes, and decreasing TBV, total GM, cerebellum, and cerebellum GM volumes with age is also in agreement with previous work (Eshaghi 2018, Bartels 2019). Additionally, the steeper slopes shown for CSF, lateral ventricle volume, and total GM in MS relative to controls, which diverge from controls at later ages, suggests progressive loss with age in MS.

For the deep GM structures in controls, negative relationships were shown for caudate, putamen, globus pallidus, and thalamus volumes, however Poisson curves were shown for these

structures previously with an initial increase during childhood/adolescence, peaking between 12-14 years for caudate, putamen, and globus pallidus, and 19-23 years for thalamus in a cross-sectional study of 5-83 year old controls (Narvacan 2017). This may reflect the lack of young (under 12 years) and elderly controls (above 65 years) in this study. Alternatively, the Poisson curves mentioned above may have been the result of overfitting, as negative linear relationships have also been shown for caudate, putamen, globus pallidus and thalamus volumes in 5-91 year old healthy controls (Treit 2022). Importantly, similar volume reductions with age were shown between this study and the other cross-sectional study after the peaks at 12-14 and 19-23 years. Control hippocampus volume did not show changes with age here, but showed a negative quadratic relationship with accelerated decline after ~60 years of age in the previous cross-sectional study, which may reflect the lack of elderly controls above 60 years in this study. However, the flat trajectory shown for control hippocampus volume with age in this study agrees with an independent measure of hippocampus volume (manual segmentation of 1 mm DWI) in the same cohort of controls if the age range was restricted to the same age range used here (Solar 2021). Interestingly, manual segmentation of the hippocampus yielded a much smaller volume for total hippocampus than volBrain (4.4 cm^3 vs 8 cm^3). Unexpectedly, control amygdala volume showed a weak positive relationship with age, although similar to the hippocampus, this may reflect the lack of elderly controls above 60 years in the study, because the other cross-sectional study showed a Poisson curve for amygdala volume in controls with age that also showed accelerated decline after ~60 years. For deep GM structures in MS, the progressive atrophy shown for caudate, putamen and hippocampus volume below controls with age is consistent with previous work (Eshaghi 2018, De Meo 2019). There were no changes shown for globus pallidus or thalamus volumes with age in MS, likely due to the marked volume reductions shown at all

ages, most notably for thalamus volume, which similar to the fornix may reflect inflammatory damage from CSF (Eshaghi 2018). Notably, the steeper slope shown for putamen volume in MS compared to controls, which diverges from controls at later ages, suggests progressive loss with age in MS.

There were several limitations in the current study, including the limited age range of controls and MS participants, which were missing very young and elderly subjects. This study analyzed all sex-matched controls within the same age range as the MS participants that had identical FLAIR-DTI from a previous normative study. Future work will analyze the remaining controls that have FLAIR-DTI, including 28 younger controls (5-12 years, 14 males), 29 male controls within the MS age range (13-62 years), and 10 elderly controls (67-74 years, 6 males). Future work should also work to recruit more elderly controls (above 74 years) and MS (above 63 years), POMS children/adults, 25-35 year old MS, PPMS/SPMS, and males with MS. The focus on a single tract of interest in this study, the fornix, was another limitation of the study as it prevented the ability to conclude whether findings were limited to the fornix or extend to other WM tracts. FLAIR-DTI has limited brain coverage as it was developed for the fornix (as detailed in Section 2.3), but future analyses will include whole brain multi-shell diffusion MRI analysis of other WM tracts in a broader age range of controls and MS. Future work should also consider longitudinal studies to better assess age-related changes within individuals, and will assess correlations between fornix volume/diffusion metrics (and other total/regional brain volumes) and clinical/cognitive scores with age, i.e. time since MS onset, EDSS, TLV, Pediatric Fatigue, MFIS, BDI-II, SDMT, BVMT-R, T25FW, and 9HPT. Nonetheless, the findings presented in this study provide useful preliminary data about fornix microstructure changes across the ‘lifespan’

in MS, and highlight a potential early degradation of fornix integrity in MS due to its location within CSF.

5. Conclusion

The results in this thesis show that the fornix is affected in child/adolescent POMS, similarly to adult MS (Chapter 3), and that there are microstructural fornix volume/diffusion abnormalities that deviate from healthy controls across the MS "lifespan" (Chapter 4). In Chapter 3, POMS fornix volume was more affected percentage wise than any other total/regional brain volume losses that were assessed in this study, including hippocampus and total GM volume, which were not different between POMS and controls. In Chapter 4, MS exhibited marked deviations from controls in fornix volume and diffusion metrics at all ages. These findings not only suggest that the fornix may be an early brain region affected in MS, but that fornix WM injury precedes injury to connected GM (i.e. hippocampus), which may be the result of its location within CSF containing soluble MS inflammatory factors early on in the disease course of MS. The use of high-resolution, CSF-suppressed FLAIR-DTI tractography identified the fornix in all MS and controls, while minimizing deleterious CSF partial voluming. These findings largely agreed with previous DTI studies of the fornix in MS and controls, and addressed some of the inconsistencies found in the results of previous fornix studies that used lower spatial resolution and no fluid-suppression.

The work presented in this thesis has several limitations. The small sample size of 11 POMS in Chapter 3 prevented any robust correlations to be made between fornix volume/diffusion metrics and clinical/cognitive scores, and the lack of very young and elderly MS and controls in Chapter 4 may have prevented more age-relationships to be found. Studies should be repeated using larger sample sizes across a wider age range, which includes more children and adult POMS, PPMS/SPMS, and males with MS. The focus on a single tract of interest, the fornix, also prevented the ability to conclude whether findings were unique to the

fornix or extend to other WM tracts. FLAIR-DTI has limited brain coverage as it was developed for the fornix, but future analyses will include whole brain multi-shell diffusion MRI analysis of other WM tracts. Future work should also consider longitudinal studies of WM tracts to clearly identify when specific age-related changes occur. Fornix findings could not be compared to histology results, which would also provide needed insight into how to interpret at the microstructural level the water diffusion changes in MS and across age.

Nonetheless, high-resolution, fluid-suppressed diffusion tractography of the fornix provided evidence for early involvement of the fornix in the disease course of MS, and suggests that fornix microstructure should not be overlooked in future work examining MS pathology. Optimistically, the short FLAIR-DTI scan could be implemented clinically in the future to analyze the fornix early on in the disease course of MS (or prior to diagnosis) if future work determines that the fornix is a unique and early target of MS.

References

Absinta M, Rocca MA, Moiola L, et al. Brain macro- and microscopic damage in patients with pediatric MS. *J Neurol Neurosurg Psychiatry* 2010; 81; 1357-1362.

Akbar N, Giorgio A, Till C, et al. Alterations in functional and structural connectivity in pediatric-onset multiple sclerosis. *PLoS One* 2016; 11; e0145906.

Aliotta R, Cox JL, Donohue K, et al. Tract-based spatial statistics analysis of diffusion-tensor imaging data in pediatric- and adult-onset multiple sclerosis. *Hum Brain Mapp* 2014; 35; 53-60.

Anderson VM, Fisniku LK, Khaleeli Z, et al. Hippocampal atrophy in relapsing-remitting and primary progressive MS: a comparative study. *Mult Scler* 2010; 16; 1083-1090.

Andersson JL, Sotiropoulos SN. An integrated approach to correction for off-resonance effects and subject movement in diffusion MR imaging. *NeuroImage* 2015; 125; 1063-1078.

Aubert-Broche B, Fonov V, Ghassemi R, et al. Regional brain atrophy in children with multiple sclerosis. *NeuroImage* 2011; 58; 409-415.

Aubert-Broche B, Fonov V, Narayanan S, et al. Onset of multiple sclerosis before adulthood leads to failure of age-expected brain growth. *Neurology* 2014; 83; 2140-2146.

Bach M, Laun FB, Leemans A, et al. Methodological considerations on tract-based spatial statistics (TBSS). *NeuroImage* 2014; 100; 358-369.

Baron CA, Beaulieu C. Acquisition strategy to reduce cerebrospinal fluid partial volume effects for improved DTI tractography. *Magn Reson Med* 2015; 73; 1075-1084.

Bartels F, Nobis K, Cooper G, et al. Childhood multiple sclerosis is associated with reduced brain volumes at first clinical presentation and brain growth failure. *Mult Scler* 2019; 25; 927-936.

Bartlett E, Shaw M, Schwarz C, et al. Brief computer-based information processing measures are linked to white matter integrity in pediatric-onset multiple sclerosis. *J Neuroimaging* 2019; 29; 140-150.

Basser PJ, Mattiello J, Le Bihan D. Estimation of the effective self-diffusion tensor from the NMR spin echo. *J Magn Reson B* 1994; 103; 247-254.

Basser PJ, Mattiello J, LeBihan D. MR diffusion tensor spectroscopy and imaging. *Biophys J* 1994b; 66; 259-267.

Beaulieu C. The basis of anisotropic water diffusion in the nervous system - a technical review. *NMR Biomed* 2002; 15; 435-455.

Bernitsas E, Yarraguntla K, Bao F, et al. Structural and neuronal integrity measures of fatigue severity in multiplier sclerosis. *Brain Sci* 2017; 7; 102.

Bernstein MA, King KF, Zhou XJ. Handbook of MRI pulse sequences. Chicago: Academic Press, 2004; pp. 631-635.

Bethune A, Tipu V, Sled JG, et al. Diffusion tensor imaging and cognitive speed in children with multiple sclerosis. *J Neurol Sci* 2011; 309; 68-74.

Bigi S, Banwell B. Pediatric multiple sclerosis. *J Child Neurol* 2012; 27; 1378-1383.

Blaschek A, Keeser D, Muller S, et al. Early white matter changes in childhood multiple sclerosis: a diffusion tensor imaging study. *AJNR Am J Neuroradiol* 2013; 34; 2015-2020.

Bodini B, Chard D, Altmann DR, et al. White and gray matter damage in primary progressive MS: the chicken or the egg? *Neurol* 2016; 86; 170-176.

Bojorquez JZ, Bricq S, Acquitter C, et al. What are normal relaxation times of tissues at 3T? *Magn Reson Imaging* 2017; 35; 69-80.

Bonacchi R, Meani A, Pagani E, et al. Association of age at onset with gray matter volume and white matter microstructural abnormalities in people with multiple sclerosis. *Neurology* 2021; e2007-e2019.

Burnham KP and Anderson DR. (2002). *Model selection and multimodel inference: a practical information-theoretic approach* (2nd Edition). Springer New York, NY. https://doi.org/10.1007/b97636

Calabrese M, Seppi D, Romualdi C, et al. Gray matter pathology in MS: a 3-year longitudinal study in a pediatric population. *AJNR Am J Neuroradiol* 2012; 33; 1507-1511.

Caranova M, Soares JF, Batista S. A systematic review of microstructural abnormalities in multiple sclerosis detected with NODDI and DTI models of diffusion-weighted magnetic resonance imaging. *Magn Reson Imaging* 2023; 104; 61-71.

Choi YJ, Lee EJ, Lee JE. The fornix: functional anatomy, normal neuroimaging, and various pathological conditions. *iMRI* 2021; 25; 59.

Concha L, Gross DW, Beaulieu C. Diffusion tensor tractography of the limbic system. *AJNR Am J Neuroradiol* 2005; 26; 2267-2274.

Concha L, Gross DW, Wheatley BM, et al. Diffusion tensor imaging of time-dependent axonal and myelin degradation after corpus callosotomy in epilepsy patients. *NeuroImage* 2006; 32; 1090-1099.

Concha L. A macroscopic view of microstructure: using diffusion-weighted images to infer damage, repair, and plasticity of white matter. *Neuroscience* 2014; 276; 14-28.

Coupé P, Tourdias T, Linck P, et al. lesionBrain: an online tool for white matter lesion segmentation. International Workshop on Patch-based Techniques in Medical Imaging (MICCAI), Sept 2018, Grenade, Spain, pp. 95-103.

De Meo E, Meani A, Moiola L, et al. Dynamic gray matter volume changes in pediatric multiple sclerosis: a 3.5 year MRI study. *Neurology* 2019; 92; e1723.

De Meo E, Storelli L, Moiola L, et al. In vivo gradients of thalamic damage in paediatric multiple sclerosis: a window to pathology. *Brain* 2021; 144; 186-197.

Dineen RA, Bradshaw CM, Constantinescu CS, et al. Extra-hippocampal subcortical limbic involvement predicts episodic recall performance in multiple sclerosis. *PLoS One* 2012; 7; e44942.

Dineen RA, Vilisaar J, Hlinka J, et al. Disconnection as a mechanism for cognitive dysfunction in multiple sclerosis. *Brain* 2009; 132; 239-249.

Donohue K, Cox JL, Dwyer MG, et al. No regional gray matter atrophy differences between pediatric- and adult- onset relapsing-remitting multiple sclerosis. *J Neuroimaging* 2014; 24; 63-67.

Douet V, Chang L, Pritchett A, et al. Schizophrenia-risk variant rs6994992 in the neuregulin-1 gene on brain developmental trajectories in typically developing children. *Transl Psychiatry* 2014b; 4; e392.

Douet V, Chang L. Fornix as an imaging marker for episodic memory deficits in healthy aging and in various neurological disorders. *Front Aging Neurosci* 2014a; 6; 343.

Edinger A, Habibi M. The evolution of multiple sclerosis disease-modifying therapies: an update for pharmacists. *Am J Health Syst Pharm* 2024; 81; 37-55.

Eshaghi A, Marinescu RV, Young AL, et al. Progression of regional grey matter atrophy in multiple sclerosis. *Brain* 2018; 141; 1665-1667.

Fabri TL, Datta R, O'Mahony J, et al. Memory, processing of emotional stimuli, and volume of limbic structures in pediatric-onset multiple sclerosis. *Neuroimage Clin* 2021; 31; 102753.

Fadda G, Brown RA, Magliozzi R, et al. A surface-in gradient of thalamic damage evolves in pediatric multiple sclerosis. *Ann Neurol* 2019; 85; 340-351.

Fadda G, de la Parra AC, O'Mahony J, et al. Deviation from normative whole brain and deep gray matter growth in children with MOGAD, MS, and monophasic seronegative demyelination. *Neurology* 2023; 101; e425-e437.

Fenu G, Lorefice L, Loi L, et al. Adult brain volume in multiple sclerosis: the impact of paediatric onset. *Mult Scler Relat Disord* 2018; 21; 103-107.

Filippi M, Cercignani M, Inglese M, et al. Diffusion tensor magnetic resonance imaging in multiple sclerosis. *Neurology* 2001; 56; 304-311.

Fink F, Eling P, Rischkau E, et al. The association between the California Verbal Learning Test performance and fibre impairment in multiple sclerosis: evidence from diffusion tensor imaging. *Mult Scler* 2010; 16; 332-341.

Fletcher E, Raman M, Heubner P, et al. Loss of fornix white matter volume as a predictor of cognitive impairment in cognitively normal elderly individuals. *JAMA Neurol* 2013; 70; 1389-1395.

Foster CM, Kennedy KM, Hoagey DA, et al. The role of hippocampal subfield volume and fornix microstructure in episodic memory across the lifespan. *Hippocampus* 2019; 29; 1206-1223.

Fritz NE, Edwards EM, Ye C, et al. Cerebellar contributions to motor and cognitive control in multiple sclerosis. *Arch Phys Med Rehabil* 2022; 103; 1592-1599.

Fuentes A, Collins DL, Garcia-Lorenzo D, et al. Memory performance and normalized regional brain volumes in patients with pediatric-onset multiple sclerosis. *J Int Neuropsychol Soc* 2012; 18; 471-480.

Ghasemi N, Razavi S, Nikzad E. Multiple sclerosis: pathogenesis, symptoms, diagnoses and cell-based therapy. *Cell J* 2017; 19; 1-10.

Giorgio A, Zhang J, Stromillo ML, et al. Pronounced structural and functional damage in early adult pediatric-onset multiple sclerosis with no or minimal clinical disability. *Front Neurol* 2017; 8; 608.

Good CD, Johnsrude IS, Ashburner J, et al. A voxel-based morphometric study of ageing in 465 normal adult human brains. *Neuroimage* 2001; 14; 21-36.

Gorman MP, Healy BC, Polgar-Turcsanyi M, et al. Increased relapse rate in pediatric-onset compared with adult-onset multiple sclerosis. *Arch Neurol* 2009; 66; 54-59.

Govindarajan ST, Liu Y, Corral MAP, et al. White matter correlates of slowed information processing speed in unimpaired multiple sclerosis patients with young age onset. *Brain Imaging Behav* 2021; 15; 1460-1468.

Hemond CC, Bakshi R. Magnetic resonance imaging in multiple sclerosis. *Cold Spring Harb Perspect Med* 2018; 8; a028969.

Houtchens MK, Benedict RHB, Killiany R, et al. Thalamic atrophy and cognition in multiple sclerosis. *Neurology* 2007; 69; 1213-1223.

Huang J, Liu Y, Zhao T, et al. White matter microstructural alterations in clinically isolated syndrome and multiple sclerosis. *J Clin Neurosci* 2018; 53; 27-33.

Jang SH, Cho SH, Chang MC, et al. Age-related degeneration of the fornix in the human brain: a diffusion tensor imaging study. *Int J Neurosci* 2011; 121;94-100.

Jenkinson M, Beckmann CF, Behrens TEJ, et al. FSL. *NeuroImage* 2012; 62; 782-790.

Kalron A, Menascu S, Givon U, et al. Is the walk ratio a window to the cerebellum in multiple sclerosis? A structural magnetic resonance imaging study. *Eur J Neurol* 2020; 27; 454-460.

Kamali A, Milosavljevic S, Gandhi A, et al. The cortico-limbo-thalamo-cortical circuits: an update to the original Papez Circuit of the human limbic system. *Brain Topogr* 2023; 36; 371-389.

Kellner E, Dhital B, Kiselev VG, et al. Gibbs-ringing artifact removal based on local subvoxel-shifts. *Magn Reson Med* 2016; 76; 1574-1581.

Kerbrat A, Aubert-Broche B, Fonov V, et al. Reduced head and brain size for age and disproportionately smaller thalami in child-onset MS. *Neurology* 2012; 78; 194-201.

Kern KC, Ekstrom AD, Suthana NA, et al. Fornix damage limits verbal memory functional compensation in multiple sclerosis. *Neuroimage* 2012; 59; 2932-2940.

Kern KC, Gold SM, Lee B, et al. Thalamic-hippocampal-prefrontal disruption in relapsing-remitting multiple sclerosis. *Neuroimage Clin* 2015; 8; 440-447.

Keser Z, Hasan KM, Mwangi B, et al. Limbic pathway correlates of cognitive impairment in multiple sclerosis. *J Neuroimaging* 2017; 27; 37-42.

Keser Z, Hasan KM, Mwangi B. Quantitative limbic system mapping of main cognitive domains in multiple sclerosis. *Front Neurol* 2018; 9; 132.

Klawiter EC, Schmidt RE, Trinkaus K, et al. Radial diffusivity predicts demyelination in ex vivo multiple sclerosis spinal cords. *NeuroImage* 2011; 55; 1454-1460.

Klistorner A, Wang C, Yiannikas C, et al. Diffusivity in the core of chronic multiple sclerosis lesions. *PLoS One* 2018; 13; e0194142.

Klistorner A, Wang C, Yiannikas C, et al. Progressive injury in chronic multiple sclerosis lesions is gender specific: a DTI study. *PLoS One* 2016; 11; e0149245.

Koenig K, Sakai KE, Lowe MJ, et al. Hippocampal volume is related to cognitive decline and fornical diffusion measures in multiple sclerosis. *Magn Reson Imaging* 2014; 32; 354-358.

Koenig KA, Sakaie KE, Lowe MJ, et al. High spatial and angular resolution diffusion-weighted imaging reveals forniceal damage related to memory impairment. *Magn Reson Imaging* 2013; 31; 695-699.

Koubiyr I, Krijnen EA, Eijlers AJ, et al. Longitudinal fiber-specific white matter damage predicts cognitive decline in multiple sclerosis. *Brain Commun* 2024; 6; fca018

Kwong KK, McKinstry RC, Chein D, et al. CSF-suppressed quantitative single-shot diffusion imaging. *Magn Reson Med* 1991; 21; 157-163.

Le Bihan D, Breton E, Lallemand D, et al. MR imaging of intravoxel incoherent motions: application to diffusion and perfusion in neurologic disorders. *Radiology* 1986; 161; 401-407.

Lebel C, Gee M, Camicioli R, et al. Diffusion tensor imaging of white matter tract evolution over the lifespan. *Neuroimage* 2012; 60; 340-352.

Longoni G, Brown RA, MomayyezSiahkal P, et al. White matter changes in paediatric multiple sclerosis and monophasic demyelinating disorders. *Brain* 2017; 140; 1300-1315.

Manjón JV, Coupé P. volBrain: an online MRI brain volumetry system. *Front Neuroinform* 2016; 10; 30.

McKay KA, Manouchehrinia A, Berrigan L, et al. Long-term cognitive outcomes in patients with pediatric-onset vs adult-onset multiple sclerosis. *JAMA Neurol* 2019; 76; 1028-1034.

McKay KA, Wickström R, Hillert J, et al. Cerebrospinal fluid markers in incident pediatric-onset multiple sclerosis: a nationwide study. Sci Rep 2021; 11; 18528.

Mesaros S, Rocca MA, Absinta M, et al. Evidence of thalamic gray matter loss in pediatric multiple sclerosis. *Neurology* 2008; 70; 1107-1112.

Metzler-Baddeley C, Hunt S, Jones DK, et al. Temporal association tracts and the breakdown of episodic memory in mild cognitive impairment. *Neurology* 2012; 79; 2233-2240.

Meyer-Moock S, Feng YS, Maeurer M, et al. Systematic literature review and validity evaluation of the Expanded Disability Status Scale (EDSS) and the Multiple Sclerosis Functional Composite (MSFC) in patients with multiple sclerosis. *BMC Neurol* 2014; 14; 58.

Mezzapesa DM, Rocca MA, Falini A, et al. A preliminary diffusion tensor and magnetization transfer magnetic resonance imaging study of early-onset multiple sclerosis. *Arch Neurol* 2004; 61; 366-368.

Michielse S, Coupland N, Camicioli R, et al. Selective effects of aging on brain white matter microstructure: a diffusion tensor imaging tractography study. *Neuroimage* 2010; 52; 1190-1201.

Mori S, Crain BJ, Chacko VP, et al. Three-dimensional tracking of axonal projections in the brain by magnetic resonance imaging. *Ann Neurol* 1999; 45; 265-269.

Multiple Sclerosis International Federation (MFIS). *Atlas of MS*. 3rd Edition. September 2020.

Narvacan K, Treit S, Camicioli R, et al. Evolution of deep gray matter volumes across the human lifespan. *Hum Brain Mapp* 2017; 38; 3771-3790.

Nygaard GO, Celius EG, de Rodez Benavent SA, et al. A longitudinal study of disability, cognition and gray matter atrophy in early multiple sclerosis patients according to evidence of disease activity. *PLos One* 2015; 10; e0135974.

Pajevic S, Pierpaoli C. Color schemes to represent the orientation of anisotropic tissues from diffusion tensor data: application to white matter fiber tract mapping in the human brain. *Magn Reson Med* 1999; 42; 526-540.

Papez JW. A proposed mechanism of emotion. *J Neuropsychiatry Clin Neurosci* 1995; 7; 103-112.

Pardini M, Brown JWL, Magliozzi R, et al. Surface-in pathology in multiple sclerosis: a new view on pathogenesis? *Brain* 2021; 144; 1646-1654

Preziosa P, Rocca MA, Mesaros S, et al. Intrinsic damage to the major white matter tracts in patients with different clinical phenotypes of multiple sclerosis: a voxelwise diffusion-tensor MR study. *Radiology* 2011; 260; 541-550.

Rocca MA, Morelli ME, Amato MP, et al. Regional hippocampal involvement and cognitive impairment in pediatric multiple sclerosis. *Mult Scler* 2016a; 22; 628-640.

Rocca MA, Sonkin M, Copetti M, et al. Diffusion tensor magnetic resonance imaging in very early onset pediatric multiple sclerosis. *Mult Scler* 2016b; 22; 620-627.

Roosendaal SD, Geurts JJG, Vrenken H, et al. Regional DTI differences in multiple sclerosis patients. *Neuroimage* 2009; 44; 1397-1403.

Rudebeck SR, Scholz J, Millington R, et al. Fornix microstructure correlates with recollection but not familiarity memory. *J Neurosci* 2009; 29; 14987-14992.

Sasson E, Doniger GM, Pasternak O, et al. White matter correlates of cognitive domains in normal aging with diffusion tensor imaging. *Front Neurosci* 2013; 7; 32.

Sicotte NL, Kern KC, Giesser BS, et al. Regional hippocampal atrophy in multiple sclerosis. *Brain* 2008; 131; 1134-1141.

Simmonds D, Hallquist MN, Asato M, et al. Developmental stages and sex differences of white matter and behavioral development through adolescence: a longitudinal diffusion tensor imaging (DTI) study. *Neuroimage* 2014; 92; 356-368.

Sinnecker T, Ruberte E, Schadelin S, et al. New and enlarging white matter lesions adjacent to the ventricular system and thalamic atrophy are independently associated with lateral ventricle enlargement in multiple sclerosis. *J Neurol* 2020; 267; 192-202.

Smerbeck AM, Parrish J, Yeh EA, et al. Regression-based pediatric norms for the brief visuospatial memory test: revised and the symbol digit modalities test. *Clin Neuropsychol* 2011; 25; 402-412.

Smith SM. Fast robust automated brain extraction. *Hum Brain Mapp* 2002; 17; 143-155.

Solar KG, Treit S, Beaulieu C. High resolution diffusion tensor imaging of the hippocampus across the healthy lifespan. *Hippocampus* 2021; 31; 1271-1284.

Song SK, Sun SW, Ju WK, et al. Diffusion tensor imaging detects and differentiates axon and myelin degeneration in mouse optic nerve after retinal ischemia. *Neuroimage* 2003; 20; 1714-1722.

Song SK, Sun SW, Ramsbottom MJ, et al. Dysmyelination revealed through MRI as increased radial (but unchanged axial) diffusion of water. *NeuroImage* 2002; 17; 1429-1436.

Stadlbauer A, Salomonowitz E, Strunk E, et al. Quantitative diffusion tensor fiber tracking of age-related changes in the limbic system. *Eur Radiol* 2008; 18; 130-137.

Stejskal EO, Tanner JE. Spin diffusion measurements: spin echoes in the presence of a time-dependent field gradient. *J Chem Phys* 1965; 42; 288-292.

Sullivan EV, Rohlfing T, Pfefferbaum A. Quantitative fiber tracking of lateral and interhemispheric white matter systems in normal aging: relations to timed performance. *Neurobiol Aging* 2010; 31; 464-481.

Syc SB, Harrison DM, Saidha S, et al. Quantitative MRI demonstrates abnormality of the fornix and cingulum in multiple sclerosis. *Mult Scler Int* 2013; 838719.

Thompson AJ, Banwell BL, Barkhof F, et al. Diagnosis of multiple sclerosis: 2017 revisions of the McDonald criteria. *Lancet Neurol* 2018; 17; 162-173.

Till C, Deotto A, Tipu V, et al. White matter integrity and math performance in pediatric multiple sclerosis: a diffusion tensor imaging study. *Neuroreport* 2011b; 22; 1005-1009.

Till C, Ghassemi R, Aubert-Broche B, et al. MRI correlates of cognitive impairment in childhood-onset multiple sclerosis. *Neuropsychology* 2011a; 25; 319-332.

Tillema JM, Leach J, Pirko I. Non-lesional white matter changes in pediatric multiple sclerosis and monophasic demyelinating disorders. *Mult Scler* 2012; 18; 1754-1759.

Tortorella P, Rocca MA, Mezzapesa DM, et al. MRI quantification of gray and white matter damage in patients with early-onset multiple sclerosis. *J Neurol* 2006; 253; 903-907.

Tournier JD, Mori S, Leemans A. Diffusion Tensor imaging and beyond. *Magn Reson Med* 2011; 65; 1532-1556.

Tournier JD, Smith R, Raffelt D, et al. MRtrix3: a fast, flexible and open software framework for medical image processing and visualization. *NeuroImage* 2019; 202; 116137.

Tovar-Moll F, Evangelou IE, Chiu AW, et al. Thalamic involvement and its impact on clinical disability in patients with multiple sclerosis: a diffusion tensor imaging study at 3T. *AJNR Am J Neuroradiol* 2009; 30; 1380-1386.

Treit S, Stolz E, Rickard JN, et al. Lifespan volume trajectories from non-harmonized T1-weighted MRI do not differ after site correction based on traveling human phantoms. *Front Neurol* 2022; 13; 826564.

Tustison NJ, Avants BB, Cook PA, et al. N4ITK: improved N3 bias correction. *IEEE Trans Med Imaging* 2010; 29; 1310-1320.

Valdés Cabrera D, Blevins G, Smyth P, et al. High-resolution diffusion tensor imaging and T2 mapping detect regional changes within the hippocampus in multiple sclerosis. *NMR Biomed* 2023; e4952.

Valdés Cabrera D, Smyth P, Blevins G, et al. Diffusion imaging of the fornix and interconnected limbic deep grey matter is linked to cognitive impairment in multiple sclerosis. *Eur J Neurosci* 2022; 55; 277-294.

Valdés Cabrera D, Stobbe R, Smyth P, et al. Diffusion tensor imaging tractography reveals altered fornix in all diagnostic subtypes of multiple sclerosis. *Brain Behav* 2020; 10; e01514.

Veraart J, Novikov DS, Christiaens D, et al. Denoising of diffusion MRI using random matrix theory. *NeuroImage* 2016; 142; 394-406.

Veraart J, Sijbers J, Sunaert S, et al. Weighted linear least squares estimation of diffusion MRI parameters: strengths, limitations, and pitfalls. *NeuroImage* 2013; 81; 335-346.

Virtanen P, Gommers R, Oliphant TE, et al. SciPy 1.0: Fundamental Algorithms for Scientific Computing in Python. *Nat Methods* 2020; 17; 261-272.

Vishwas MS, Chitnis T, Pienaar R, et al. Tract-based analysis of callosal, projection, and association pathways in pediatric patients with multiple sclerosis: a preliminary study. *AJNR Am J Neuroradiol* 2010; 31; 121-128.

Vishwas MS, Healy BC, Pienaar R, et al. Diffusion tensor analysis of pediatric multiple sclerosis and clinically isolated syndromes. *AJNR Am J Neuroradiol* 2013; 34; 417-423.

Vos SB, Jones DK, Viergever MA, et al. Partial volume effect as a hidden covariate in DTI analyses. *Neuroimage* 2011; 55; 1566-1576.

Vrenken H, Pouwels PJW, Geurts JJG, et al. Altered diffusion tensor in multiple sclerosis normal-appearing brain tissue: cortical diffusion changes seem related to clinical deterioration. *J Magn Reson Imaging* 2006; 23; 628-636.

Waubant E, Chabas D, Okuda DT, et al. Difference in disease burden and activity in pediatric patients on brain magnetic resonance imaging at time of multiple sclerosis onset vs adults. *Arch Neurol* 2009; 66; 967-971.

Weier K, Till C, Fonov V, et al. Contribution of the cerebellum to cognitive performance in children and adolescents with multiple sclerosis. *Mult Scler* 2016; 22; 599-607.

Welton T, Kent D, Constantinescu CS, et al. Functionally relevant white matter degradation in multiple sclerosis: a tract-based spatial metaanalysis. *Radiology* 2015; 275; 89-96.

Westin CF, Peled S, Gudbjartsson H, et al. Geometrical diffusion measures for MRI from tensor basis analysis. *ISMRM* 1997; 5; 1742.

Wilbur C, Yeh EA. Improving outcomes in pediatric multiple sclerosis: current and emerging treatments. *Paediatr Drugs* 2019; 21; 137-152.

Yeh EA, Weinstock-Guttman B, Ramanathan M, et al. Magnetic resonance imaging characteristics of children and adults with paediatric-onset multiple sclerosis. *Brain* 2009; 132; 3392-3400.

Yu HJ, Christodoulou C, Bhise V, et al. Multiple white matter tract abnormalities underlie cognitive impairment in RRMS. *Neuroimage* 2012; 59; 3713-3722.

Zhou F, Zee CS, Gong H, et al. Differential changes in deep and cortical gray matters of patients with multiple sclerosis: a quantitative magnetic resonance imaging study. *J Comput Assist Tomogr* 2010; 34; 431-436.

Appendix A: Volumetric Studies in POMS Children and Adolescents (ordered chronologically since 2008)

Author, journal, year	**Subjects**	**Protocol**	**Core Findings** **L-left, R-right, N.d.-no difference**
Mesaros, *Neurology*, 2008	28 POMS 14.4 years (7-16)	1.5T 1 mm^3 isotropic	N.d. TBV, ICV, total GM MS vs controls ↓ Th ↓Th ∝ lesion volume (Wallerian degeneration?)
Aubert-Broche, *NeuroImage*, 2011	30 POMS 15.4 years RRMS	1.5T 1 mm^3 isotropic or 0.98x0.98x1.5 mm^3	↓ Th, CC (splenium), GP ↑ LVs ↓CC (splenium) ∝ lesion volume
Till, *Neuropsychology*, 2011a	35 POMS 16.3 years	1.5T 0.98x0.98x1.5 mm^3	↓ Th (12%), TBV (4%), total GM (4%) volumes CC area ∝ EDSS Th, TBV, total GM, CC ∝ lesion volume Th volume ∝ IQ, SDMT
Calabrese, *AJNR Am J Neuroradiol*, 2012	35 POMS 13.2 years (8-16)	1.5T 120 1.2 mm axial slices	**Baseline:** N.d. GMf MS vs controls **Follow-up (3 years):** ΔGMf MS > ΔGMf controls ΔGMf ∝ cortical lesion volume
Fuentes, *J Int*	32 POMS	1.5T	↓TBV, Amyg (7%), Th (14%)

Neuropsychol Soc, 2012	16.3 years (11-19) RRMS	0.98x0.98x1.5 mm^3	N.d. Hippo MS vs controls Th, Hippo $\propto$ IQ TBV, Th, Hippo, Amyg (weak) $\propto$ memory performance Memory performance N.d. MS vs controls
Kerbrat, *Neurology*, 2012	38 POMS 15.2 years (10.1-19.6) RRMS	1.5T 0.98x0.98x1.5 mm^3	$\downarrow$ICV, TBV, total WM, total GM, deep GM (Th, GP) $\downarrow$TBV, Th $\propto$ lesion volume
Aubert-Broch e, *Neurology*, 2014	36 POMS 13.8 years (5.1-17.7) Longitudinal (2-11 scans, 1.1-7.7 year follow-up)	1.5T 0.98x0.98x1.5 mm^3	Failure of age-expected TBV, Th, GP volumes N.d. Caud, Put $\downarrow$Th $\propto$ lesion volume
Rocca, *Mult Scler*, 2016a	53 POMS 15.1 years (8-18)	3T 0.89x0.89x0.8 mm^3	$\downarrow$TBV, total GM, Hippo (total and regional) Hippo atrophy (only regional) $\propto$ lesion volume, cognitive impairment, attention, language
Weier, *Mult Scler*, 2016	28 POMS 16.2 years RRMS	1.5T 0.98x0.98x1.5 mm^3	N.d. Cb MS vs controls Cb (posterior lobe) $\propto$ SDMT, vocabulary Cb (infratentorial) lesion volume $\propto$ vocabulary
Bartels, *Mult Scler*, 2019	37 POMS 15 years (10-17)	1.5T 0.89-2.5 mm slice thickness	**Baseline:** $\downarrow$TBV (6%), total GM (8%), total WM (4%) $\uparrow$CSF (25%) **Follow-up (2 years):**

			↓TBV (7%), total GM (7%), total WM (7%) ↑CSF (40%) (N.d. total GM, no progression) ↓TBV (baseline and follow-up) ∝ lesion volume, EDSS ↑CSF (baseline and follow-up) ∝ lesion volume, relapses
De Meo, *Neurology*, 2019	68 POMS 15.1 years RRMS (baseline) 30 POMS 15.5 years RRMS (3.5 year follow-up)	3T 0.89x0.89x0.8 mm^3	**Baseline:** ↓ Bg, FL, PL, TL, OL, Cb ↓ Hippo, Th, Prec, Insula, Cn, Amyg GM atrophy (Th, L Cn, L IFg, R Prec) ∝ EDSS GM atrophy (CingC, Th, FL, TL, PL, OL, Cb) ∝ worse IQ GM atrophy (Th, Cn, FL, TL) ∝ lesion volume **Follow-up (3.5 years):** ↓Th, Put, Prec, FL, PL, TL, OL, CingC, Insula, Hippo, Amyg, cerebellum (GM atrophy progression) GM atrophy progression (CingC, FL, PL, TL, OL) ∝ worse IQ GM atrophy progression (Th) ∝ lesion volume
Fadda, *Ann Neurol*, 2019	27 POMS 12-13 years	1.5T 0.98x0.98x1.5 mm^3	↓Th (especially regions adjacent to WM) Th atrophy ∝ distance from ventricular CSF
Fabri, *Neuroimage Clin*, 2021	65 POMS 18.3 years (8-27)	3T 0.9x0.9x1	↓Hippo (7%), Amyg (5%), Th (13%), TBV (2%), total GM (3%)

		mm^3	Hippo and Th volumes ∝ word memory performance
Fadda, *Neurology*, 2023	26 POMS 14.6 years (13.6-15.6) Longitudinal (median 5.1 years)	1.5T 0.98x0.98x1.5 mm^3 or 3T 0.94x0.94x1 mm^3	Failure of age-expected Th, GP volumes

Amg, amygdala; Bg, basal ganglia; Caud, caudate; Cb, cerebellum; CC, corpus callosum; CingC, cingulate cortex; Cn, caudate nucleus; FL, frontal lobe; GMf, gray matter fraction; GP, globus pallidus; Hippo, hippocampus; ICV, intracranial volume; IFg, frontal gyrus; LVs, lateral ventricles; OL, occipital lobe; PL, parietal lobe; Prec, precuneus; Put, putamen; TBV, total brain volume; Th, thalamus; TL, temporal lobe

Appendix B: DTI Studies in POMS Children and Adolescents (ordered chronologically since 2004)

Author, journal, year	**Subjects**	**Protocol**	**DTI Analysis**	**Core Findings L-left, R-right, N.d.-no difference**
Mezzapesa, *Arch Neurol*, 2004	13 POMS 14.1 years (7-16)	1.5T 24 5 mm axial slices 8 b=1044 s/mm^2	Voxel-based	**NABT:** ↑MD
Tortorella, *J Neurol*, 2006	23 POMS 14.1 years (7-16)	1.5T 10 5 mm axial slices 8 b=1044 s/mm^2	Voxel-based	**NAWM:** ↑MD, ↓FA **NAGM:** N.d. MS vs controls
Absinta, *J Neurol Neurosurg Psychiatry*, 2010	30 POMS 14.7 years (7-18) RRMS	1.5T 10 5 mm axial slices 8 b=1044 s/mm^2	Voxel-based	**NAWM:** ↑MD, ↓FA **GM:** N.d. MS vs controls
Vishwas, *AJNR Am J Neuroradiol*, 2010	10 POMS 16.6 years (15.1-18) RRMS	1.5T 1.72x1.72x6 mm^3 12-30 b=1000 s/mm^2 (8 patients) 2.29x2.29x3 mm^3 29 b=1000 s/mm^2	ROI, tract-based	**CC ROI**: ↑ADC, ↓FA, NAWM (↑ADC genu, splenium; ↓FA splenium) **PLIC ROI**: ↑ADC, ↓FA, NAWM (↑ADC) **CP ROI:** ↑ADC, NAWM (↑ADC) **LAF ROI:** ↑ADC, ↓FA, NAWM (↑ADC/↓FA SLF, IFOF, UF)

		(1 patient) 2.2 mm^3 isotropic 29 b=1000 s/mm^2 (1 patient)		**CC TB:** ↑ADC, ↓FA, NAWM (↑ADC genu, splenium; ↓FA splenium) **PLIC TB:** ↑ADC, ↓FA, NAWM (↑ADC/↓FA) **CP TB:** ↑ADC, ↓FA, NAWM (↑ADC/↓FA) **LAF TB:** ↑ADC, ↓FA, NAWM (↑ADC/↓FA SLF, IFOF, UF)
Bethune, *J Neurol Sci*, 2011	33 POMS 16.1 years	1.5T 32 5 mm axial slices 25 b=1000 s/mm^2	ROI	**CC NAWM:** ↑MD (posterior body), ↓FA (genu, splenium), avg FA ∝ lesion volume, ↑MD/↓FA ∝ worse VM/SDMT **FL NAWM:** N.d. MS vs controls **PL NAWM:** ↓FA L/R **TL NAWM:** ↑MD L, ↓FA L/R **OL NAWM:** ↓FA L/R **Th NAWM:** N.d. Avg hemispheric NAWM FA ∝ lesion volume
Till, *Neuroreport*, 2011b (follow-up study to Bethune, *J Neurol Sci*, 2011)	31 POMS 16.4 years	1.5T 32 5 mm axial slices 25 b=1000 s/mm^2	ROI	**CC:** avg FA ∝ better math performance **FL:** R avg FA ∝ better math performance **PL:** R avg FA ∝ better math performance

Tillema, *Mult Scler*, 2012	18 POMS 15.4 years	1.5 T 3 mm^3 isotropic (interpolated to 1.5x1.5x3 mm^3) 15 b=1000 s/mm^2	ROI	**CC NAWM:** ↓FA, ↓AD, ↑RD **IC NAWM:** ↓FA
Blaschek, *AJNR Am J Neuroradiol*, 2013	14 POMS 15.1 years (12-17)	3T 1.8x1.8x4 mm^3 20 b=1000 s/mm^2	TBSS, mean WM skeleton	↓FA (splenium CC, R TL, L/R PL) ↑MD (CC, SLF, Fx, CR, CST, UF) ↑AD < ↑RD Mean skeletal FA $\propto$ disease duration
Vishwas, *AJNR Am J Neuroradiol*, 2013	20 POMS 15.9 years (8.4-18)	1.5T 1.72x1.72x6 mm^3 or 0.86x0.86x2.2 mm^3 6-29 b=1000 s/mm^2	ROI, tract-based	**CC ROI:** ↑ADC, ↓FA **CP ROI:** ↑ADC, ↓FA **PLIC ROI:** ↑ADC, ↓FA **LAF ROI:** ↑ADC, ↓FA **CC TB:** ↑ADC, ↓FA, NAWM (↑ADC/↓FA splenium, anterior/posterior midbody) **CP TB:** ↑ADC, ↓FA **PLIC TB:** ↑ADC, ↓FA **LAF TB:** ↑ADC, ↓FA NAWM (↑ADC/↓FA SLF, IFOF, UF)
Akbar,	19 POMS	3T	TBSS, mean	**WM:** ↓FA (entire skeleton, CC,

PLoS One, 2016	19 years (12-24)	2.0x2.0x3.0 mm^3 64 b=1000 s/mm^2	WM skeleton	posterior ThR, ILF, IFOF, CR), ↑MD, ↑RD, N.d. AD MS vs controls FA, AD, RD ∝ lesion volume, thalamic volume
Rocca, *Mult Scler*, 2016b	11 POMS 11.1 years RRMS (Cohort 1) 11 POMS 13.4 years RRMS (Cohort 2)	1.5 T 1x1x5 mm^3 25 b=1000 s/mm^2 (Cohort 1) 3T 2.14x2.6x2.3 mm^3 35 b=900 s/mm^2 (Cohort 2)	Probabilistic Tractography	Cohort 1 **CC NAWM:** ↑MD 5%, ↓FA 5% **SLF NAWM:** L/R ↑MD (L 5%, R 5%), L/R ↓FA (L 6%, R 8%) **CST NAWM:** L ↑MD (4%) **ILF NAWM:** R ↓FA (7%) Cohort 2 **CC NAWM:** ↑MD 4% , ↓FA 7% **SLF NAWM:** L/R ↑MD (L 3%, R 3%), L/R ↓FA (L 4%, R 4%) **CST NAWM:** L/R ↓FA (L 3%, R 5%) **ILF NAWM:** L ↓FA (5%) Avg CC NAWM FA ∝ lesion volume HC age ∝ ↑FA and ↓MD (correlation lost in POMS)
Longoni, *Brain*, 2017	58 POMS <20 years	1.5 T 2x2x5 mm^3 25 b=1000 s/mm^2	Voxel-based, NAWM mask	↑MD (females only) with age ↓FA with age
Bartlett, *J Neuroimaging*, 2019	15 POMS 17.9 years	3T 2.5 mm^3 isotropic 64 b=1000 s/mm^2	ROI	**CC:** ↓FA **TL:** ↓FA **Th:** ↑FA WM FA (CC, UF, TL, OL) ∝ reaction time (but not BICAMS -

				SDMT, BVMT-R, CVLT-II, RAVLT)
De Meo, *Brain*, 2021	70 15.6 years	3.0T 55 2.3 mm axial slices 35 b=900 s/mm^2	TBSS, mean WM skeleton	**Th:** ↓FA (whole, WM), ↑MD (WM) ↓FA and ↑MD ∝ bands closer to CSF
Govindarajan, *Brain Imaging Behav*, 2021	25 POMS 20.8 years	3T 2.5 mm^3 isotropic 64 b=1000 s/mm^2	Voxel-wise analysis, WM tract atlas (avg FA, MD, RD, AD)	**AR:** ↓FA, ↑RD **CC:** ↓FA, ↑MD, ↑RD, ↑AD **Cing:** ↓FA, ↑MD, ↑RD **CST:** ↓FA, ↑MD, ↑RD, ↑AD **IFOF:** ↓FA, ↑RD **SFOF:** ↓FA, ↑MD, ↑RD, ↑AD **OR:** ↓FA, ↑MD, ↑RD, ↑AD **SLF:** ↓FA, ↑MD, ↑RD, ↑AD MD, RD, AD (CC, L CST, L SFOF) ∝ worse processing speed (SDMT)

AR, acoustic radiation; BICAMS, Brief International Cognitive Assessment for MS; CC, corpus callosum; Cing, cingulum; CP, cerebral peduncle; CR, corona radiata; CST, corticospinal tract; FL, frontal lobe; Fx, fornix; HC, healthy control; IC, internal capsule; IFOF, inferior fronto-occipital fasciculus; ILF, inferior longitudinal fasciculus; LAF, long association fibers; NABT, normal-appearing brain tissue; OL, occipital lobe; OR, optic radiation; PL, parietal lobe; PLIC, posterior limb of internal capsule; RAVLT, Rey Auditory Verbal Learning Test; SFOF, superior fronto-occipital fasciculus; SLF, superior longitudinal fasciculus; TB, tract-based; Th, thalamus; ThR, thalamic radiation; TL, temporal lobe; UF, uncinate fasciculus; VM, Visual Matching

Appendix C:

Pediatric Fatigue: Participants must answer 1-5 for each statement; the total score is the number sum of all answers.

Neuro-QOL Item Bank v2.1 –Pediatric Fatigue

Pediatric Fatigue

Please respond to each question or statement by marking one box per row.

	In the past 7 days…	None of the time	A little bit of time	Some of the time	Most of the time	All of the time
NQFTGped01	I felt tired……..	☐ 1	☐ 2	☐ 3	☐ 4	☐ 5
NQFTGped04	I had trouble starting things because I was too tired……..	☐ 1	☐ 2	☐ 3	☐ 4	☐ 5
NQFTGped05	I had trouble finishing things because I was too tired……..	☐ 1	☐ 2	☐ 3	☐ 4	☐ 5
NQFTGped06	I needed to sleep during the day……	☐ 1	☐ 2	☐ 3	☐ 4	☐ 5
NQFTGped08	Being tired made it hard to play or go out with my friends as much as I would like...	☐ 1	☐ 2	☐ 3	☐ 4	☐ 5
NQFTGped11r1	I was too tired to eat……..	☐ 1	☐ 2	☐ 3	☐ 4	☐ 5
NQFTGped12	Being tired makes me sad……..	☐ 1	☐ 2	☐ 3	☐ 4	☐ 5
NQFTGped13	Being tired makes me mad……	☐ 1	☐ 2	☐ 3	☐ 4	☐ 5
NQFTGped07	I got upset by being too tired to do things I wanted to do……	☐ 1	☐ 2	☐ 3	☐ 4	☐ 5
NQFTGped09	I needed help doing my usual things at home……..	☐ 1	☐ 2	☐ 3	☐ 4	☐ 5
NQFTGped10	I felt weak……..	☐ 1	☐ 2	☐ 3	☐ 4	☐ 5

English
June 13, 2014

Page **1** of **1**

Modified Fatigue Impact Scale (MFIS): Participants must answer 0-4 for each statement; the total score is the number sum of all answers.

Modified Fatigue Impact Scale (MFIS)

Fatigue is a feeling of physical tiredness and lack of energy that many people experience from time to time. But people who have medical conditions like MS experience stronger feelings of fatigue more often and with greater impact than others.

Following is a list of statements that describe the effects of fatigue. Please read each statement carefully, the circle the one number that best indicates how often fatigue has affected you in this way during the past 4 weeks. (If you need help in marking your responses, tell the interviewer the number of the best response.) Please answer every question. If you are not sure which answer to select choose the one answer that comes closest to describing you. Ask the interviewer to explain any words or phrases that you do not understand.

Because of my fatigue during the past 4 weeks

		Never	Rarely	Sometimes	Often	Almost Always
1.	I have been less alert.	0	1	2	3	4
2.	I have had difficulty paying attention for long periods of time.	0	1	2	3	4
3.	I have been unable to think clearly.	0	1	2	3	4
4.	I have been clumsy and uncoordinated.	0	1	2	3	4
5.	I have been forgetful.	0	1	2	3	4
6.	I have had to pace myself in my physical activities.	0	1	2	3	4
7.	I have been less motivated to do anything that requires physical effort.	0	1	2	3	4
8.	I have been less motivated to participate in social activities.	0	1	2	3	4
9.	I have been limited in my ability to do things away from home.	0	1	2	3	4
10.	I have trouble maintaining physical effort for long periods.	0	1	2	3	4
11.	I have had difficulty making decisions.	0	1	2	3	4
12.	I have been less motivated to do anything that requires thinking	0	1	2	3	4
13.	My muscles have felt weak	0	1	2	3	4
14.	I have been physically uncomfortable.	0	1	2	3	4
15.	I have had trouble finishing tasks that require thinking.	0	1	2	3	4
16.	I have had difficulty organizing my thoughts when doing things at home or at work.	0	1	2	3	4
17.	I have been less able to complete tasks that require physical effort.	0	1	2	3	4

	Never	Rarely	Sometimes	Often	Almost Always
18. My thinking has been slowed down.	0	1	2	3	4
19. I have had trouble concentrating.	0	1	2	3	4
20. I have limited my physical activities.	0	1	2	3	4
21. I have needed to rest more often or for longer periods.	0	1	2	3	4

Instructions for Scoring the MFIS

Items on the MFIS can be aggregated into three subscales (physical, cognitive, and psychosocial), as well as into a total MFIS score. All items are scaled so that higher scores indicate a greater impact of fatigue on a person's activities.

Physical Subscale

This scale can range from 0 to 36. It is computed by adding raw scores on the following items: 4+6+7+10+13+14+17+20+21. 0

Cognitive Subscale

This scale can range from 0 to 40. It is computed by adding raw scores on the following items: 1+2+3+5+11+12+15+16+18+19. 0

Psychosocial Subscale

This scale can range from 0 to 8. It is computed by adding raw scores on the following items: 8+9. 0

Total MFIS Score

The total MFIS score can range from 0 to 84. It is computed by adding scores on the physical, cognitive, and psychosocial subscales. 0

Beck's Depression Inventory-II (BDI-II): Participants must answer 0-3 for each statement; the total score is the number sum of all answers.

BDI - II

Instructions: This questionnaire consists of 21 groups of statements. Please read each group of statements carefully. And then pick out the one statement in each group that best describes the way you have been feeling during the past two weeks, including today. Circle the number beside the statement you have picked. If several statements in the group seem to apply equally well, circle the highest number for that group. Be sure that you do not choose more than one statement for any group, including Item 16 (Changes in Sleeping Pattern) or Item 18 (Changes in Appetite).

1. Sadness
   0. I do not feel sad.
   1. I feel sad much of the time.
   2. I am sad all the time.
   3. I am so sad or unhappy that I can't stand it.

2. Pessimism
   0. I am not discouraged about my future.
   1. I feel more discouraged about my future than I used to.
   2. I do not expect things to work out for me.
   3. I feel my future is hopeless and will only get worse.

3. Past Failure
   0. I do not feel like a failure.
   1. I have failed more than I should have.
   2. As I look back, I see a lot of failures.
   3. I feel I am a total failure as a person.

4. Loss of Pleasure
   0. I get as much pleasure as I ever did from the things I enjoy.
   1. I don't enjoy things as much as I used to.
   2. I get very little pleasure from the things I used to enjoy.
   3. I can't get any pleasure from the things I used to enjoy.

5. Guilty Feelings
   0. I don't feel particularly guilty.
   1. I feel guilty over many things I have done or should have done.
   2. I feel quite guilty most of the time.
   3. I feel guilty all of the time.

6. Punishment Feelings
   0. I don't feel I am being punished.
   1. I feel I may be punished.
   2. I expect to be punished.
   3. I feel I am being punished.

7. Self-Dislike
   0. I feel the same about myself as ever.
   1. I have lost confidence in myself.
   2. I am disappointed in myself.
   3. I dislike myself.

8. Self-Criticalness
   0. I don't criticize or blame myself more than usual.
   1. I am more critical of myself than I used to be.
   2. I criticize myself for all of my faults.
   3. I blame myself for everything bad that happens.

9. Suicidal Thoughts or Wishes
   0. I don't have any thoughts of killing myself.
   1. I have thoughts of killing myself, but I would not carry them out.
   2. I would like to kill myself.
   3. I would kill myself if I had the chance.

10. Crying
   0. I don't cry anymore than I used to.
   1. I cry more than I used to.
   2. I cry over every little thing.
   3. I feel like crying, but I can't.

11. Agitation
   0. I am no more restless or wound up than usual.
   1. I feel more restless or wound up than usual.
   2. I am so restless or agitated, it's hard to stay still.
   3. I am so restless or agitated that I have to keep moving or doing something.

12. Loss of Interest
   0. I have not lost interest in other people or activities.
   1. I am less interested in other people or things than before.
   2. I have lost most of my interest in other people or things.
   3. It's hard to get interested in anything.

13. Indecisiveness
   0. I make decisions about as well as ever.
   1. I find it more difficult to make decisions than usual.
   2. I have much greater difficulty in making decisions than I used to.
   3. I have trouble making any decisions.

14. Worthlessness
   0. I do not feel I am worthless.
   1. I don't consider myself as worthwhile and useful as I used to.
   2. I feel more worthless as compared to others.
   3. I feel utterly worthless.

15. Loss of Energy
   0. I have as much energy as ever.
   1. I have less energy than I used to have.
   2. I don't have enough energy to do very much.
   3. I don't have enough energy to do anything.

16. Changes in Sleeping Pattern

0. I have not experienced any change in my sleeping.
1a I sleep somewhat more than usual.
1b I sleep somewhat less than usual.
2a I sleep a lot more than usual.
2b I sleep a lot less than usual.
3a I sleep most of the day.
3b I wake up 1-2 hours early and can't get back to sleep.

17. Irritability

0. I am not more irritable than usual.
1. I am more irritable than usual.
2. I am much more irritable than usual.
3. I am irritable all the time.

18. Changes in Appetite

0. I have not experienced any change in my appetite.
1a My appetite is somewhat less than usual.
1b My appetite is somewhat greater than usual.
2a My appetite is much less than before.
2b My appetite is much greater than usual.
3a I have no appetite at all.
3b I crave food all the time.

19. Concentration Difficulty

0. I can concentrate as well as ever.
1. I can't concentrate as well as usual.
2. It's hard to keep my mind on anything for very long.
3. I find I can't concentrate on anything.

20. Tiredness or Fatigue

0. I am no more tired or fatigued than usual.
1. I get more tired or fatigued more easily than usual.
2. I am too tired or fatigued to do a lot of the things I used to do.
3. I am too tired or fatigued to do most of the things I used to do.

21. Loss of Interest in Sex

0. I have not noticed any recent change in my interest in sex.
1. I am less interested in sex than I used to be.
2. I am much less interested in sex now.
3. I have lost interest in sex completely.

Total Score: _____

Symbol Digit Modalities Test (SMDT): Participants must read out loud (in order; left to right, line by line) as many numbers, which each correspond to a different symbol, as possible in 90 seconds. The total score is the number of correct number-symbol matches within 90 seconds.

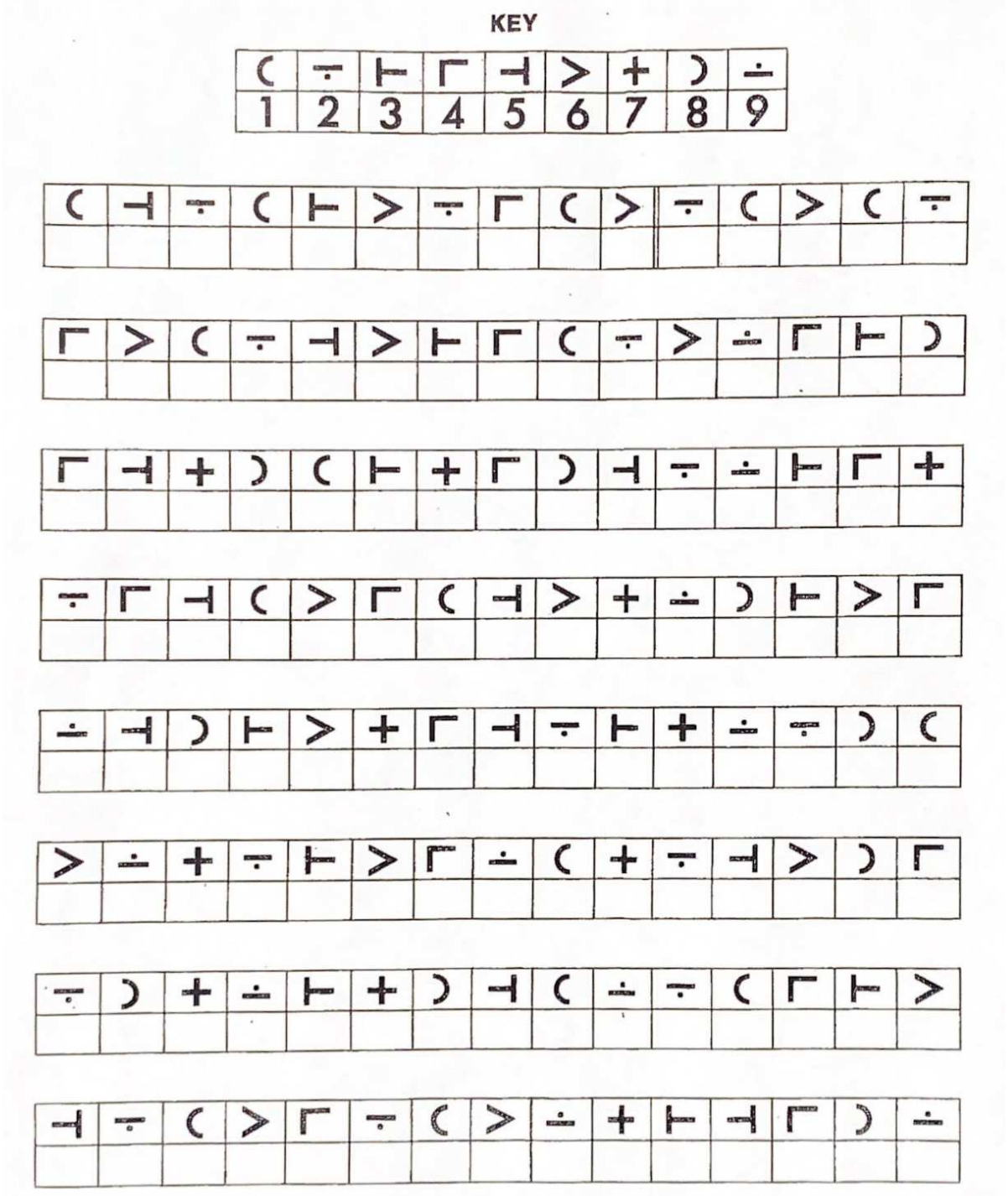

Brief Visuospatial Memory Test-Revised (BVMT-R): Participant is instructed to look at the test stimuli (below) for 10 seconds, after which point the test stimuli page is put away and the participant is given unlimited time to draw as many figures as they remember on a separate blank sheet of paper (participant advised to draw exact shape, size, and location on the page). This is repeated three times using the same test stimuli page for all three trials with a new blank sheet of paper each time. The total score is the number sum of all three trials, which are each scored out of 12, based on correct shape/size and location.

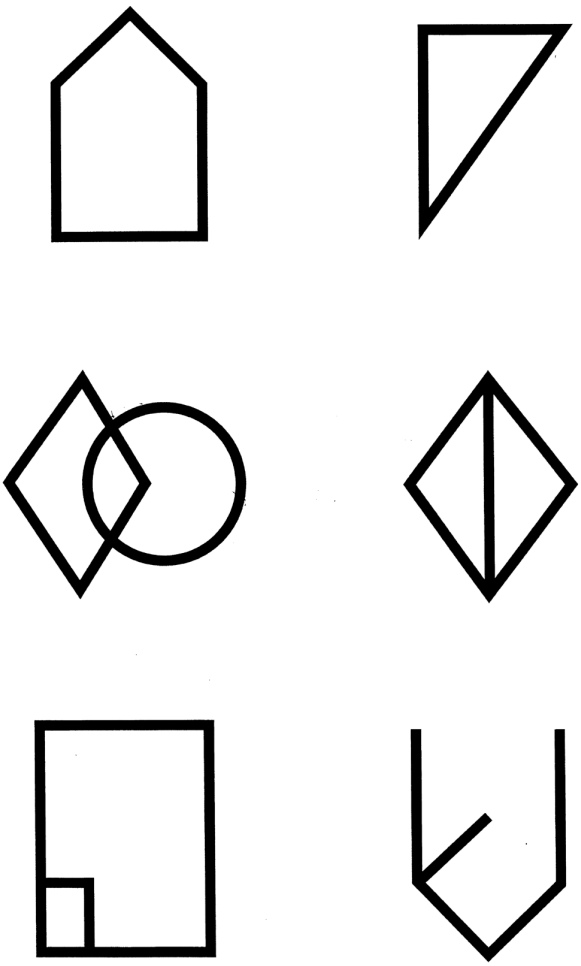

Timed 25-Foot Walk (T25FW): Participant is asked to walk 25 ft as quickly, but safely (i.e. participant may use assistive walking device if needed) as possible, and is timed. This is repeated a second time, and the total score is the average time (seconds) of both trials.

Nine-Hole Peg Test (9HPT): Participant is given 9-hole-peg board and 9 pegs, and is asked to fill the board and empty the board with the pegs one at a time as quickly as possible. This is repeated two times with their dominant hand and then two times with their non-dominant hand; each of the four trials is timed and the total score is the average time (seconds) of all four trials.